AAiT

ADDIS ABABA UNIVERSITY
SCHOOL OF GRADUATE STUDIES
Institute of Technology
Department of Chemical Engineering

CFD Modeling and Simulation on Hydrodynamics of CFB Biomass Gasifier using FLUENT

By

Beniyam Kebede W/kidane

Advisor: **Dr.-Ing. Zebene Kiflie**

A Thesis Submitted to the Graduate Studies of Addis Ababa University in Partial Fulfillment of the Degree of Masters of Science in Chemical Engineering

(Process Engineering)

Addis Ababa Institute of Technology (AAiT)
Addis Ababa, Ethiopia
July, 2011

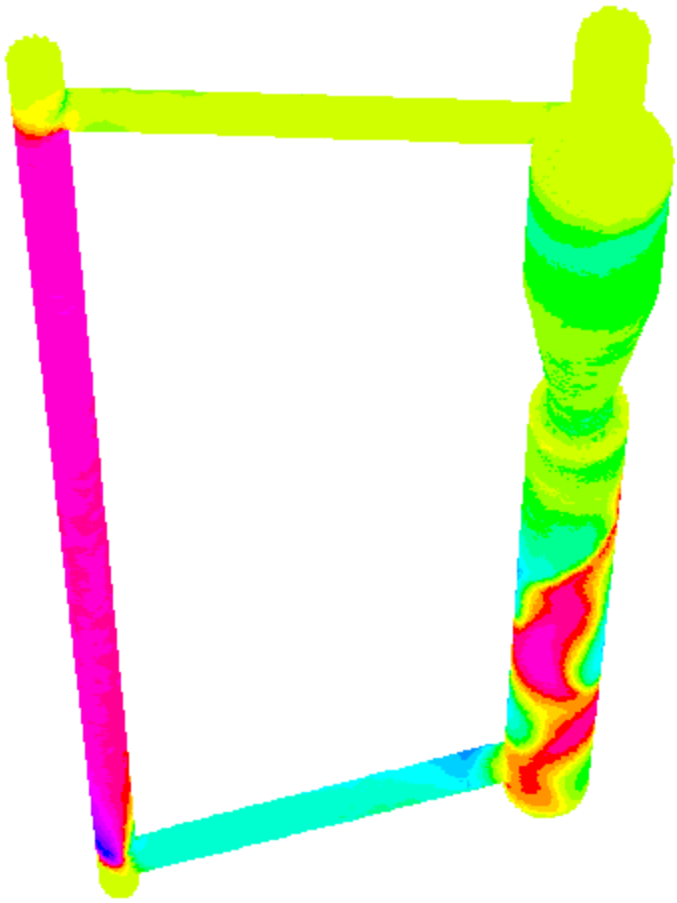

CFD Modeling and Simulation on Hydrodynamics of Circulating Fluidized Bed Biomass Gasifier using FLUENT

CFD Modeling and Simulation on Hydrodynamics of CFB Biomass Gasifier using FLUENT

A Thesis Submitted to School of Graduate Studies of Addis Ababa University in Partial Fulfillment of the Requirements for the Degree of Master of Science in Chemical Engineering

(Process Engineering Stream)

Candidate

Beniyam Kebede

Approved by the Examining Board:

	Date	Signature
_____	_____	_____

Chair man, Department's Graduate Committee

Dr.-Ing. Zebene Kiflie _____ _____
Advisor

Dr.-Ing. Nurelegne Tefera
_____ _____ _____
Internal Examiner

Dr.-Ing. Demiss Alemu _____ _____
External Examiner

DECLARATION

I hereby declare that the work which is being presented in this thesis entitled "CFD Modeling and Simulation on Hydrodynamics of CFB Biomass Gasifier using FLUENT" is original work of my own, has not been presented for a degree of any other university and all the resource of materials used for the thesis have been duly acknowledged.

_____ _____

Beniyam Kebede Date

(Candidate)

This is to certify that the above declaration made by the candidate is correct to the best of my knowledge.

_____ _____

Dr.-Ing. Zebene Kiflie Date

(Project advisor)

Acknowledgments

First I would like to thank God for giving me the health, the patience and the blessing that I have received from the beginning to the end of the Master's study. Next, I would like to express my deepest gratitude to my advisor Dr.-Ing. Zebene Kiflie, Head of chemical engineering department at AAiT. It would not have been possible to accomplish this thesis work without his sincere help, guidance, and support. I am also heartily thankful to Moges Ashagrie, Surafel Shemeles and Mesay, for their valuable contributions and support towards the success of this work.

I would like also to take this opportunity to thank all my friends for their valuable ideas and moral support during my thesis work. Last but not least, I would like to thank all my family members who have given me fresh impetus along all my journeys to reach the goal I have been aiming for.

Abstract

Biomass gasification in Circulating fluidized beds (CFB) is one of the most promising conversion processes in meeting future ecologically compatible and sustainable energy demand, based on a combination of flexibility, efficiency, and environmental acceptability. Widespread industrial use of CFB technology in coal and biomass combustion and gasification depends on improved control of the fluidization process that demands a better understanding of fluidized bed hydrodynamics. However, its application to CFB systems is limited due to the high computational requirements for understanding complex fluid flow behavior. The effect of different operating parameters on the hydrodynamic behavior of a two-phase gas-solid CFB biomass gasifier were studied in this thesis work systematically using computational fluid dynamics (CFD) software FLUENT.

Both 2-D and 3-D computational fluid dynamics (CFD) model based on Eulerian-Eulerian approach coupled with granular kinetic theory is developed to simulate the hydrodynamics and flow structures of the CFB under different operating conditions. A parametric analysis is performed to comprehensively investigate the influences of particle properties (Bagasse, sand and its sizes), operating parameters (gas velocity and solid circulation rate) and gasifier geometries (inlet structure/position).

The dynamic characteristics obtained from CFD simulation have been compare ed with the some similar conditions experimental data obtained from open literatures and in general a good agreement has been observed. Eulerian-Eulerian granular multiphase flow model approach is capable of predicting the core-annulus structure in CFB. The lower region of the CFB riser is denser than the upper-dilute region. Back-mixing behavior or accumulation of particles near the wall has been perfectly exist in the CFB. Increasing solids flux slows down the flow development, but increasing superficial gas velocity makes the flow development faster. Superficial gas velocity has a strong influence on the axial solids velocity. The volume fraction of big particles is lower in the upper. This hydrodynamics model provides the powerful theoretical basis for next steps on CFB designs. This study proposes that the operating parameters (solid circulation rate and gas velocity) and solid inlet geometry may be the critical consideration in order to reduce non-uniform distribution of gas and solid in CFB gasifier.

Table of contents

List of Tables

List of Figures

Acronyms

ρ_k	Density of phase k= g (gas), s (solid)
ε_k	Volume fraction of phase k= g (gas), s (solid)
v_k	Velocity of phase k= g (gas), s (solid)
$\mu_{g,l}$	Gas phase laminar viscosity
P_s	Pressure (Pa)
ε	Dissipation rate of turbulent kinetic energy
ϕ_s	Sphercity
ϕ_s	Exchange of fluctuating energy between the gas and solid phase
d_p	Particle diameter, (m)
k_s	solid phase turbulent kinetic energy by unit of mass (m^2/s^2)
P_g	Gas pressure (Pa)
t	Time, (s)
u	Velocity component in radial direction, (m/s)
v	Velocity component in axial direction, (m/s)
β	Interface drag function, (kg/m^2s)
μ	Dynamic viscosity, (kg/ms)
θs	Solid phase granular temperature (m^2/s^2)
τ_i	Viscous stress tensors, (Pa),
C	Instantaneous velocity vector of phase
k_s	Diffusion coefficient of granular temperature
R_e	Particle Reynolds number
Z	Height along axial (m)
C_D	Drag coefficient
e_{ss}	Coefficient of restitution between particles of solid phase s
Gs	Solids volume flux per unit area, (m/s)
g	Vector representation of acceleration due to gravity, 9.81 m/s^2
g_o	Radial distribution function between particles belonging to a solid phase s
K_{sg}	Momentum exchange coefficient between phase s and phase g
R_{es}	Reynolds number
γ_s	Collisional dissipation of granular temperature

S_Φ	Source term
F	Convective flux
D,	Diffusive flux
Γ	Transport coefficient

Subscripts

(g) and (s)	gas and solid phase
o	Initial condition
max	Maximum

Abbreviation

CFD	Computational Fluid Dynamics
FVM	Finite Volume Method
HHV	Higher Heating Value
PEBG	Pressurized Entrained flow Biomass Gasification
BC	Boundary Condition
2-D	Two Dimensional
3-D	Three Dimensional
CFB	Circulating Fluidized bed
CAD	Computer Aided Design
FB	Fluidized Bed
TFM	Two Fluid Models
KTGF	Kinetic Theory of Granular fluid
PEM	Particle Element Method
DEM	Discreet Element Method
PDE	Partial Differential Equations

CVM	Constant Viscosity Model
EMMS	Energy-minimization multi-scale
CFBBG	Circulating Fluidized Bed Biomass Gasifier
TDMA	Tri-Diagonal Matrix Algorithm
MFIX	Multiphase Flow with Interphase eXchanges
GAMBIT	Geometry And Mesh Building Intelligent Toolkit
SIMPLE	Semi-Implicit Method for Pressure-Linked Equations
GUI	Graphical User Interface
UDF	User Define Function

1. INTRODUCTION

1.1 Background

Currently, most of the electrical or thermal energy consumed in the world is generated through the use of nonrenewable energetic sources that, in the future, will increase strongly their price due to their potential shortage in the market. On the other hand, there are the renewable energetic sources that can in the long term be used permanently without any exhaustion threat. This is the case of biomass, which is currently being considered a promising energy source. The world's existing preoccupation about the contamination of the atmosphere with harmful gases for the stability of the planet's weather is combined with the necessity to valorize agricultural wastes like cane bagasse, rice husk and sawdust, among others.

Ethiopia has large amount of agricultural wastes. These wastes are used as a source of energy in some industries such as pulp and paper, sugar industry, etc. Currently, all sugar factories use bagasse based energy cogeneration for their energy production. Most of the sugar factories face energy loss problem in the boiler and in production process. Due to this, exporting electricity to the national grid is not yet practiced. Minimizing this loss, in order to increase the efficiency of the boiler mostly doesn't give significant effect rather it is better to focus on using efficient equipment that would replace the boiler to fully exploit the energy potential of bagasse [1].

Nowadays, energy saving opportunities in sugar industry focus on identifying opportunities for increasing cogeneration in a way that much of the rural electrification need in cane growing region could be meet. So it is better for all sugar factories to focus on using efficient cogeneration system to minimize the process low pressure steam demand and using other convectional cycle such as Biomass Integrated Gasification-Combined Cycle (BIG-CC) with Circulating fluidized bed (CFB) gasifier.

Indeed, among the technologies available for using bagasse for producing electricity, gasification is relatively new. Even until now there is no installed Circulating Fluidized Bed Gasifier (CFBG) in Ethiopia for any purpose but, there are some interesting steps toward this technology. Some of them are projects under study on the designing of 2MW biomass gasifcation plant by Live Energy [2]. The other one is done by Jimma University on manufacturing of different types of

gasifiers for producing syngas or the producer gas by gasification of wood chips and saw dust of Jimma University's wood work shop wastes and scrap papers of each faculty and administrative office of the university which are being burned in the garbage pit as a waste, grass and other agricultural wastes [3].

Thus, there is a demand in terms of understanding its characteristics of CFB gasifier so that in the near future can be design and improve the current technology that start's Jimma University in the direction of whole rural people need without depending on foreign technology. To focus on developing renewable energy equipment like CFB gasifier that has high efficiency and less impact on the environment. A good understanding on the hydrodynamics in circulating fluidized beds is necessary to further optimize and improve the design of existing small scale CFB biomass gasifier and to provide more information for CFB modeling.

Application of computational fluid dynamics (CFD) to analyze bed behavior is advantageous because predictions of hydrodynamics can be made in geometries and locations that would be impossible to measure using conventional experimental techniques, or that would require highly specialized equipment. The resulting abundance of hydrodynamic data can also assist in identifying important details that affect global bed performance, such as heat and mass transfer or reactor conversion and yield.

In order to comprehensively understand the biomass gasification in CFB gasifier and provide the theoretical basis for the optimized operation and scale-up designs, detail experimental and numerical techniques are required on the hydrodynamics investigation of fluidized beds, the thermodynamic equilibrium model and the CFD reactor model which are the three integral parts to comprehensively understand biomass gasification in CFB gasifier.

To better understand the CFB boiler/gasifier behavior, detailed information is needed in terms of, for example, the dynamic mixing of gas and solid fuels both horizontally and vertically, the effects of various non-uniform geometries such as biomass-feed inlets, solid return valves and secondary air-injection nozzles, and the pressure balance over the whole loop of CFB circulation. All these considerations necessitate 2D and 3D full-loop CFD simulations, which may even be viewed as "virtual experimentation" if with reliable models. But, there are only a few reports with regard to 3D, full-loop simulation of CFB [4].

1.2 Statement of the Problem

CFB-fluidized bed (CFB) has wide range of applications in petrochemical, mineral and metallurgical industries. Despite its extensive use, an understanding of the complex behavior of these units is incomplete. Since, the basic design goal of biomass fluidization using CFB for any purpose is to spread the particle evenly throughout the CFB riser in order to increase the efficiency of the reactions taking place, in CFB riser operation is usually that the solid material distribution is non-uniform. Additionally at higher production rates, which require a higher solid flux, the down-flow of solids near the wall occurs, and causes back mixing. These are further complicated by the effects of the inlet and outlet configurations. Besides, most of previous studies are done for fluid catalytic cracking (FCC) and coal. Definitely coal gasifier and biomass gasifier are different things as coal char in gasification reactivity is significantly different from biomass reactivity. Furthermore the know-how in this field is almost blank. So, detailed experimental and numerical techniques are required to study the flow structures pertaining in CFB gasifier.

In the past, researchers have attempted to understand the hydrodynamics of fluidized-bed reactors by performing laboratory-scale experiments. Unfortunately, the laboratory-scale data does not necessarily scale up accurately. This is due to the complicated transient gas and solid motion occurring in the fluidized bed. It is well known that the existing hydrodynamics theory that describe this motion has not been sufficiently verified by experiment, especially where there is more than one solid in the bed [6].

To gain a better understanding on hydrodynamics behavior for a commercial-scale fluidized bed, it is necessary to study a vessel of that size. However, the capital cost of such a program can be prohibitive. Alternatively, new CFD software like FLUENT With new modeling methods that can simulate gas-solid flows to a, much higher level of reliability [7]. Once a good numerical model has been defined, physical modeling of small scale pilot plants validates the numerical model, which will in turn be used to predict characteristics of large scale production plant. This will reduce the number of pilot plants required, hence, reducing the time and cost of scale-up.

1.3 Objective

1.3.1 General Objective

The general objective of this research was to study the effect of different operating parameters on the hydrodynamic behavior of a two-phase gas-solid CFB biomass gasifier numerically using CFD software FLUENT (version **6.3**)

1.3.2 Specific Objective

- To model and simulate the hydrodynamic of CFB using bagasse particle.
- To identify and characterize the flow regime and structure in CFB for different gas velocity and solid flux.
- To investigate the effect of particle size and inlet geometry on bed expansion (bed voidage) and velocity distribution.

2. LITERATURE REVIEW

2.1 Introduction

Today the world thrives on power. Energy or power in its various forms permeates the modern society; urban and rural alike. However, while the uses that energy can be put to are endless, the conventional sources of energy are finite. There is a need to explore other sources of energy that are more sustainable and would complement or even supplement the existing sources.

One of the non-conventional sources of energy is biomass that is available mainly as a by-product of crop production, agro processing or the wood industry. Today, energy generated from biomass sources accounts for 12% of the energy consumed at a global level, 3-5 % among the industrialized countries, and 18-49% in developing countries. Efficiency improvements of existing energy systems, and putting huge quantities of biomass, mostly in the form of agricultural residues and wastes, which are currently disposed by burning or dumping, could potentially increase the energy supply from biomass substantially. The growing importance of biomass energy is also reflected in the intensification of related research and development efforts, as a result of which a number of biomass/wood energy technologies have matured in the recent years. These include:

- Modern wood fired plant
- Biomass integrated gasification combined cycle (BIGCC) technology
- Gasifier-engine system
- Cogeneration in Sugar industry
- Ethanol
- Biodiesel

The use of agricultural residues as bio-energy resource represents an appropriate option to be considered. The anticipated advantages of using agricultural residues for energy production are reduction in air emissions. Their utilization also contributes to waste management, reduction in electricity purchase at the generating facility (e.g. sugar mills) and even profit from selling surplus electricity to the grid.

2.2 Biomass based Power Cogeneration in Ethiopia

In Ethiopia hydro-electric and biomass energy are the two renewable energy sources that receive high priority for support by the government. Around 95% of the country electricity is generated from hydro-electric, the high proportion of hydropower is rational considering the facts that Ethiopia is rich in water resources and hydropower is relatively cheap [8]. However, the rainfall in Ethiopia varies considerably from year to year and therefore, over dependence on hydropower makes the energy supply very unstable.

In the case of agricultural based country like Ethiopia, biomass is considered a renewable source with the highest potential. There is considerable potential for energy production from large commercial farms and from agro-processing industries. Potential sources include sugar cane bagasse, cotton stalk, coffee hull and oil seed shells. At present only sugar cane bagasse is used in significant scale for energy production.

The use of biomass residues to generate electricity and thermal power to support weak grids is therefore important for the economic sustainability, as well as a key component of sustainable energy demand growth. Cogeneration power from sugar cane residual would be located where it is most needed: in the countryside. Over 75% of our country population lives in rural areas, more than 65% of our populations still have a problem of access to electricity. Bagasse based energy cogeneration for export to the national grid is not yet practiced in Ethiopia. Although all of them are not on the potential to supply electricity in a way that can help rural people, finding new energy efficient process equipment like BIG-CC, indigenous, low cost source of power, profitable and optimally operated sugar factory is becoming critical for continuing development.

In Ethiopia currently there are three sugar factories with crushing capacities ranging from 3,100 to 5,000 metric tons of cane per day (TCD). Table 1 shows the capacity of the sugar factories including expansion of new sugar factories by the government and the foreign investors now and in the next 5 years [9].

Table 1 : Production capacity of Ethiopian Sugar Factories

Name of Sugar Factory	Present Crushing Capacity, TCD	Crushing Capacity after 5 years, TCD	Annual Sugar Production, Tons	Annual Sugar Production after 5 years, Tons
Wonji Shoa	3100	6,000	70,000	150,000
Metehara	5000	5,000	120,000	120,000
Fincha	4000	13,000	100,000	194,400
AL-Habasha	-	8,000	-	155,520
Tendaho	-	13,000	-	260,000
Hiber sugar S.C	-	12,500	-	290,000

Bagasse, the fibrous residue of the cane stalk after crushing and extraction of the juice, consists of water, fibers and relatively small quantities of soluble solids. Its composition varies according to the variety of cane, its maturity, the method of harvesting, and finally the efficiency of the milling plant.

In sugar mills steam is used for both power generation and as source of heat in process operation. In Ethiopia this is the case in sugar factories and all of them use conventional steam cycle for co-generation. Some of the fundamental properties of steam which govern its use for generation of power and for heating as well as boiling in process are (i) High pressure and temperatures of steam are desirable for generating power. (ii) Low pressure steam is required in process operation. High pressure steam from boiler is fed to prime movers for some units like mills as also to the power generating turbines and the exhaust steam from these prime movers is utilized for process operations.

Conventional steam cycle use a byproduct bagasse as a fuel for steam generation unit (boilers) and treated water as a boiler feed and the boiler produce high steam pressure than required for the process. This steam is passed through a steam turbine where some of the energy is used to generate mechanical power for driving an alternator for electricity. The steam exits the turbine at a reduced pressure and is then returned to the boiler as condensate or hot water. The primary objective of the energy system is the production of steam hence the electricity that is produced is governed by the demand for process steam. In some cases the electricity becomes a primary product when the steam is excess to requirements such as is the case after milling season. The turbine would then be a condensing one where the steam is returned to the boiler without having

to pass through the process. Under these circumstances the plant operates as a bagasse fired power station.

However the case is quite different in some Sugar Factory, which suffers from lack of bagasse during off season and as a matter of fact it is forced to cut trees of the surrounding to deliver it to its boilers during stoppage of mill and even in Metahara Sugar Factory, which is the largest sugar factory in Ethiopia with an installed crushing capacity of 5000 TCD [10]. The factory currently generates around 6.6MW of electricity from its 3 turbines (3.3MW capacity each, one on standby) and consumes all of it. The factory still imports power from the national grid only during the low season.

The average combustion efficiency of the boilers of Metehara Sugar Factory is 65.3% [11] and in Shoa Sugar Factory is 56%. Both of them have very low efficiency when compared to the minimum accepted efficiency of boiler that uses bagasse as a fuel (70 %) [10]. The main causes of heat losses for most types of boiler and especially for solid fuels like bagasse furnaces are: Heat loss due to dry gas, Heat loss due to moisture from burning of hydrogen in the fuel, Heat loss due to moisture in the fuel, Heat loss from the formation of CO, Heat loss due to unburned carbon in the ash and Heat loss due to radiation and unaccounted. A lot of alternative solutions for efficiency improvement are suggested by different researchers, but that is not the objective of this work.

2.3 New Technology to Enhance Bagasse Cogeneration

When steam demand in the process is high and the simple medium pressure steam cycle is used, surplus power generation is difficult. However, by minimizing the process low pressure steam demand and using other cycles such as high pressure steam cycle and BIG-CC and recovering part of the sugarcane trash that is burned or wasted in the field to supplement the bagasse fuel, the power deficit can be reduced. In other words, by improvement of the co-generation plant in sugar factories, selling additional power to the national grid will be possible. This also offers an excellent opportunity for the sugar mills to generate additional revenue.

The cane sugar industry has long recognized the enormous potential in the use of bagasse for the production of energy. Many sugar factories are presently producing considerable amounts of

electricity for export to the utility grid while at the same time meeting on-site energy needs by installing modern condensing-extraction steam turbines for cogeneration. However, biomass gasification technology applied to bagasse gasification in conjunction with gas fired turbines, which could become commercially available in the near future, offer higher thermodynamic efficiencies compared to the conventional steam cycle using condensing turbo-generator sets.

A promising alternative to the steam-turbine cycle for biomass power generation is a set of biomass integrated gasifier/ gas turbine technologies. These technologies involve coupling combined power generating or co-generating cycles, which have already been developed for coal applications, to biomass gasifiers. The gas produced by the gasifier is used to fuel a gas turbine-generator unit; further energy can be recovered from the gas turbine exhaust.

This study assumes the BIGCC option as an emerging energy technology for sugar industry that will be introduced for the coming decade years and examined with favorable results the use of bagasse and cane residues as input fuels in a BIG-CC plant. By some estimates, BIG-CC system has a net electricity generation potential of 180 kWh/tc which means producing up to twice as much electricity per unit of biomass consumed and are expected to have lower capital investment requirements per kW of capacity than conventional cycles [12].

Since, using of the sugarcane trash after green harvesting is another way to increase further the surplus power generation. A large amount of residues as dry and green leaves, as well as tops left on the field is one of the major characteristics of green harvesting. Studies show, the surplus power generation can be raised from the present level of 50 to 60 kWh/tc to 100-120kWh/tc with existing technology, or to 250-300kWh/tc with BIG-GT system. Of importance, there are costs involved in gathering and transporting cane trash to a mill [13].

2.4 Biomass Gasification Technology

Gasification is thermo-chemical process at high temperature that converts carbon containing fuels, such as coal and biomass, into a combustible gas containing mainly “producer gas” carbon monoxide, hydrogen, methane and inert gases, through incomplete combustion and reduction. It contains a series of steps: drying, devolitisation, char gasification and gas phase reactions. Also, the final product gas composition is a result of twelve important endothermic and exothermic

chemical reactions that take place inside the gasifier. The exothermic reactions provide heat to support the endothermic reactions through partial combustion. Eventually a steady state will be reached and the gasifier will maintain its operation at a certain temperature.

Gasification and combustion are two closely related thermochemical processes, but there is an important difference between them. Gasification packs energy into chemical bonds in the product gas; combustion breaks those bonds to release the energy. The gasification process adds hydrogen to and strips carbon away from the feedstock to produce gases with higher hydrogen-to-carbon (H/C) ratio, while combustion oxidizes the hydrogen and carbon into water and carbon dioxide, respectively. Gasification, on the other hand, requires a gasifying medium like steam, air, or oxygen to rearrange the molecular structure of the feedstock in order to convert the solid feedstock into gases or liquids; it can also add hydrogen to the product. For a given throughput of fuel processed, the volume of gas obtained from gasification is much less compared to that obtained from a combustion system. The reduced volume of gas needs smaller equipment, and hence results in lower overall costs. Thus, gasification provides an attractive option for remote locations.

2.4.1 Gasifying Mediums

The thermo-chemical conversion of carbonaceous feed stock during gasification process is usually undergone in oxidant starved environment (i.e. under stoichiometric gasification conditions). Depending on the required quality of the product gas intended to be produced; oxygen, air, steam or a combination of these can be used as the oxidizing agent. As such, the quality of the product gas downstream the gasifier could vary in great extent both in terms of energy density and mixture components, depending on both the carbonaceous feed stock used and the type of oxidant.

Table 2 : Heating Values for Product Gas

Medium	Heating Value (MJ Nm^{-3})
Air	4–7
Steam	10–18
Oxygen	12–28

Table 2 and 3, show that heating value and the composition of the gas produced in a gasifier are strong functions of the nature and amount of the gasifying agent used. If air is used instead of oxygen, the nitrogen in it greatly dilutes the product. From Table 2, we can see that oxygen gasification has the highest heating value followed by steam and air gasification [12].

Table 3 : Product gas composition and heating value gasification process

Gas	HHV	LHV
	(MJ Nm^{-3})	
Hydrogen	12.65	12.65
Carbon Monoxide	12.77	10.8
Methane	39.79	35.86
Ethane	70.39	64.45
Propane	101.73	93.68
Butane	132.37	122.27

2.4.2 Types of Gasifiers

The main challenge in gasification is enabling the pyrolysis and gas reforming reactions to take place using the minimum amount of energy in reactors that are economical to construct. With a history going back to the late 18^{th} Century, there have been an extraordinary number of different designs and process configurations. Prior to the development of fluidized bed technologies in the 1920s, the majority of the gasifiers were so called fixed bed units.

Depending on the end application of the product gas and plant size, there are different gasifier designs. Small, packed-bed gasifiers (updraft, downdraft or crossdraft) may be suitable for stationary internal combustion engine operation (with electricity generation) or for gas burner application. Fluidized bed gasifiers (bubbling, circulating or pressurized) can be quite large and are thus applied for larger plants, which for example may involve gas turbines, steam boilers, methanol synthesis etc. Pressurized entrained flow gasifiers are commercialized for coal as fuel and under development for black-liquor gasification to produce bio fuels.

The main advantage of fluidized bed gasifiers over fixed bed gasifiers is their uniform temperature distribution in the gasification zone. This is achieved using fine particles of an inert material like sand or alumina. The inert particles are heated at start-up, and then serve as an ignition source and thermal energy carrier at steady state conditions.

Atmospheric CFB is the most suitable technology for use in a BIGCC system. CFBs allow for more complete carbon conversion and permit higher specific throughputs than bubbling beds. Some of its additional benefits are: [11]

- Good fuel flexibility
- Compact gasifier even at atmospheric pressure, cost-effective large scale construction
- Good controllability
- Uniform process temperature due to highly turbulent movement of solids

2.5 Mechanism of Gas-Solid Fluidization

When a fluid is passed upwards at a low velocity through a packed bed of particles, the fluid percolates through the void spaces between the stationary particles. By increasing the gas velocity, the drag force imparted by the fluid on the particles becomes greater. A point is reached where the drag force counterbalances the weight of the particles; the particles are lifted and separation of the particles occurs. At this point, the bed of particles has attained minimum fluidization.

Beyond the minimum fluidization velocity of gas-solids systems, two-phase theory dictates that any gas in excess of the minimum fluidization velocity will form gas bubbles; and the bed becomes a heterogeneous suspension of gas and solids. At elevated gas velocities the heterogeneous nature of the gas-solids flow begins to deteriorate, and the bed behaviour incrementally becomes dominated by a single-phase suspension of gas and solids. This incremental change in the behaviour of the bed, from heterogeneous to homogeneous gas-solids flow, is the basis for classification of fluidization regimes.

2.5.1 Fluidization Regimes

Kunni et al. [14] has defined fluidization as a "phenomena through which fine solids behave like a fluid through contact with a gas or liquid" and classify the different flow regimes in gas-solid fluidized bed, depending on the superficial gas velocity. At low fluid flow rates, the fluid percolates through the void spaces between the solids, which remains a packed bed; the force acting on the bed due to the flow of the fluid is less than the weight of the bed. When the flow

rate is increased over a certain threshold, known as the minimum fluidization velocity, the solids become levitated due to the interaction between the fluid and the particles, and the bed behaves like a fluid.

Minimum Fluidization

Minimum or incipient fluidization occurs at the point where the upward drag on the solid packing is equal to the weight of the packing. The height of the bed will be the same as for a fixed bed, or marginally higher than that of the fixed bed. The particles move about slightly, but only on a small scale. In most cases the particles just "vibrate" in their local positions in the bed.

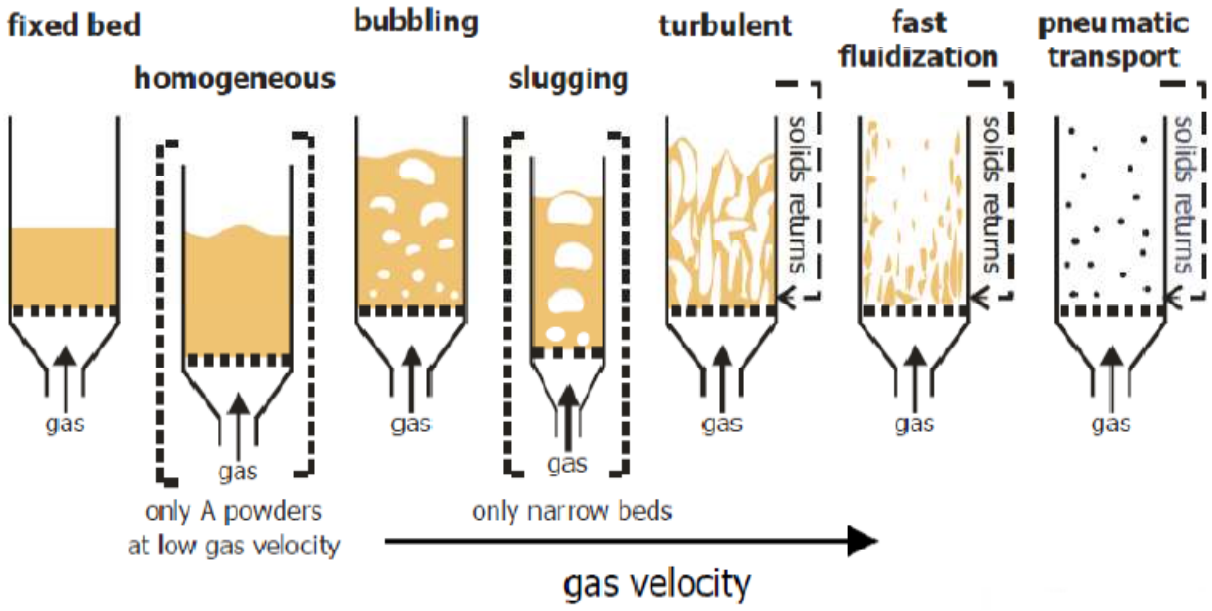

Figure 1 : Fluidization regimes

Grace in 1986 has also classified different types of fluidized beds on the basis of gas velocity as shown in the Fig. 1 above. As the gas velocity is increased in bubbling fluidized bed (BFB), the bubbling action becomes very violent which results in bubbles coalesce and form a core space in the dense region of the column. At the same time, the cloud and emulsion merge and retreat to walls of the vessel. In this state, we have a fast fluidized (FF). Between BFB and FF regimes, he has described "Turbulent Bed (TB)". At further higher velocity, the column enters in the

pneumatic conveying region (PC). On the basis of change in gas velocities, the solid move from one state or regime to another. These regimes, arranged in order of increasing velocities, are: Packed Bed (fixed), Bubbling Bed, Turbulent Bed, Fast Bed (Circulating Fluidized Bed) and Transport Bed (Pneumatic or Entrained Bed) [15].

2.5.2 Solid Classification

Different types of solids fluidize differently as many different factors such as drag, particle interactions, etc influence the behavior of these particles during fluidization. Geldart was the first to classify the fluidization behavior of the different types of solids in a gas and group them into four different types, namely the Geldart A, B, C and D powders. An illustration of the layout of the famous Geldart chart can be seen in Figure 2 below [16].

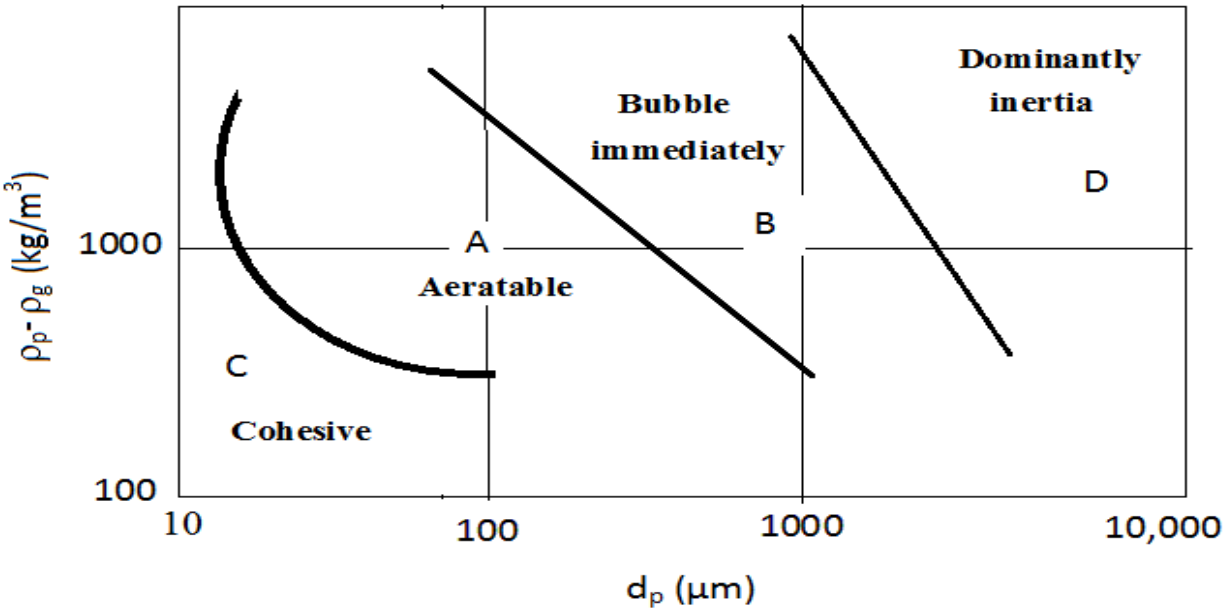

Figure 2 : Geldart Particle classification

Group C

This class of solids includes very fine and cohesive powders, e.g. cement, flour, starch etc. With this class, normal fluidization is extremely difficult and channeling takes place when fluidized. This difficulty in fluidization is as a result of the large inter-particle forces associated with such small solids.

Group A

Solid particles having a small mean particle size or low particle density. Typical examples of this class are catalysts used for fluid catalytic cracking (FCC) processes. These solids fluidize easily, with smooth fluidization at low gas velocity and bubbling/turbulent fluidization at higher velocity.

Group B

Similar in behavior to sand, these powders fluidize well but not homogeneously. Bubbles start to appear as soon as the minimum fluidization velocity is passed. These bubbles will grow in size up to bed diameter, when the bed will start to slug. Most biomass particle is arranged in this group.

Group D

These particles have large diameters compared to the other Geldart classifications. A stable spouted bed can easily be formed with these powders, but it is hard to fluidize.

2.5.3 Advantages and Disadvantages of Fluidized Beds

Fluidized-bed reactors afford excellent gas-solid contacting and particle mixing, facilitate the control of highly exothermal reactions, provide good gas-to-particle and bed-to-wall heat transfer, fuel can be burnet at a much lower temperature compared with conventional boiler technology. The lower temperature reduces the amount of NO_x produced. Also, limestone and dolomite can be added to a fluidized bed which can absorb SO_2 and, consequently, the emission can be made acceptably low. However, they also have disadvantages, such as gas-bypassing in the form of gas bubbles, channeling, the erosion of bed internals and the attrition of the bed material, agglomeration and defluidization of the bed material if the fuel contains a high content of some low melting point inorganic species and scale-up can be difficult due to the behavior of fluidized bed which can change significantly as its size is increased.

The two most important fluidized beds with regards to investigating new technology for power generation industry are the bubbling fluidized bed and circulating fluidized bed. This thesis work is limited to gas-solid circulating fluidized beds (fast fluidization).

2.6 Circulating Fluidization Bed (CFB) Gasifier

CFB or Fast fluidized bed is a high velocity gas–solid suspension where particles, elutriated by the fluidizing gas above the terminal velocity of individual particles, are recovered and returned to the base at a rate sufficiently high to cause a degree of solid refluxing that will ensure a minimum level of temperature uniformity in the furnace. CFB technology has evolved from conventional bubbling bed combustion as a means to overcome some of the drawbacks associated with conventional bubbling bed combustion like gas by passing.

The operation of circulating fluidized bed systems requires that both the gas flow rate and the solids circulation rate are controlled, in contrast to the gas flow rate only in a dense phase fluidized bed system. The solids circulation is established by a high gas flow. The integral parts of a CFB loop are the riser, gas-solid separator, downcomer, and solids flow control device. The CFB is thus a fluidized bed system in which solid particles circulate between the riser and the downcomer, as shown below in Figure 3 below. The riser is the main component of the system. The name riser is generally used to characterize a tall vessel or column that provides the principal reaction zone. On average, the particles travel upwards in the riser, though the motion at the wall may be downwards. The fluidized gas is introduced at the bottom of the riser, where solid particles from the downcomer are fed via a control device and carried upwards in the riser. The fast fluidization regime is the principal regime under which the CFB riser is operated. The particles exit at the top of the riser into the gas-solid separators which are normally cyclones. In lean-phase fluidized beds, the rate of entrainment is far larger than in turbulent fluidized beds, and bigger cyclone collectors outside the bed are usually necessary. The separated particles then flow to the downcomer and return to the riser. The entrance and exit geometries of the riser often significantly affect the gas and solid flow behavior in the reactor. The efficiency of the cyclones determines the particle size distribution and solids circulation rate in the system. The downcomer provides hold volume and a static pressure head for particle recycling to the riser. The downcomer can be a large reservoir which aids in regulating the solids circulation rate, a heat exchanger, a spent solid regenerator, hopper or a standpipe. CFB risers normally contain a relatively dense region near the bottom and a dilute zone towards the top [14].

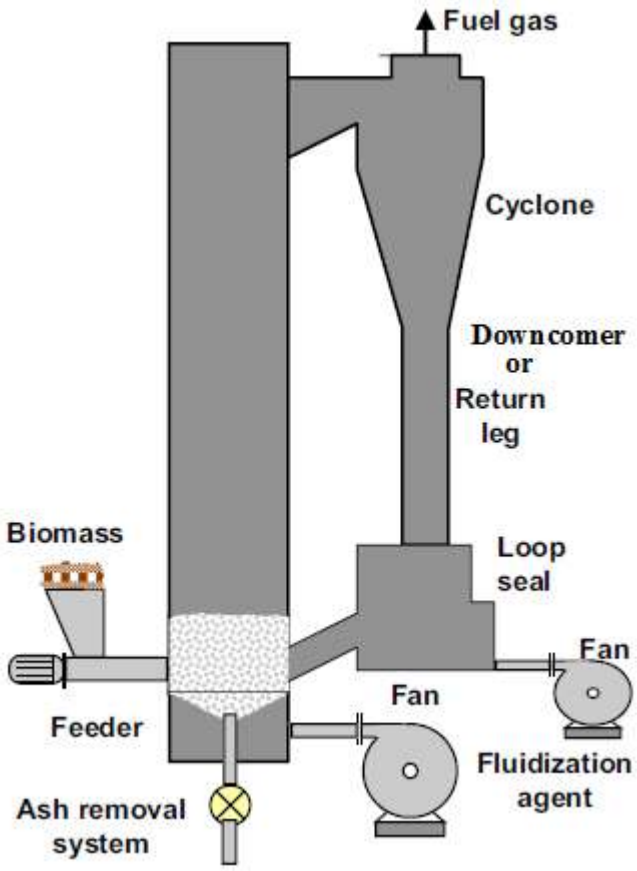

Figure 3 : Circulating fluidized bed (CFB)

Zones in a CFB

In a fluidized bed reactor distinct zones can be found. These zones all have their own specific properties and unique hydrodynamic behavior, which are used to identify the zones and which influence the conditions and events inside the zones. An illustration of the most important zones can be seen in Figure 2.3. Dense region near the bottom and a dilute zone towards the top are the most important zones in CFB riser. The dense bed is found at the bottom of the vessel and this is the zone in the fluidized bed where most of the particles are found. It is the zone with the highest solid hold-up and lowest voidage, ε. The interface between the dense bed and the zone above the dense bed is called the splash zone. It is in this zone where all the solids are ejected into the freeboard. When the fluidized bed is in the fast fluidization regime, the splash zone is difficult or even impossible to distinguish from the dense bed. The zone above the splash zone has a more gradual decrease in solids concentration up to a point where the solids concentration remains

constant for all practical purposes. This distance from the bed surface up to the point where the solids concentration remains constant is called the transport disengagement height (TDH).

Commonly used names for the region of large solids volume fraction are dense region, bottom bed and choked bed. The transitional zone is frequently referred to as the acceleration, splash or developed flow regime. The regime of low solid volume fraction is as dilute, transported or fully developed flow regime.

Different experimental results from literature shows that the dens zone of CFB operate in the bubbling regime, if the gas velocity increased to three times the terminal velocity of the average sized particle. The upper (dilute) zone has the solids volumetric concatenation very low. The fast fluidization is primarily affected by parameters like solids circulation rate, superficial gas velocity through the column and particle size. Hence, the main task in achieving smooth operation of a CFB system is to control such parameters in the riser [18].

2.6.1 Transition to Fast Fluidization

A clear picture of the transition to and from fast fluidization is lacking at the moment. Thus, a description of the process, based on present available condition is shown in Figure 4. Imagine that gas is flowing upwards through a vertical column to which a solid is fed at a certain rate, so the suspension is initially in pneumatic transport. If the superficial gas velocity through the column is decreased without changing the solid feed rate, the pressure drop per unit height of the column will decrease due to the reduced fluid friction on the wall (C–D). However, the suspension will become increasingly denser with decreasing gas velocities. Thus, the gas–solid drag will dominate the pressure drop across the column. There would be a pressure drop across the column due to both wall-gas friction and gas–solid drag (friction). Under steady-state conditions the solid–gas friction is equal to the weight of the solids. With a continued decrease in the superficial velocity in Figure 4, the bed becomes denser and the pressure drop begins to increase (D–E). The point of reversal (D) marks the onset of fast-bed from pneumatic transport.

If the gas velocity is decreased further, the solid concentration in the column increases up to a point where the column is saturated with solids, the gas being unable to carry any more. The solids start accumulating, filling up the column, and causing a steep rise in the pressure. This

condition (E) is called choking. In smaller diameter columns, the bed starts slugging, while in larger ones it undergoes transformation into a non-slugging dense-phase fluidized bed, such as a turbulent bed. The gas–solid regimes below this velocity have the generic name of captive state. The captive state may include turbulent, slugging, bubbling, and fixed beds [17].

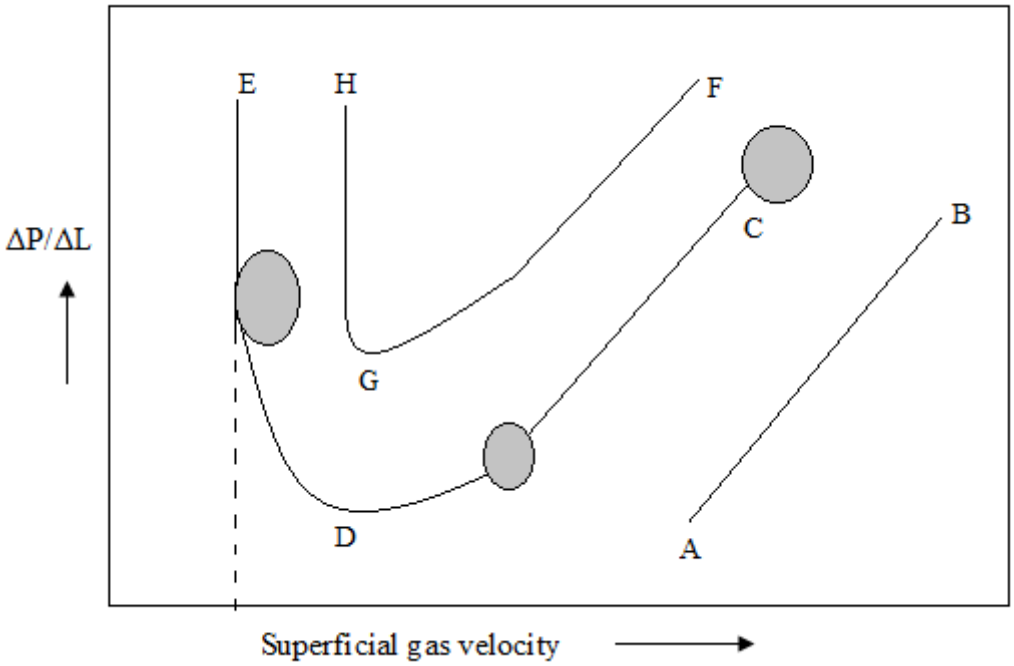

Figure 4 : Schematic representation of different regimes of gas-solid flow through a vertical column

A qualitative flow regime diagram, developed by Reddy-Karri and Knowlton [17], is presented in Figure 5. The regimes are shown on a plot of solid circulation rate and fluidizing or superficial velocity. The line A–B (locus of choking velocity) marks the boundary between the captive and fast-bed conditions. Figure 5 further shows that at higher circulation rates, the transition to fast fluidization occurs at higher velocities and for each solid circulation rate there are two limiting velocities for the fast bed: the choking velocity on the lower side and another velocity on the higher side that marks the transition from fast fluidization to pneumatic transport. This is also the velocity at which, for a given circulation rate, the average pressure drop across the height of the column reaches a minimum value (point D, in Figure 4).

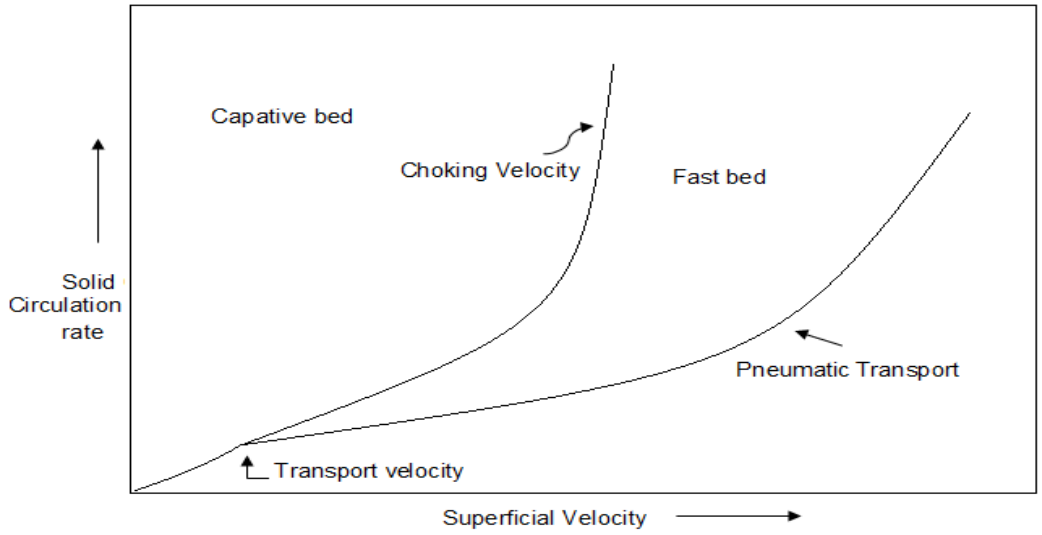

Figure 5 : Fast fluidization regime boundary

Choking velocity, U_{ch} used to mark the transition from captive state to fast fluidization. Transport velocity U_{tr} is a minimum velocity below which fast fluidization cannot occur, irrespective of the circulation rate. If a bed is fluidized above the terminal velocity of the individual bed particles, all solids will be entrained out of the column unless they are replaced simultaneously. However, it takes a certain amount of time to empty the column. As the velocity in excess of the terminal velocity increases, the time needed to empty the vessel decreases gradually until a critical velocity is reached, above which there is a sudden drop in the time for emptying the vessel. An empirical relation for the transport velocity is given by [17].

$$U_{tr} = 1.45 * \frac{\mu}{(\rho_g d_p)} Ar^{0.484} \qquad Ar = \frac{g\rho_g(\rho_p - \rho_g)d_p^3}{\mu_g^2} \qquad (2.1)$$

Where: Ar represents the Archimedes Number, $20 < Ar < 50{,}000$

: U_{tr} is the transport velocity for the solids.

Transport velocity is significantly larger than the terminal velocity when fluidizing Geldart A and B powders, but the two boundary velocities are more or less equal when fluidizing Geldart D powders. This means that there is a very narrow range of velocities in Geldart D powders where turbulent fluidization occurs. These powders proceed from bubbling fluidization straight to fast fluidization. Fast fluidization cannot be achieved if no solids return is present in the fluidized bed, otherwise the contents of the bed will be lost after a short period of operation. The main

difference between fast fluidization and pneumatic transport is that fast fluidization is operated at a flow rate closer to U_{tr}, which results in a dense phase and a lean phase inside the bed, while pneumatic transport has a homogeneous distribution of solids throughout the bed. In the case of fast fluidization, the dense phase, or 'annulus' is close to the wall of the vessel with solids flowing down while the lean phase, or 'core' is in the centre of the vessel where the solids flow up [19].

2.6.2 Hydrodynamics Behavior of CFB

The performance of a gasifier is governed by how effectively gases are transported from the gasifier entrance to the surface of the fuel particles, their reaction rate on the surface of particles and transport of the product gas to the exit of the gasifier. Reaction kinetics decides the reaction rate for a given temperature and gas concentration at the reaction site on the particle, but the transport of gases from and to the reaction site is determined by the hydrodynamics of the gasifier. Therefore, study on hydrodynamic plays a vital role in defining the operation of a CFB. It leads to understanding of several aspects of gas-solid suspension behavior in the CFB of different sizes and shapes, operated under a variety of conditions.

The basic difference between a fluidized gasifier or boiler and a reactor is in the hydrodynamics of the gas–solid motion in their boiler or reactors. Interestingly, most of their environmental and operating characteristics are a direct result of the hydrodynamics of gas–solid interaction. For this reason, the performance of a fluidized bed boiler or gasifier drops significantly when the operation of its furnace deviates from the designed fluidization regime. Thus, a good understanding of the gas–solid motion in the furnace or reactor of a fluidized bed unit is very important. The next discussion presents a brief summary of the hydrodynamics of circulating fluidized beds.

The two most popular uses of circulating fluidized bed process are boilers and FCC reactors. There is a basic difference between these two prominent applications of the CFB process it is in the flow regime of operation of their risers. Some important differences are listed in Table 4 below.

Table 4 : Difference between CFB Boiler and CFB Reactors

Application	Boiler	Reactor
Regime	Fast	Dense phase suspension up-flow
Geldart particle group	B or D	A,AC,C or B
Particle diameter (μm)	200	70
Suspension density in upper region (kg/m^3)	1-10	10-100
External circulation rate (kg/m^3)	10-50	500-1100
Solid circulation rate (sec)	30-600	3-15
Velocity (m/s)	<6	<25
Temperature (^oC)	850	550

Auxiliary power consumption being a major concern, boiler furnaces require minimum pressure drop across the riser and maximum internal solid circulation. For this reason, CFB boilers use a low (1 to 10 kg/m^2 sec) external solid circulation rate and a relatively dilute suspension density of about 1 to 5 kg/m^3 in the upper part of the riser. In CFB catalytic reactors, on the other hand, internal back-mixing is not desirable as it decreases the yield. Therefore, they use large external solid circulation rates (500 to 1100 kg/m^2 sec), yielding high suspension densities in the range of 10 to 100 kg/m^3. This regime is more appropriately called dense suspension up-flow instead of fast-bed as in CFB boilers. Additionally, CFB boilers or gasifier use group A, B, or even D particles, while FCC reactors use mostly Group AC, A particles [13].

In a circulating fluidized bed (CFB) boiler, hot solids circulate around a loop carrying heat from burning fuel (coal or biomass) to heat-absorbing surfaces, and finally leave the furnace with the flue gas. Here, solids move through a number of hydrodynamic regimes while passing through different sections of the boiler. In a typical CFB boiler or gasifier the solids are in the turbulent fluidized bed regime in the lower furnace, fast fluidized bed regime in the upper furnace and swirling flow in the cyclone are the common one.

Since 1970s, circulating fluidized beds (CFBs) have been widely applied in the chemical, petrochemical, metallurgical, environmental and energy industries. In order to continuously improve the design efficiency and performance of the existing industrial processes and facilitate

new applications, intensive studies have been conducted to obtain more detailed and reliable fundamental knowledge about CFB. Although the hydrodynamics of CFBs have been investigated to some extent both in industry and in academia, much remains to be known about this special multi-phase fluidization system. The hydrodynamic model can predict mean voidage, annulus and core voidages, core radius, upward solids flow in the core, downward solids flow in the annulus and external circulation solid flux, all as functions of height [20].

There is huge amount of papers on hydrodynamics of CFBs which are very useful for modeling CFBBGs. Concerning the modeling of fluidized bed gasifiers, the field of coal is well ahead of that of biomass. There are a lot of works on modeling CFB coal combustors and gasifiers which contain very valuable information and help to model CFBBGs. They will be used in different parts of the modeling of CFBBGs presented here. Nevertheless, it is well known and accepted that thermochemical processing of biomass has some important differences with respect to the processing of coal. Two of them are important for the CFBBG modeling: (1) biomass is much more reactive than coals, it pyrolyzes very quickly and its ash content is usually very low. For these and other reasons, another solid, sometimes called fluidizing, has to be used in the gasifier. It is usually silica sand. Besides, an additive (dolomite or limestone) is also used in the gasifier for tar cracking and alkali capture sulfur dioxide. The particle size of these two solids (silica sand and additive) is an important variable in the process. (2) Biomass gasification below $1000^{O}C$ always produces important amounts of tar whose content in the flue gas has to be estimated with a good model for it to be it useful. Literature on biomass is therefore more important for CFBBG modeling than coal, but it is less abundant and the existing approaches are not yet as rigorous and developed as those for coal [21].

Literature on modeling CFB for biomass gasification is even scarcer as compare with papers on modeling CFB for fluid catalytic cracking (FCC). The absence of details in the literature on CFBBG modeling is not surprising because, besides the very few existing commercial CFBBGs, it was mainly written for marketing purposes. Models claimed to exist can neither be checked nor used by readers because most of the key information is missing. Most of the manufacturers and users of CFB biomass gasifiers at commercial and pilot scales claim to operate a good own model but not much more is said about it. This is one of the reasons why this work is devoted to

develop a hydrodynamic model and simulate as good as possible for atmospheric Circulating fluidized bed biomass gasifier (CFBBGs).

A significance amount of experimental study on the hydrodynamic and other characteristics behavior of two phase fluidization has been carried out. Most of the studies related to two phase fluidization have been directing toward the understanding of the complex hydrodynamics, and its influence the phase hold up and transport property. To create a better understanding on hydrodynamics of CFB some review work is being discussed below under core-annulus structure and radial and axial voidage distribution:

2.6.2.1 Core-Annulus Structure of CFB

The macroscopic hydrodynamic behavior of a CFB was firstly studied by Yerushalmi and Cankurt et al. in 1978 about the effects solid mass flux and gas velocity on pressure drop, slip velocity and bed expansion in CFB. Diameter column operating in different fluidization regimes, has presented of a fluidization map, which depicts the solid volumetric concentration (ε) at the bottom of the bed versus the slip velocity (U_{slip}). A unique relation between the slip velocity and the solids volume concentration over the bubbling and the turbulent regimes was obtained. In the fast fluidization regime, however, this relation also depends on the solid rates (G_S) [22].

$$U_{slip} = \frac{U}{\varepsilon} - \frac{G_S}{(1-\varepsilon)\rho_p} \tag{2.2}$$

Gasdos and Bierl [23] found a lean core surrounded by a dense annulus when they investigated the radial variation of particle concentration in a CFB using the local solids flux probe and X-rays. After a few years, the basic core-annular distribution of particle concentration model was confirmed by other different researcher. These results clearly indicated the existence of a core-annulus flow structure with very significant radial concentration gradients. The boundary between core and annulus was not clearly defined. A low particle concentration in the center and high concentration in the wall region was confirmed by each of the above mentioned researcher.

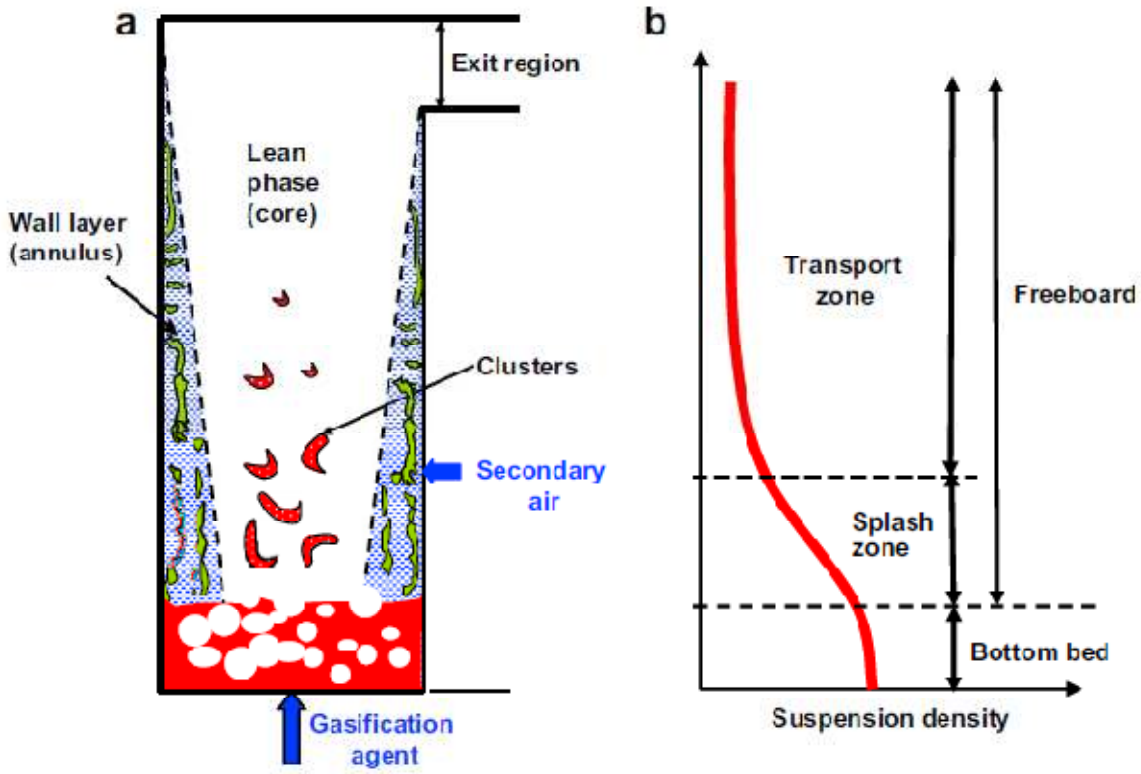

Figure 6 : Core-annulus structure in CFB (a) and Simplified solid density profile at different zone (b)

Brereton et al. [24] developed a simple hydrodynamic model for circulating fluidized beds. The model predicts the two phase flow characteristics. The model postulates a core annulus type of flow structure, the core being a dilute suspension flowing upward and the annulus, a denser film of particles moving close to the riser wall. This model can predict the radius of core region, the voidage in the core and gas and solid velocities as functions of reactor length.

Shuyan et al. [25] from experimental results suggested that riser flow is characterized by continuous formation and disintegration of clusters. In the dilute region, the number and size of clusters increase towards the wall and were found maximum near corners. Core clusters moved upwards or downwards, however, wall clusters generally moved downwards. The number of clusters decreased with increasing elevation, especially near the center of the cross-section.

A typical CFB riser may be split into two vertical regions: core and annulus, as shown in Figure 6. The velocity of the gas in the annulus is low, while that in the core is well above the superficial velocity through the riser. Solids move upwards through the core in a dilute

suspension, with the occasional presence of clusters. When the clusters drift sideways due to hydrodynamic interactions they are exposed to gas velocities that are too low or even negative to carry the cluster upwards. As a result the clusters start to fall in the low-velocity annular region on the wall. The up-and-down movement of solids in the core and annulus sets up an internal circulation in the bed, in addition to the external circulation, where solids captured by the cyclone are returned to the bed. Different experimental measurement has shown the internal circulation rate to be many times the external circulation rate. The temperature uniformity of the bed is a direct result of this internal solid circulation. The core-annular structure leads to two main problems: (1) inefficient gas-solids contact, and (2) back mixing due to non-uniform radial distributions.

2.6.2.2 Radial and Axial Distribution of Voidage

Radial Voidage Profile

The distribution of solid particles in circulating fluidized bed risers has been widely studied because of its importance in design. Radially, the upper region consists of a dilute core surrounded by a relatively dense annulus, with solids downflow along the wall. The few available studies on the bottom dense region also show that the solids concentration increases significantly towards the wall.

A number of correlations have been proposed to estimate local voidage profiles in CFB risers. Most experimental work shows that local solids concentration profiles were self-similar, i.e., functions of the cross-sectional average voidage only. Other different researchers also suggest that the local voidage ε is a function of only the cross-sectional average voidage ε_m, and the nondimensional radial distance (r/R), from the axis of the bed. This was supported by Tung et al. and Zhang et al. for several types of particles at different superficial gas velocities and solids circulation rates in risers of various diameters. Zhang et al. proposed [13]:

$$\varepsilon = \varepsilon_m^{0.191+\varphi^{2.5}+3\varphi^{11}} \tag{2.3}$$

$$1-\varepsilon = (1-\varepsilon_m)\left[0.191+\left(\frac{r}{R}\right)^{2.5}+\left(\frac{r}{R}\right)^{11}\right] \tag{2.4}$$

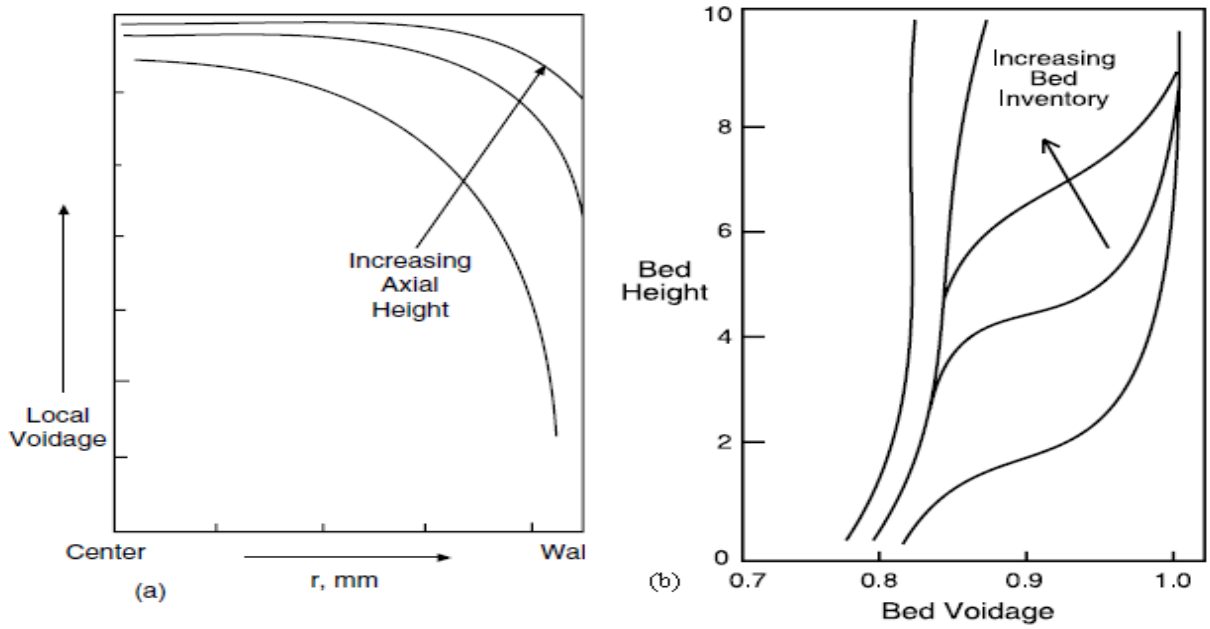

Figure 7 : Radial vodage profile and Axial voidage profile [13]

Axial Voidage Profile

Figure 7 (b) shows that the higher solids concentration at the wall and a lower concentration in the center of the riser were found. Axial voidage along the length of the riser is obtained from the experimental pressure drop data using the following relation:

$$\frac{\Delta P}{H} = g(\rho_s - \rho_g)(1 - \varepsilon) \tag{2.5}$$

Kato, et al. [26] measured particle hold up and axial pressure drop in a fast fluidized bed. There is a dense region of particles in the lower part of the bed and dilute region of particles in the upper part of the bed. The height of the inflection point between the dense region of particles and the dilute region of particles was determined from an axial pressure drop profile. Its location is effected by superficial gas velocity, the circulation rate of particles and the particle Reynolds number. An empirical equation for the location of the inflection point was reported. Particle hold up in a fast fluidized bed is affected by superficial gas velocity, circulation rate of solids, particle Reynolds number, tube diameter, location of the inflection point and axial distance from the distributor.

2.7 Review on CFD Modeling Approach for Biomass CFB Gasifier

Circulating fluidized bed technology has been successfully used in coal and petroleum industry for more than two decades but it still lacks practical wide-scale application in the biomass gasification. The application of biomass modeling for fluidized bed gasification is not as common as in case of coal gasification. Although a large number of models for fluidized bed coal gasifier is available, these models may not be directly applicable to biomass gasification. The thermo-chemical processing of biomass has some differences that should be taken into consideration while applying models developed for coal to biomass. Few of the differences are as below [21]:

- Biomass is more reactive than coal, and it pyrolyzes much quickly and its ash content is usually very low.
- Gasification of biomass below 1000°C always produces a measurable amount of tar.
- Coal is predominantly aromatic material whereas the aromatic component of biomass is relatively less.
- Biomass is relatively rich in oxygen, which decomposes during pyrolysis process to produce oxygenated gases like CO, CO_2, and H_2O.

2.7.1 CFD Modeling

Computational fluid dynamics (CFD) is a branch of fluid mechanics that involves numerical methods and algorithms in the analysis of systems that involve fluid flow, heat transfer, solid and fluid interaction, chemical reaction and other related phenomena. CFD serves as an aiding tool in many general engineering aspects such as component design, product development and refinement, system analyses, optimization and verification. Furthermore, the applications of CFD in many industries have been instigated since about two decades or more. For instance, chemical process industries such as in thermo-chemical conversion process, significant effort has been made on the development of numerical models of thermo-chemical reactors such as on gasifiers, pyrolyzers, boilers, combustors, and incinerators [6].

Though CFD has passed through many development stages to the level of providing qualitative information in many cases, there are still significant challenges for effective application of CFD

in areas of biomass thermo-chemical conversion. This is mainly due to complexity of biomass feedstock and the thermo-chemical process.

Beside some of the difficulties mentioned above, there have always been continuous interests in the use of CFD modelling for thermo-chemical conversion specifically in biomass gasification and combustion. For instance, practical experience and scale up through existing plant is limited to a level where one can't easily and completely predict the performance for a certin CFBBG plant. In this context, performance of a gasifier is governed by how effectively gases are transported from the gasifier entrance to the surface of the fuel particles, their reaction rate on the surface of particles and transport of the product gas to the exit of the gasifier. Reaction kinetics decides the reaction rate for a given temperature and gas concentration at the reaction site on the particle, but the transport of gases from and to the reaction site is determined by the hydrodynamics of the gasifier, hydrodynamic predictions through numerical simulation has recently got new impetus and has taken the prime position for research and development involving sphere of interests in areas of biomass combustion and gasification. It is strongly believed that biomass is still one of the untapped potential for manufacturing of premium thermal power, electricity and synthesis gas via the process of thermo-chemical conversion. To make hydrodynamics prediction and improving the operating efficiency of gasifier and combustor, there are needs for CFD predictions of solid distribution, effects of fluidizing gas velocity, particle size, solid circulation rate and geometry of CFB pertinent to the hydrodynamics of CFB.

Even though a large number of experimental studies have been directed toward the quantification of flow structure and flow regime identification for different process parameters and physical properties, the complex hydrodynamics of these are not well understood due to the interaction of two phases simultaneously. It has been a very tedious task to analyze the hydrodynamics property in experimental way of two phase fluidized bed gasifier. So another advanced modeling approach based on CFD techniques have been applied for investigating of two phase for accurate design and scale up. Some of the various investigations done by researchers on gas-solid fluidization in CFB using CFD are mentioned below:

Corella et al. [21] have worked on 1-D, model for an atmospheric circulating fluidized bed biomass gasifier (CFBBG) under stationary stat. The model is based on the kinetic equations for

the reaction network solved together with mass and heat balances and with several hydrodynamic considerations. Hydrodynamics in the model were checked with a survey carried out worldwide among the existing pilot and commercial CFBBGs. Axial profiles of concentration of different species and temperature have been calculated to optimize both design and operation of CFBBGs.

Gungor [27] tried to explain about the numerical simulation of CFBs for prediction of its flow behavior. Specifically has been given to predicting the axial pressure profile which is major difficulties in modeling a CFB. A model using a Particle Based Approach (PBA) is developed to accurately predict the axial pressure profile in CFBs. axial and radial distribution of voidage and velocity of the gas and solid phases, and for the solids volume fraction and particle size distribution of the solid phase have been simulated.

Idris et al. [28] have studied 3-D, using a commercial code ANSYS CFX 11.0 to describe the hydrodynamic behavior of gas-solid flow in a FCC/CFB riser. The model was based on Eulerian-Eulerian two-fluid modelling approach, incorporating the kinetic theory constitutive model for a dilute assemblies of the particulate solid, a Gidaspow's drag model for gas-particles interaction. Axial and radial distribution of voidage, velocity and pressure drop for gas and solid phase, and solids volume fraction and particle size distribution for solid phase have been simulated.

Almuttahar et al. [29] have used 2-D, Eulerian–Eulerian model incorporating the kinetic theory of granular flow (KTGF) was developed to describe the hydrodynamics of gas– solid flow in the riser section of a high density circulating fluidized bed. The model was capable of predicting the main features of the complex gas–solids flow, including the cluster formation of the solid phase along the walls, for different operating conditions. The model also predicted the coexistence of up-flow in the lower regions and downward flow in the upper regions at the wall of the riser for high gas velocity and solid mass flux.

Yanping et al. [30] have worked in 2-D, Eularian multifluid approach for gas-solid in CFB. Kinetic theory granular flow (KTGF) for describing the particle phase and K-ε based turbulent model for gas phase have been used. The developed model was validated by comparing the simulation results with the experimental data, and the model was used for the examination of the effects of the feeding configuration on the gas/solid two-phase flow.

Zhou et al. [31] have studied in 2-D CFD approach simulate the air-coal two phase flow and combustion characteristics in a 50 kW circulating fluidized bed (CFB) combustor. Eulerian–Granular multiphase model with a drag coefficient correction based on the extended energy-minimization multi-scale (EMMS) model was used to study the gas–solid hydrodynamics. The model consists of hydrodynamic model, heat transfer model and mass transfer model including homogeneous and heterogeneous reactions. The obtained result have shown that reasonable distributions of temperature, solid volume fraction, solid velocity, gas velocity and gas compositions in the combustor and the results are in good agreement with the experimental data.

2.7.2 Working on CFD

CFD codes are structured around the numerical algorithms that can be tackle fluid problems. In order to provide easy access to their solving power all commercial CFD packages include sophisticated user interfaces input problem parameters and to examine the results. Hence all codes contain three main elements:

1. Pre-processing.
2. Solver
3. Post-processing.

2.7.2.1 Pre-processing

This is the first step in building and analyzing a flow model. Preprocessor consist of input of a flow problem by means of an operator friendly interface and subsequent transformation of this input into form of suitable for the use by the solver. The user activities at the Preprocessing stage involve:

- Definition of the geometry of the region: The computational domain.
- Grid generation the subdivision of the domain into a number of smaller, non-Overlapping sub domains (or control volumes or elements Selection of physical or chemical phenomena that need to be modeled).
- Definition of fluid properties
- Specification of appropriate boundary conditions at cells, which coincide with or touch the boundary.

The solution of a flow problem (velocity, pressure etc.) is defined at nodes inside each cell. The accuracy of CFD solutions is governed by number of cells in the grid. In general, the larger numbers of cells better the solution accuracy. Both the accuracy of the solution & its cost in terms of necessary computer hardware & calculation time are dependent on the fineness of the grid. Efforts are underway to develop CFD codes with a (self) adaptive meshing capability. Ultimately such programs will automatically refine the grid in areas of rapid variation.

Geometry and mesh generating software GAMBIT is used to draw complex geometry. GAMBIT is a state-of-the-art preprocessor for engineering analysis. With advanced geometry and meshing tools in a powerful, flexible, tightly-integrated, and easy-to use interface, it can dramatically reduce preprocessing times for many applications. Complex models can be built directly within GAMBIT's solid geometry modeler, or imported from any major Computer Aided Design (CAD) system. Using a virtual geometry overlay and advanced cleanup tools, imported geometries are quickly converted into suitable flow domains. A comprehensive set of highly-automated and size function driven meshing tools ensures that the best mesh can be generated, whether structured, unstructured, or hybrid.

2.7.2.2 Solver

The CFD solver does the flow calculations and produces the results. FLUENT, CFX and POLYFLOW are some of the types of solvers. FLUENT is used in most industries. POLYFLOW is also used in a wide range of fields, with emphasis on the materials processing industries. FLUENT and CFX two solvers have a number of things in common, but they also have some significant differences. Both are control-volume based for high accuracy and rely heavily on a pressure-based solution technique for broad applicability. They differ mainly in the way they integrate the fluid flow equations and in their equation solution strategies. The CFX solver uses finite elements (cell vertex numerics), similar to those used in mechanical analysis, to discretize the domain. In contrast, the FLUENT solver uses finite volumes (cell centered numerics). CFX software focuses on one approach to solve the governing equations of motion (coupled algebraic multigrid), while the FLUENT product offers several solution approaches (density, segregated and coupled-pressure-based methods)

The FLUENT CFD code has extensive interactivity, so can make changes to the analysis at any time during the process. This saves time and enables to refine designs more efficiently. Graphical user interface (GUI) is intuitive, which helps to shorten the learning curve and make the modeling process faster. In addition, FLUENT's adaptive and dynamic mesh capability is unique and works with a wide range of physical models. This capability makes it possible and simple to model complex moving objects in relation to flow. This solver provides the broadest range of rigorous physical models that have been validated against industrial scale applications, so we can accurately simulate real-world conditions, including multiphase flows, reacting flows, rotating equipment, moving and deforming objects, turbulence, radiation, acoustics and dynamic meshing. The FLUENT solver has repeatedly proven to be fast and reliable for a wide range of CFD applications. The speed to solution is faster because suite of software enables us to stay within one interface from geometry building through the solution process, to post-processing and final output.

In the numerical solution technique, there are three different streams that form the basis of the solver. There are finite differences, finite element and finite volume methods. The differences between them are the way in which the flow variables are approximated and the discretization processes are done.

Finite volume method (FVM) it was originally developed as a special finite difference formulation. The main computational commercial CFD codes packages using the FVM approaches. Basically, the numerical algorithm in these CFD commercial packages involved the formal integration of the governing equation over all the finite control volume, the discretization process involves the substitution of variety FDM types to approximate the integration equation of the flow problem and the solution is obtained by iterative method.

Discretization in the solver involves the approaches to solve the numerical integration of the flow problem. Usually, two different approaches have been used and once at a time.

1. Explicit approach: Usually, this is the most approach that makes sense. It is relatively simple to set up and program. The limitation is that for a given Δt and Δx , must be less than some limit imposed by stability constraints. In some cases, Δt must be very small to maintain the stability and consequently long running time required for the calculation over a given time interval, t.

2. Implicit approach: For this approach, the stability can be maintained over a large value of Δt and fewer time steps required making calculation. Thus resulting less computer time. Adversely, it is complicated to set up and program. The computer time per time step is much larger than the explicit approach due to the matrix manipulation which is required for each time step. This approach is very accurate to follow the exact transients i.e. the time variations of the independent variables.

Solver is very important in solving the flow problem. FLUENT 6.3 have many solvers and segregated (implicit) has been used to solve the gasification process in gasifier. This is because it can solve both compressible and incompressible flow problems. Besides that it can be used to solve the unsteady flows.

2.7.2.3 Post-processing

This is the final step in CFD analysis, and it involves the organization and interpretation of the predicted flow data and the production of CFD images and animations. Most flow properties such as pressure, temperature, species concentration and density for the combustion reaction can be displayed and analyze after simulation. FLUENT is a computational fluid dynamics (CFD) software package to simulate fluid flow problems. It uses the finite-volume method to solve the governing equations for a fluid. It provides the capability to use different physical models such as incompressible or compressible, inviscid or viscous, laminar or turbulent, etc.

Problem solving

In the computational fluid dynamic, using the FLUENT codes provide to solver the problem numerically. The fundamental involves determining the convergence, whether the solution is consistent and stable for all range of flow variables.

- Convergence – is a property of a numerical method to produce a solution that approaches the exact solution of which the grid spacing, control volume size is reduced to a specific value or to zero value
- Consistent – to produce the system of algebraic equations which can be equivalent to the original governing equation

- Stability – associates with the damping of errors as a numerical method proceeds. If a technique chosen is not stable, even the round-off error in the initial data can leads to wild oscillations or divergence.

3. CFD MODELING OF TWO PHASE CFB BIOMASS GASIFIER

3.1 Introduction

Gas-solids fluidized beds are widely used in many operations in chemical, metallurgical, energy generation and especially petrochemical industries. Major applications are fluid catalytic cracking (FCC) risers and CFB combustor or gasifier systems. The efficiency of such systems relies primarily on their hydrodynamic behavior. Although fluidized beds are successfully and widely used in commercial industrial operations, much remains to be done due to the complexity of the gas-solid flow. Therefore, the prediction of CFB hydrodynamics has been an active area of research for many years.

Thanks to the increase in the computational speed and improved numerical algorithms, CFD has become a promising tool for simulating CFB hydrodynamics. The availability of affordable high performance computing hardware and the introduction of user-friendly interfaces have led to the development of CFD packages available both for commercial and research purposes. The various general-purpose CFD packages in use are CFX, FLUENT and FLOW3D etc. Most of these packages are based on the finite volume method and are used to solve fluid flow and heat and mass transfer problems. Further understanding of the hydrodynamic phenomena, including turbulence characteristics is necessary so that a better closure relationship for turbulence can be developed for CFD modeling. So it is significant to research the gas-solid fluidized bed for designing, operating and testing of reactors [2].

3.2 Approaches to Gas-Solid Fluidization Modeling

According to the way the particle phase is treated, CFD models of gas-solid systems can be classified into two approaches: the discrete element method (DEM) based on the Eulerian-Lagragian and the continuous method based on the Eulerian-Eulerian approach or two-fluid model (TFM) models. Both methods consider the gas phase as a continuous phase. The fundamental difference between these two models lies in the way the particles are treated.

The Lagrangian-Eulerian models describe the solids phase at the particle level (point mass representation), In this representation the particle is much smaller than the grid spacing on which the gas velocity is calculated and does not influence the gas domain or its discretization. The

point masses techniques are used to model large numbers of particles without regard to the specifics of the gas-solid fluid mechanics (e.g. boundary layer effects). In the point mass representation the trajectory of the particles through the gas phase is determined by integration of the particle equation of motion (PEM) which is based on the forces that are assumed to act on the particle (i.e. the Newton's laws are applied to describe the motion of the particles).

The Eulerian-Eulerian approach treats even the particles as a continuum, and the two phases form an interpenetrating continuum. Owing to the continuum representation of the particle phases, Eulerian models require additional closure laws to describe the rheology of particles phase, and there is an absence of consensus concerning the stress terms in the particulate momentum equation. The TFM model is generally less computationally demanding than the DEM and has thus been extensively used by the CFD code packages.

The Eulerian approaches have several advantages over the Lagrangian approach. The primary one being less computational expense for about the same type of problem. And also its grid based, memory and the computational requirements do not change radically with the introduction of additional particles. However, a number of problems exist with two-fluid models including: the type and nature of the boundary conditions for wall-bound flows, where the tangential particle velocity will not be zero as it is for the fluid phase.

3.2.1 Advanced CFD Modeling Approach for CFB

The hydrodynamics of CFBs has been investigated by using different modeling approaches. In the Eulerian approach to model gas/solid fluidized beds closures are required for the internal momentum transfer in the particulate phase. Because the concept of particles has disappeared in the TFM, one can only include indirectly the effect of particle-particle interactions, via an effective solid's pressure P_s and an effective solid's shear μ_s and bulk viscosity λs, for which appropriate closures should be used. In the early hydrodynamic models a fundamental problem encountered in modeling the hydrodynamics of a gas-solid fluidized bed by the two-fluid method is how to include the stress of the particle phase in the particulate momentum equation. Therefore, numerical models can be classified into two kinds according to how the effective viscosity of the particle is determined: a constant viscosity of the solid phase (CVM) and kinetic theory of granular flow (KTGF) [32].

In the past 20 years, researchers have used the TFM to study a wide number of different systems relevant to chemical engineering science, and a full survey of all past and present developments is beyond the scope of this thesis work. Only a limited list of some selected applications and developments are discussed below. Tsuo and Gidaspow were among the first to predict annular flow regime using multiphase flow equations. The viscosity is defined as an empirical constant i.e. CVM, and also the dependence of the solid's phase pressure on the solid's volume fraction are determined from experiments. The advantage of this model is its simplicity; the drawback is that it does not take into account the effect of non-uniform characteristics on the particle phase viscosity.

In recent years, one step forward in the understanding of gas-solid systems has been taken by the development of kinetic theory for two-phase flows based on the theory for non-uniform dense gases. The phases interact through additional source terms in the conservation equations. The kinetic theory of granular flow is based on the analogy between the thermal motion of the gas molecules in the kinetic theory of gases and the random motion of solid particles described by Chapman and Cowling 1970. In this theory, the inter particle interactions are taken into account by adding the contribution of collisions between particles, which are the main mechanism of transport due to particulate phase properties. In 1994 Gidaspow, has re-viewed this theory and extended his previous work into formulation to both dilute and dense cases by considering a velocity distribution. Such a formulation, besides the CFBs, has been applied to the analysis of liquid-solid flows and to full-scale CFB loops. Currently the kinetic theory of granular flow has become one of the most useful tools to model fluid-solid flows in dilute to dense bed regimes [33].

Fluid dynamics of circulating fluidized beds (CFB) can be computed with a variety of methods. Typically the simulations are conducted with Eulerian-Eulerian models based on the kinetic theory of granular flow. These models require a fine computational mesh and, in addition, that the simulations are run as transient, which for large industrial processes leads to unfeasibly long computations. To improve the modeling capabilities it is necessary to develop faster simulation methods. The most attractive approach seems to be time-averaged modeling, easing steady state simulation of fluidization. An order of magnitude slower but still feasible alternative would be using a coarse mesh and special mesh dependent closure equations in a transient simulation.

The present studies aims to model and simulate a two-dimensional two-phase flow model, based on the kinetic theory of granular flow (KTGF), using time-averaged modeling to come up to steady state fluidization and to predict the behavior of a gas-solid fluidized bed, using a computational fluid dynamics technique.

3.3 Computational Flow Model

Computational fluid dynamics could have an important role in the modeling of fluidized bed gasifier. A computational fluid dynamics (CFD) based code involves solution of conservation of mass, momentum and turbulent over a defined domain or region. These equations could be written for each phases, where flux of above phases moving in and out of the element is considered with suitable boundary conditions.

3.3.1 Assumptions of the Model

In the present work, basic assumptions considered in the model are isothermal non-reactive, unsteady state gas-solid CFB gasifier, Eulerian multi-fluid model is adopted where both gas and solid phases are treated as continua, inter-penetrating and interacting with each other everywhere in the computational domain. The single pressure field is assumed to be shared for both phases, in proportion to their volume fraction. Gas phase has been modeled with k-ε turbulent model and particle phase have been modeled with the kinetic theory of granular flow, the motion of each phase is governed by respective mass and momentum conservation equations are described below, where the energy balance is not shown as the system is isothermal in the cold-mode operation. Particles are assumed to be perfectly spherical ($\phi_s = 1$) and mono-sized. Therefore, the solid phase is supposed to have a uniform particle size distribution. For CFD simulation, system temperature and pressure are set to 300K and 1 atm.

3.3.2 Conservation Equation for Gas and Solid Phase

Continuity equation:

The motion of each phase is governed by respective mass and momentum conservation equations and locally averaged transport equations for two-fluid models is given as follow:

$$\frac{\partial\left(\rho_g \varepsilon_g\right)}{\partial t} + \nabla.\left(\rho_g v_g \varepsilon_g\right) = \sum \dot{m}_{sg} \tag{3.1}$$

$$\frac{\partial(\rho_s \varepsilon_s)}{\partial t} + \nabla.(\rho_s v_s \varepsilon_s) = \sum \dot{m}_{sg} \tag{3.2}$$

Where v_s is velocity of solid, v_g is velocity of gas and $\dot{m}_{sg}$ is of characterizes of mass transfer from solid phase to gas phase.

From mass conservation equation

$\dot{m}_{sg} = -\dot{m}_{sg}$ and $\dot{m}_{ss} = \dot{m}_{gg} = 0$

Usually, the source term $\sum \dot{m}_{ij}$ on the right side of the Eq. 3.1 and Eq. 3.2 are zero.

Momentum equation:

$$\frac{\partial\left(\rho_g \varepsilon_g v_g\right)}{\partial t} + \nabla.\left(\rho_g v_g v_g \varepsilon_g\right) = -\nabla P - K_{sg} + \nabla.\left(\tau_g \varepsilon_g\right) + \rho_g\, g \tag{3.3}$$

τ_g - is the gas phase stress viscosity and is related to the gradients of velocity components by

$$\tau_g = \mu_g\left[\nabla v_g + \left(\nabla v_g\right)^T\right] - \frac{2}{3}\mu_g\left(\nabla \cdot v_g\right) I \tag{3.4}$$

$$\frac{\partial(\rho_s \varepsilon_s v_s)}{\partial t} + \nabla \cdot (\rho_s v_s v_s \varepsilon_s) = -\nabla P - K_{sg} + \nabla \cdot (\tau_s \varepsilon_s) + \rho_s\, g \tag{3.5}$$

Where: $\tau_s = (-P_s + \xi_S \nabla \cdot v_s) I + \mu_S[\nabla v_S + (\nabla v_s)^T] - \frac{2}{3}(\nabla \cdot v_s) I$ (3.6)

In the expression of τ_s, μ_s and ξ_s are particle phase laminar viscosity and bulk viscosity respectively.

Volume Fraction

The description of multiphase flow as interpenetrating continua incorporates the concept of phase volume fractionsε_i. Volume fractions represent the space occupied by each phase, and the laws of conservation of mass and momentum are satisfied by each phase individually.

Where: $\varepsilon_s + \varepsilon_g = 1$ (3.7)

3.3.3 Interphase Momentum Exchange

The interphase momentum exchange terms K_{gs} are composed of a linear combination of different interaction forces between different phases such as the drag force (K_D), the lift force (K_L) and the added mass force (gravity) (K_{VM}), etc., and is generally represented as

$$K_{gs} = K_D + K_L + K_{VM} \tag{3.8}$$

Since, the momentum exchange term is proportional to the velocity differential between phases i.e. slip velocity ($v_g - v_s$) and a drag function i.e momentum exchange coefficient (β_{gs}) which is obtained empirically for a specific flow regime as follows.

$$K_i = \beta_{gs}(v_s - v_g) \tag{3.9}$$

In fluidized systems, gravity and drag forces are expected to be the dominant forces for the majority of flows, except for very dense flow where the frictional stresses became more important. For relatively small particles with density much larger than the continuous phase density, the interphase drag force dominates the other forces such as lift and virtual mass. Therefore, the gas–solid momentum exchange coefficient, β_{gs}, is assumed to have only the drag contribution. Since the gas–solid flow in the CFB riser possesses a non-uniform solid volume fraction distribution, a proper model to specify the gas–solid drag coefficient for wide range (i.e., dilute to dense) of solid volume fraction should be used. There are several drag models applicable to the gas–solid flow in CFB risers in the literature. In this paper Syamlal and O'Brien drag model has been considered to select the best fitted model.

The Syamlal and O'Brien drag model with a modification for the actual particle minimum fluidization condition, which is reported to provide a good description of the hydrodynamics of fluidized beds with similar particles, was used in this study to model the gas–solid interphase exchange coefficient as follows:

$$K_{sg} = \frac{3\varepsilon_s \varepsilon_g \rho_g}{4 v_{r,s}^2 d_s} C_D \left(\frac{Re_s}{v_{r,s}}\right)(v_s - v_g) \tag{3.10}$$

$$C_D = \left(0.63 + \frac{4.8}{\sqrt{Re_s / v_{r,s}}}\right)^2 \tag{3.11}$$

$$v_{r,s} = 0.5\left(A - 0.06Re_s + \sqrt{(0.06Re_s)^2 + 0.12\,Re_s\,(2B - A)}\right) \quad (3.12)$$

The coefficient A and B are as follows

$$A = \varepsilon_g^{4.14} \qquad B = 0.8\varepsilon_g^{1.28} \qquad \varepsilon_S \leq 0.85 \quad (3.13)$$

$$A = \varepsilon_g^{4.14} \qquad B = \varepsilon_g^{2.65} \qquad \varepsilon_S > 0.85 \quad (3.14)$$

Gidaspow drag model, it is combination of Wen and Yu model and the Ergun equation describe as follow is also used in some of simulation:

$$K_{sg} = \beta\left(v_g - v_s\right) \quad (3.15)$$

$$\beta = 150\frac{\varepsilon_s^2\mu_g}{\varepsilon_g(d_s\emptyset_s)^2} + 1.75\frac{\varepsilon_s\rho_s|v_g - v_s|}{d_s\emptyset_s} \quad ; \quad \varepsilon_s < 0.8 \quad (3.16)$$

$$\beta = \frac{3}{4}C_d\frac{\varepsilon_s\rho_g|v_g - v_s|}{d_s\emptyset_s}\varepsilon_g^{-2.65} \quad ; \quad \varepsilon_s \geq 0.8 \quad (3.17)$$

C_d - is the drag coefficient between the gas and a single particle, defined as

$$C_d = \frac{24}{Re_s}(1 + 0.15Re_s^{0.687}) \quad ; Re_s \leq 1000 \quad (3.18)$$

$$C_d = 0.44 \quad ; \; Re_s > 1000 \quad (3.19)$$

with the particle Reynolds number Re_S given by:

$$Re_s = \frac{|v_g - v_s|\varepsilon_s\rho_g d_s\emptyset_s}{\mu_g} \quad (3.20)$$

3.3.4 Turbulence Modeling

In order to account for the effects of turbulence fluctuation of velocity the number of terms to be modeled in the momentum equations in multiphase is large and this makes the modeling of turbulence in multiphase simulation extremely complex. The turbulence model used for the current simulations is based on dispersed turbulence model.

The k-ε model is one of the most common turbulence models. It includes two transport equations to represent the turbulent properties of the flow. This allows a two equation model to account for history effects like convection and diffusion of turbulent energy. The first transported variable

"k" is turbulent kinetic energy. The second transported variable "ε" in this case is the turbulent dissipation. It is the variable that determines the scale of the turbulence, whereas the first variable, k, determines the energy in the turbulence. The turbulence kinetic energy and its rate of dissipation are obtained from the following transport equations

Gas phase turbulent kinetic energy equation (k)

The above equations are closed by the modified $k-\varepsilon$ model similar to the single-phase flow $k-\varepsilon$ model supplemented with an extra term. The turbulence kinetic energy, k_g, is modeled by the following transport equation:

$$\frac{\partial(\varepsilon_g \rho_g k_g)}{\partial t} + \nabla \cdot (\varepsilon_g \rho_g v_g k_g) = \nabla \cdot \left(\varepsilon_g \frac{\mu_g}{\sigma_k}\right) \nabla k_g + G_{kg} - \varepsilon_g \rho_g + S_{kg} \qquad (3.21)$$

Where: G_{kg} is represents the generation of turbulence kinetic energy due to the mean velocity gradients. This production term given by

$$G_{kg} = \mu_{gT} \left[\nabla v_g + (\nabla v_g)^T\right] : \nabla v_g \qquad (3.22)$$

The last term on the right-hand side of Eq. (3.21) S_{kg} is user-defined source term due to interaction between the gas phase and particle phase i.e. produced gas from biomass gasification. This term is not considered in for this model since cold non-reactive model is considered.

Gas phase turbulent kinetic energy dissipation rate equation (ϵ)

The differential equation for the dissipation of turbulent kinetic energy ϵ_g is given by:

$$\frac{\partial(\varepsilon_g \rho_g \epsilon)}{\partial t} + \nabla \cdot (\varepsilon_g \rho_g v_g \epsilon) = \nabla \cdot \left(\varepsilon_g \left(\frac{\mu_g}{\sigma_\varepsilon}\right) \nabla \epsilon\right) + \frac{\epsilon}{k_g} \left[C_1 (G_k + G_p) - C_2 \varepsilon_g \rho_g \, \epsilon\right] \qquad (3.23)$$

Some empirical constants associated with k-ε turbulence model are given in Table 6.

Table 5 : Empirical constants for gas phase turbulence model

C_1	C_2	C_μ	σ_k	σ_ϵ
1.44	1.92	0.09	1.0	1.3

Closure law for turbulence

The gas phase effective viscosity μ_g can be expressed as linear combination of both laminar and turbulent viscosity.

$$\mu_g = \mu_{gl} + \mu_{gT} \tag{3.24}$$

Where: gas phase turbulent viscosity is modeled as $\mu_{g,T} = \frac{C_\mu \varepsilon_g \rho_g k^2}{\varepsilon}$ (3.25)

and $\mu_{g,l}$ is the gas phase laminar viscosity. C_μ is the constant, which is set as 0.09.

3.3.5 Particle-Particle Interaction and Kinetic Theory for Granular Flow

Appropriate constitutive equations have to be specified to describe the physical rheological properties of each phase and to close the conservation equations. Bagnold is credited for starting the kinetic theory approach of granular flow. In this model, solids viscosity and pressure are derived by considering the random fluctuation of particle velocity and its variations due to particle-particle collisions and the actual flow field. Such a random kinetic energy, or granular temperature, can be predicted by solving, the mass and momentum equations, besides, the fluctuating kinetic energy equation for the particles. The solids viscosity and pressure can then be computed as a function of granular temperature at any time and position. Particles are considered smooth, spherical, inelastic, and undergoing binary collisions.

Particle phase Granular-temperature (Θ) equation

There are two possible mechanisms inducing the fluctuations of particle velocity: inter-particle collisions and particle interactions with turbulent fluctuations in the gas phase. Inter-particle collisions play a crucial role in sufficiently dense suspensions. Equivalent to the thermodynamic temperature for gases, the granular temperature can be introduced as a measure for the energy of the fluctuating velocity of the particles. The granular temperature, Θ, according to Lun et al's theory, the kinetic energy of fluctuations is accounted in the granular kinetic theory. The granular temperature of solid phase 's' is defined as one-third the mean square velocity of the random motion of particles, by defining a granular temperature defined as [34]:

$$\frac{3}{2}\Theta = \frac{1}{2}\langle v^2 \rangle \tag{3.26}$$

Where: $\boldsymbol{v}$ - is the particle fluctuating velocity.

The equation of conservation of solids fluctuating kinetic energy can be found

$$\frac{3}{2}\left[\frac{\partial(\varepsilon_s\rho_s\Theta)}{\partial t}+\nabla\cdot(\varepsilon_s\rho_s v_s\Theta)\right]=(-P_S I+\tau_S):\nabla v_S+\nabla\cdot(k_\Theta\nabla\Theta)-\gamma_\Theta+\phi_s \quad (3.27)$$

The left-hand side of equation 3.27 represents the net change of fluctuating energy. The first term on the right hand side represent the fluctuating energy due solid pressure and solid viscous forces. The second term is the diffusion of fluctuating energy in the solid phase. γ_Θ represent the dissipation of fluctuating energy , ϕ_s is the exchange of fluctuating energy between the gas and solid phase. In this work the algebraic form of this equations has been used in FLUENT.

The transport (diffusion) coefficient for granular temperature for the solid-phase energy fluctuation is defined by

$$k_\Theta=\frac{150\,\rho_s d_s\sqrt{\Theta\,\pi}}{384(1+e)g_o}\left[1+\frac{6}{5}\varepsilon_s g_o(1+e)\right]^2+2\varepsilon_s^2 d_s\rho_s g_o(1+e)\sqrt{\frac{\Theta}{\pi}} \quad (3.28)$$

The collision energy dissipation between particles γ is calculated

$$\gamma_\Theta=3(1-e^2)\varepsilon_s^2\rho_g g_o\Theta\left(\frac{4}{\mathrm{d_s}}\sqrt{\frac{\Theta}{\Pi}}-\nabla\cdot v_\mathrm{s}\right) \quad (3.29)$$

The dissipation of energy fluctuation due to interaction of particles with the gas phase is not considered. The term $\boldsymbol{\nabla\cdot v_s}$ in Eq 3.29 can be positive or negative depending on the direction of the flow in the CFB riser. Since the term $\boldsymbol{\nabla\cdot v_s}$ is about two orders of magnitude less than the positive term on its left side of Eq. 3.29 will always be a dissipative term in the granular temperature Equation 3.27.

The energy exchange between two phases is represented as follows and it represents the loss of particle kinetic energy to the gas-phase due to particle–gas drag forces.

$$\phi_s=-3\beta\Theta \quad (3.30)$$

Solid Phase Pressure

The solid pressure, P_s represents the solid-phase normal forces due to particle-particle interactions and can be written in two parts, a kinetic contribution and a collisional contribution:

$$P_s = \varepsilon_s \rho_s \Theta[1 + 2(1+e)\varepsilon_s g_o] \tag{3.31}$$

Where: e, is the particle-particle collision coefficient (coefficient of restitution).

Coefficient of restitution is a measure of the elasticity of the collision between two particles, and relates to how much of the kinetic energy of the colliding particles, before the collision remains after the collision. A perfectly elastic collision has a coefficient of restitution of 1. The coefficient of restitution is defined as the ratio of the difference in the velocities of the two colliding particles after the collision, to that in their velocities before the collision, A perfectly plastic, or inelastic, collision has a coefficient of restitution of 0. *i.e.*,

$$\mathrm{e} = \frac{\text{speed of separation}}{\text{speed of approach}} \tag{3.32}$$

The kinetic part, expressed by the first term on the right hand side of Eq. 3.32, is due to the momentum transferred by the shear stress caused by the flow of particles, and the second term, related to the collisional contribution, is due to the momentum transferred between particle collisions.

g_0 -is a radial distribution function which can be expressed as

$$g_o = \frac{3}{5}\left[1 - \left(\frac{\varepsilon_s}{\varepsilon_{s,max}}\right)^{\frac{1}{3}}\right]^{-1} \tag{3.33}$$

and $\varepsilon_{s,max}$ is the particle volume fraction at maximum packing. The radial distribution function, g_o, is related to the Maxwellian distribution of the probability of finding N particles of diameter d_S in a volume control with a given fluctuation velocity, i.e., it describes the probability of inter-particle collisions. The function g_o is a distribution function that governs the transition from the "compressible" condition with $\varepsilon < \varepsilon_{s,max}$, where the spacing between the solid particles can

continue to decrease, to the "incompressible" condition with $\varepsilon = \varepsilon_{s,max}$, where no further decrease in the spacing can occur.

Solid Shear Viscosity

At a packed state, the bed is crammed with particles, hence the frictional force prevails over the other forces, while at a fluidized state, lasting contact gives way to free flight and brief collisions among particles. The competition and transformation of dominating forces lead to flow transition from the packed bed to fluidization. Subsequently, three mechanisms of the particle-phase transport result in two types of flow states, as shown in Fig. 8. The frictional transport determines the behaviors at a close packed state, while the kinetic and collisional transports cause a two-phase flow. So, the total stress may be approximated as the sum of frictional kinetic and collisional contributions as if each of them acts alone. So, the solids stress tensor contains shear and bulk viscosities arising from particle momentum exchange due to translation and collision.

Therefore, the collisional and kinetic parts, and the optional frictional part, are added to give the solids shear viscosity:

$$\mu_s = \mu_{s,col} + \mu_{s,kin} + \mu_{s,fr} \tag{3.34}$$

The collisional and kinetic parts are added as follow

$$\mu_s = \frac{10\rho_s d_s\sqrt{\pi\Theta}}{96(1+e)g_o}\left[1+\frac{4}{5}(1+e)g_o\varepsilon_s\right]^2 + \varepsilon_s^2\rho_s d_s g_o(1+e)\sqrt{\frac{\Theta}{\pi}} \tag{3.35}$$

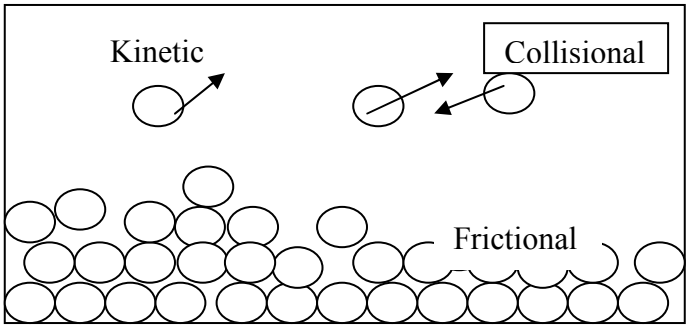

Figure 8 : Particle transport mechanisms: Kinetic, collisional, and frictional transport

In dense flow at low shear, where the secondary volume fraction for a solid phase nears the packing limit, the generation of stress is mainly due to friction between particles. A frictional component of viscosity can also be included to account for the viscous-plastic transition that occurs when particles of a solid phase reach the maximum solid volume fraction. Frictional viscosity generation due to friction between particles, and between particles and walls, becomes especially significant as the solids volume fraction approaches the packing limit [34,35]. Friction stress, which plays a significant role when the solid-phase volume fraction gets, close to the packing limit, and the frictional viscosity is included in the calculation, **FLUENT** uses Schaeffer's [34,35] expression:

$$\mu_{s,fr} = \frac{P_s \sin \emptyset}{2\sqrt{I_{2D}}} \tag{3.36}$$

Where: P_s is the solids pressure, $\emptyset$ is the angle of internal friction, and I_{2D} is the second invariant of the stress tensor.

Solid Bulk Viscosity

The solid bulk viscosity can be defined as the resistance of the particle suspension against compression, and given by Lun et al. and Gidaspow 1994, is

$$\xi_s = \frac{4}{3}\varepsilon_s^2 \rho_s d_s g_o (1+e)\sqrt{\frac{\Theta}{\pi}}. \tag{3.37}$$

Table 6 : Summary of model parameter

Parameter	Model in (Fluent 6.3)	Eq No.
Solid viscosity	Gidaspow	3.35
Solid bulk viscosity	Lun et al.	3.37
Frictional viscosity	Scheaffer	3.36
Solid pressure	Lun et al.	3.31
Radial distribution function	Lun et al.	3.33
Drag law (gas-solid)	Gidaspow	3.10 - 3.14
	Syamlal and O'Brien	3.15 - 3.20

4. NUMERICAL METHODOLOGY

Numerical methods are at the heart of the CFD process. Since, the focus in numeric's is to devise efficient, robust, and reliable algorithms for the solution of PDEs. PDEs are a combination of differential terms (rates of change) that describe a conservation principle. Without loss in generality, all physical processes can be described by PDEs. Now, the CFD process requires the discretization of the governing PDEs, i.e. the derivation of equivalent algebraic relations that should faithfully represent the original PDEs. This is done by transforming each differential term into an approximate algebraic relation.

In this work, bagasse was used as a solid material having uniform size which was initially in static condition inside the fluidized bed column and forms a desire height in the bed. The air i.e. the gas phases was introduced from the bottom of the CFB column so the fluidization starts.

4.1 Research Method

The model equations described in previous section are solved using the commercial CFD software package Fluent 6.3. Figure 9 shows the general procedure for the simulation using Fluent software**.** FLUENT is state-of-the-art computer software for modeling of fluid flow and heat transfer in complex geometry. GAMBIT a pre-processor CAD program used for the geometry set-up and mesh generation both two and three-dimensional setup for CFB. All simulations were performed on laptop computer in order to speedup computational time and transfer all results data's to Academic Computer Centre in AAU. All general procedures done in GAMBIT and FLUENT are listed in Appendix 1.

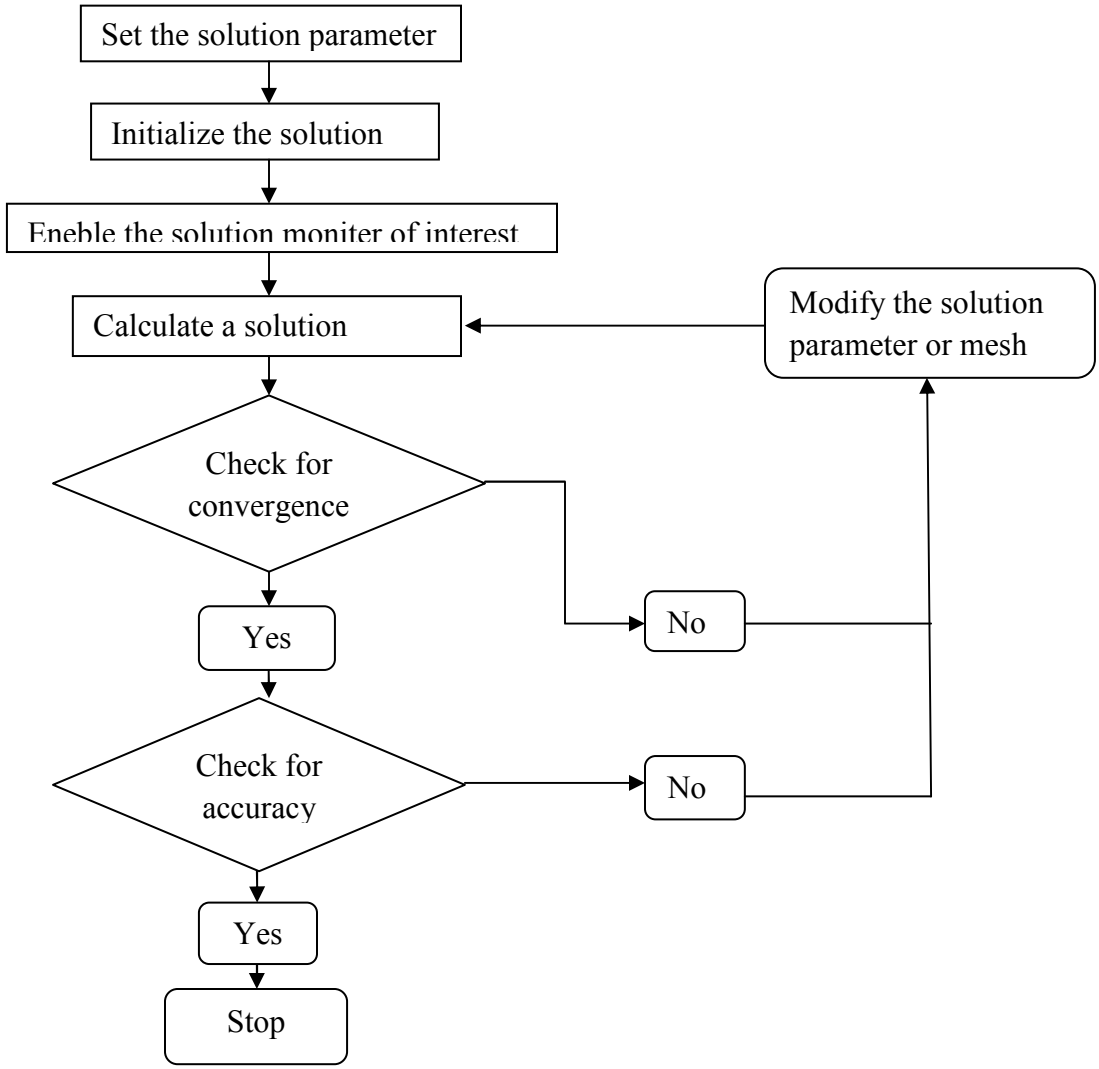

Figure 9 : Flowchart showing the general procedure for the simulation using Fluent.

4.2 Geometry and Mesh Generation

The geometrical dimensions of laboratory scale CFB from Chulalongkorn University having a diameter of 5 cm and 2.0 m height and downcomer with a diameter of 0.10 m and 1.2 m height was used for this simulation work. Since, the dimension of this lab-scale CFB is small and easy for simulate using fine meshes with less computational time. Besides, some experimental work on biomass gasification was done on this lab-scale CFB. Somchai Suaysa-ard was one of the researchers used this experimental set up to study about hydrodynamics of mixed feed in a circulating fluidized bed. The experimental tests were conducted using four different solids

(Sand, Sawdust, Rice husk and Bagasse) [36]. For this simulation work bagasse and sand are the main focus for CFB biomass gasification. Detail geometrical setup of the CFB is shown below in the Figure 10.

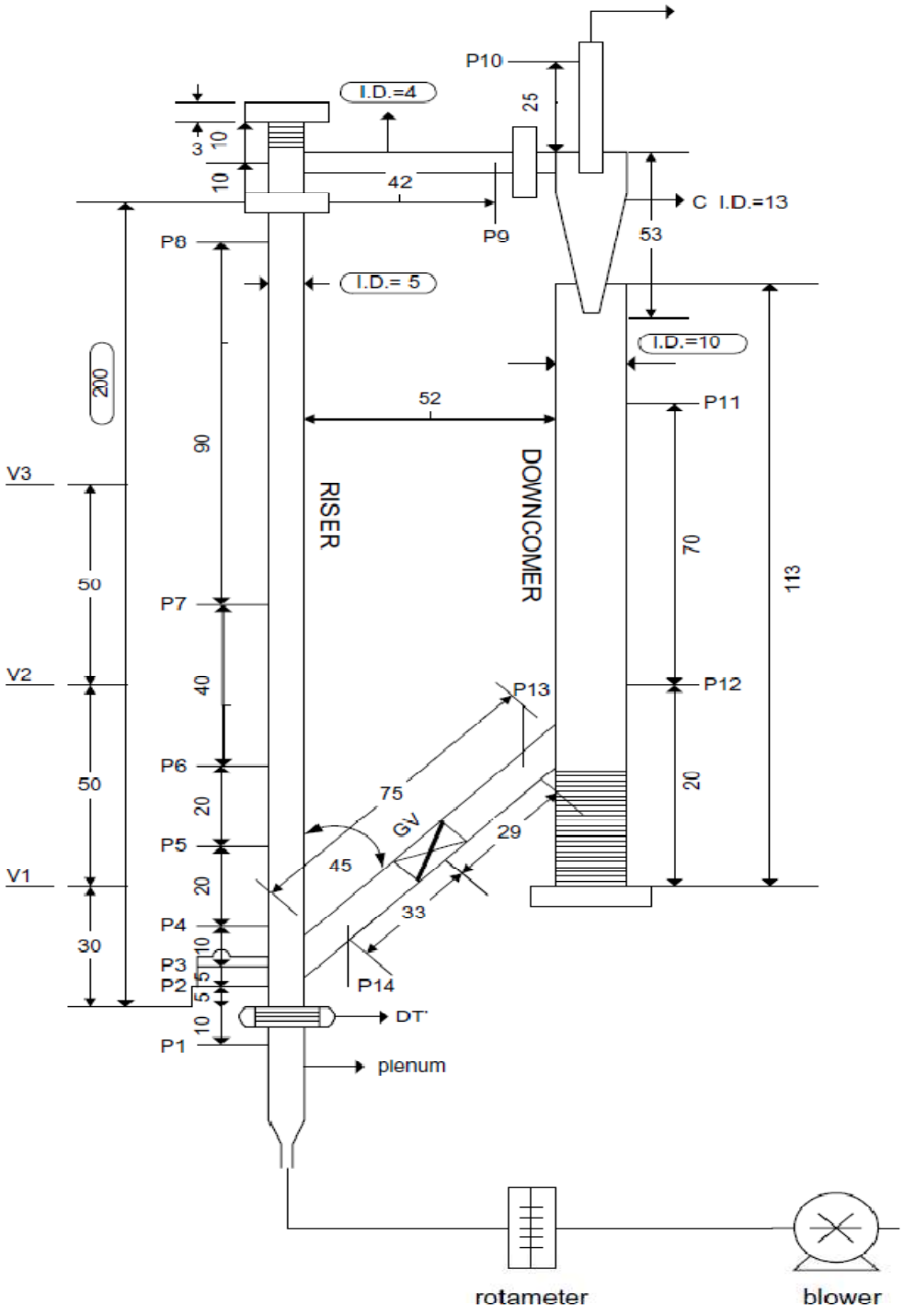

Figure 10 : Geometry of Circulating Fluidized Bed: CFB

The partial differential equations that govern fluid flow are not usually amenable to analytical solutions, except for very simple cases. Therefore, to analyze fluid flows, flow domains are split into smaller sub-domains made up of geometric primitives like tetrahedral in 3D and quadrilaterals in 2D. The governing equations are then discretized and solved inside each of these sub-domains. Typically, finite volumes approximate method is used to solve the system of equations. Care must be taken to ensure proper continuity of solution across the common interfaces between two sub-domains, so that the approximate solutions inside various portions can be put together to give a complete picture of fluid flow in the entire domain. The sub-domains are often called elements or cells, and the collection of all elements or cells is called a mesh or grid.

The first step in CFD simulation of circulating fluidized bed is preprocessor, which has been done by GAMBIT tool, to design the problem geometrical configuration and mesh the geometry. Before hydrodynamics fluid flow problem can be solved in the gasifier. FLUENT need the domain in which the flow takes place to evaluate the solution. The flow domains into the specific domain have been created in GAMBIT by drawing the geometry of CFB. Then, meshing is very important step to get the solution with high quality results. Exporting the model domain to the FLUENT will be the final task.

GAMBIT has been used to create the geometry of cylindrical with desired dimension. Both the 2-D and 3-D have been created and meshed to form the grid. In 3-D geometry tetrahedral meshing has been done with element type hex/wedge. In 2 m height column dividing using cooper hex/wedge schemes 138,109 cells, 289,158 faces, and 29,981 nodes have been created. In 2-D geometry of 2 m height CFB riser column dividing 6,200 cells 12,670 faces and 6,471 nodes have been created. After meshing, the FLUENT 5/6 solver need to be specified so that GAMBIT knows what types of boundary conditions ware allowed. The boundary conditions such as velocity-inlet, pressure outlet, wall and default interior have been set. Then grid has been exported as a mesh file from GAMBIT to be used in FLUENT for solution.

In the first part of numerical simulations, both 2-D and 3-D geometry of the pilot CFB biomass gasifier have been created using GAMBIT. Some of simulation work was done using 2-D model created because it is easier to model the simulation comparable to 3-D in terms of computer

processor's time consuming when running the simulation and it is simplest way to control solid some operating parameters and to see their effects. While 3-D model it takes long simulation time, it is better one to see the reality on CFB. So, most of the simulation on this work was done on 3-D model CFB.

4.3 Boundary and Initial Conditions

The definition of appropriate initial and boundary conditions is critical for the carrying out of a realistic simulation. The implementation of correct inlet conditions is critical for a successful simulation of flow hydrodynamics. The initial and boundary condition used for the gas phase and particle phase applied in the simulation are given in Fig. 11 (a) and 11 (b). Two different cases conditions were considered to observe the effects of inlet geometry on solid particle mixing. The simulation was assumed to be non-reactive and a cold flow fluidization system therefore the operating conditions for both cases was assumed to be operated at 300K temperature and pressure of 1 atm. Besides, most experimental work used to validate this simulations work ware done at this similar atmospheric condition.

For case one: Figure 11 (a) shows the full closed CFB gasifier geometry. Where solid initially in static condition inside the fluidized bed column at 0.5 m initial static height at fluidization conditions ($\varepsilon_{s,}$ = 0.1158). So, solid particle velocity was set at zero, and the inlet gas velocity at the bottom of CFB was assumed to be uniform along the axial direction. The pressure was not specified at the inlet because of the incompressible gas phase assumption (relatively low pressure drop system). All velocities and volume fractions $(\varepsilon_g, \varepsilon_s, v_g, v_s)$ of both phases are specified below. At the outlet, only pressure boundary condition is specified. Average static pressure of zero has been set, based on the atmospheric inlet reference pressure. The other variables ware subjected to the Newman boundary condition. The effects of particle-wall collisions within CFB risers play a significant part on the shear stress at the walls. The boundary condition at the walls for the gas phase was assumed that the tangential and normal velocities of zero, namely no-slip boundary conditions. However, this condition is unrealistic for solid phase particles. Free slip boundary conditions for the solid phase was assumed. The higher viscous effect and higher velocity gradient near the wall have been dealt with the standard wall function method is used to

compute particle phase velocity gradient, which is proposed by Launder and Spalding [34], and have been most widely used for industrial flows.

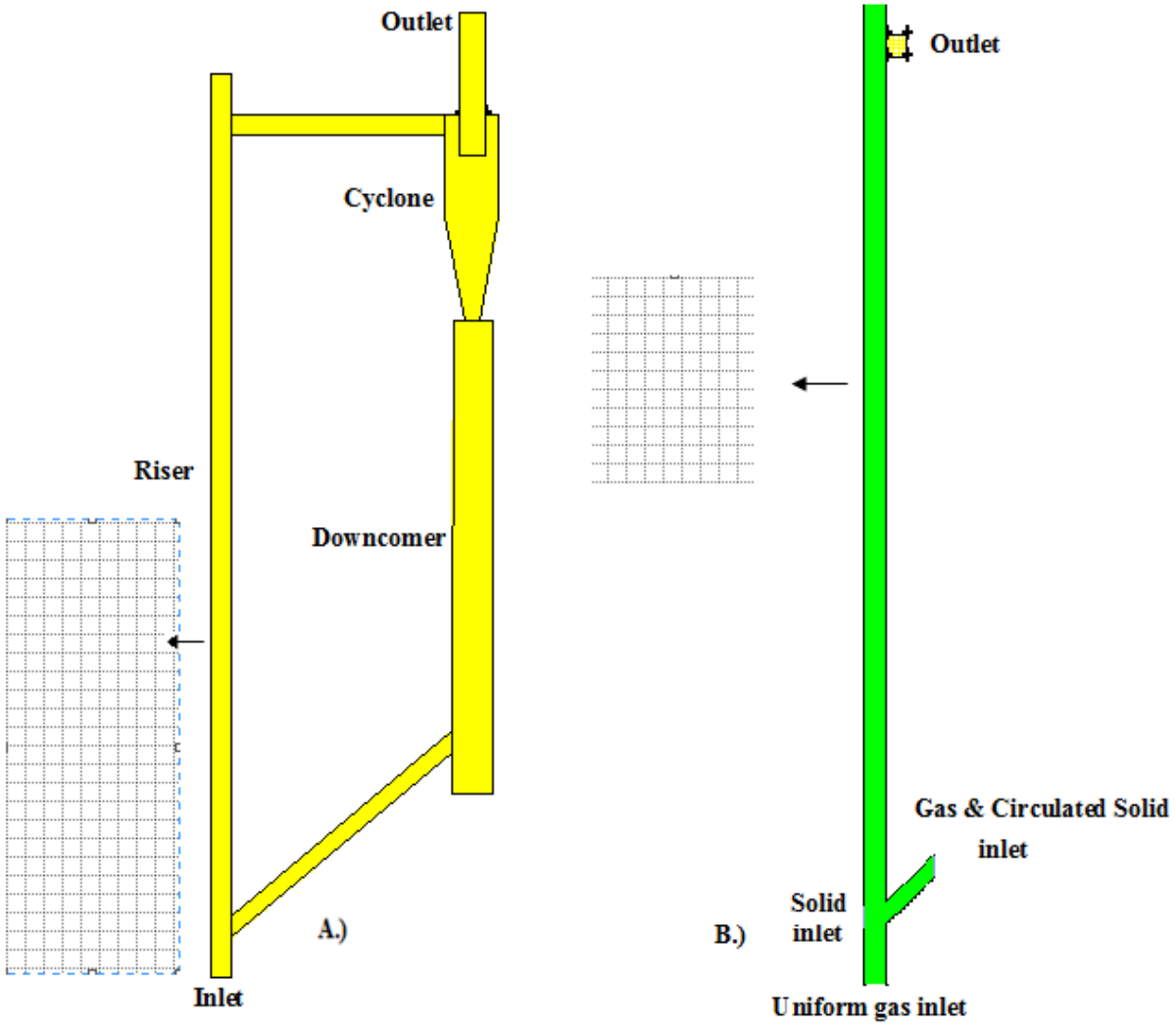

Figure 11 : 2D meshed front view of CFB with boundary conditions (A) full loop CFB (B) CFB rise

For case two: It is important to note that the real geometry of the riser is cylindrical with the solid entering from one side only. To obtain mixing at the entrance zone similar to the 3-D CFB, two-inlet geometry was considered. Figure 11 (b) shows only the riser section of CFB with two side solid inlet, the one for fresh bagasse inlet and the other side for unconverted circulated

bagasse char inlet, the later side is used to control the bagasse circulation rate to the riser for the simulation work, instead of using valve to control the solid circulation inlet in industrial scale operation. Bagasse solid particles were fed from both sides of the riser with voidage fraction of $\varepsilon_{s,} = 0.1158$. A one-inlet CFB for the 3-D CFB could lead the inlet gas to flow to the opposite side of the solid inlet, therefore, to create uniform mixing throughout the height of the CFB riser. The effect of inlet geometry condition was also demonstrated in this case, although the effect of mechanical design geometry is not the concern of this paper. Just to come up to uniform distribution of the solid particle observed on the way. All the other initial and boundary conditions are the same as the previous case.

Table 7: Summary of Boundary Conditions for two cases

	Case 1	Case 2
Model	Setting	Setting
Space	3-D	2-D
Initial condition	Closed loop CFB with initial solid packing - $T=25^oC$ - $\varepsilon_{solid} = 0.1158$	Riser with initial solid packing - $T=25^oC$ - $\varepsilon_{solid} = 0.1158$
Initial boundary conditions	Uniform gas velocity - $U_g = 5.2$ m/s $= U_{y,o}$ and - $U_{x,o} = U_y = 0$ For solid phase - $U_{x,o} = 0$ and $U_{y,o} = 0$	Uniform gas velocity - $U_g = 5.2$ m/s $= U_{y,o}$ and - $U_{x,o} = U_y = 0$ For solid phase - $U_{x,o} = 0$ and $U_{y,o} = 0$
Outlet boundary condition	- P=101325 pa	- P=101325 pa
Wall boundary condition	No-slip condition for gas phase Free-slip condition for solid phase	No-slip condition for gas phase Free-slip condition for solid phase
Computational conditions	138,109 quadrilateral cells 289,158 faces 29,981 nodes $\Delta x = 0.01$, $\Delta y = 0.01$	- 6,200 quadrilateral cells - 12,670 faces - 6,471 nodes

The gas and solid flow parameters for two different cases used in the model are summarized in Table 8. And all operating parameters that affect the hydrodynamics of the CFB varied in the simulation are listed in the Table 9. Standard data for designing CFB also listed and the parameter varied in the simulation was taken on referring standard range.

Table 8 : Solid physical properties and simulation model parameters

Description	Value	Unit	Comment
Gas density	1.2	kg/m^3	(air)
Gas viscosity (air)	$1.7894*10^{-5}$	Pa.s	
Density of solid	630	kg/m^3	(bagasse)
Density of inert solid	2650	kg/m^3	Sand
Particle size	250 – 450	µm	
Diameter of column	0.05	m	Fixed
Height of column	2	m	Fixed
Initial static bed height	0.5	m	
Initial solid holdup (ε_{so})	0.1158		
Initials gas velocity	3 - 6.2	m/s	(air)
Solid circulation rate	5.5 – 14.9	kg/m^2s	
Maximum solids packing (ε_{max})	0.63		Fixed
restitution coefficient, *e*	0.99	-	
CFD time step	$1*10^{-4}$	sec	
Convergence criteria	10^{-3}	-	

Table 9 : Parameter varied in the simulation

Description	Run 1	Run 2	Run 3	Run 4	Run 5	Run 6	Run 7	Run 8	Run 9	Run 10
Gas inlet velocity (m/sec)	3	4.2	5.2	6.2	5.2	5.2	5.2	3	3	3
Solid circulation rate (kg/m^2 sec)	-	-	-	-	5.5	9.1	14.9	-	-	-
Mean Patrice diameter (µm)	337	337	337	337	337	337	337	250	350	450
Key design operating conditions for CFB in fast fluidization (Standard data) [17]										
Mean particle diameter (µm)					50-500					
Gas velocity (m/s)					3- 6					

4.4 Solution procedures

4.4.1 Coordinate system

Two-dimensional cylindrical r, z. coordinates has been applied for the description of the riser for case two. With cylindrical coordinates, simulations have been performed assuming no symmetry conditions with respect to the axis of the riser. Uniform grid spacing has been used in the axial direction for 3-D CFB and more cells are placed closer to the wall to capture the complex flow behavior in this region for 2-D CFB riser.

4.4.2 Discretization

To obtain an approximate solution numerically, it is better use a discretization method which approximates the differential equation by a system of algebraic equations, which can then be further solved. The approximations are applied to small domains in space and time so the numerical solutions provide results at discrete locations in space and time. It concerns the process of transferring continues models and equations into discrete counterparts. This process is usually carried out as a first step toward making them suitable for numerical evaluation and implementation on digital computers. The accuracy of numerical solution depends on the quality of discretization used. In the present work discretization based on finite volume methods has been used since, it's simple to understand, to program and can accommodate any type of grid, so it is suitable for complex geometries like 3-D CFB.

The governing equations given in previous section are solved by a finite volume method, where the calculation domain is divided into a finite number of non-overlapping control volumes. Physical parameters are stored at main grid points placed in centre of the control volumes. Figure 12 shows a scalar control volume for a two-dimensional situation and velocity control volumes are shown. Nodal point N, E, W and S represent north, east, west and south direction from the desired nodal point P.

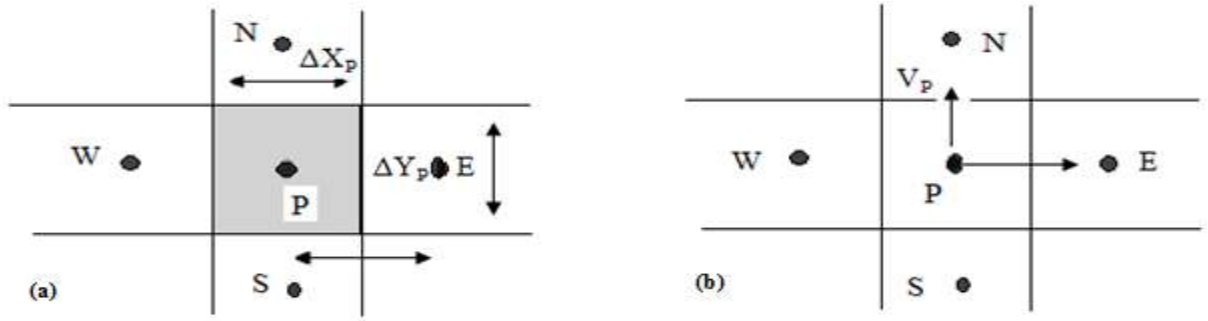

Figure 12 : Scalar control volume for a 2-D situation (a) and velocity control volumes (b)

4.4.3 Differencing schemes

The conservation equations are integrated in space and time. This integration is performed using second-order upwind differencing in space has been used for discretization of momentum, turbulence kinetic energy and turbulence dissipation rate and first-order upwind differencing in space has been used for discretization of volume-fraction equations and fully implicit in time. The set of algebraic equations is solved by a tri-diagonal matrix algorithm (TDMA), except for the volume fraction where a point iteration method is used. Semi-Implicit Method for Pressure-Linked Equations (SIMPLE) algorithm was used to take care of the coupling between the continuity and the velocity equations.

First-order upwind differencing (FOU)

A general differencing equation can be written as;

$$\frac{\partial}{\partial t}(\rho\Phi) + \frac{\partial y}{\partial x}(\rho U_i \Phi) = \frac{\partial}{\partial t}\left(\Gamma \frac{\partial \Phi}{\partial x_i}\right) + S_\Phi \qquad (4.1)$$

Where S_Φ is the source term, the discretization equation for the dependent variable Φ for a one dimensional system is obtained as

$$a_P \Phi_P = a_E \Phi_E + a_W \Phi_W + b \qquad (4.2)$$

Where the constant part of the source term is included in b. the values of Φ in point P become linear combinations of Φ in the neighbor points W and E. The coefficient in the neighbor point depend on how Φ varies between the main grid nodes, and included convection and diffusion. For the FOU difference schema the coefficients of the neighboring points can be written as:

$$a_w = \mathrm{Max}\,(F_w, 0) + D_w \qquad a_E = \mathrm{Max}\,(-F_e, 0) + D_E \qquad (4.3)$$

The variable, F and D, represent the convective and the diffusive fluxes at the cell faces and are defined according to:

$$F_e = (\rho U)_e \Delta y + D_W \qquad F_w = (\rho U)_w \Delta y + D_E \qquad (4.4)$$

$$D_e = \frac{\Gamma_e \Delta y}{\delta x_e} \qquad D_w = \frac{\Gamma_w \Delta y}{\delta x_w}$$

The transport coefficient, Γ at the east control volume surface is expressed as:

$$\Gamma_{\Phi e} = \frac{\delta X_e \Gamma_P \Gamma_E}{\Delta X_E \Gamma_E + \Delta X_P \Gamma_E} \qquad (4.5)$$

Second order upwind differencing (SOU)

In this work second order upwind scheme (SOU) is introduced in to avoid the problem with false diffusion.

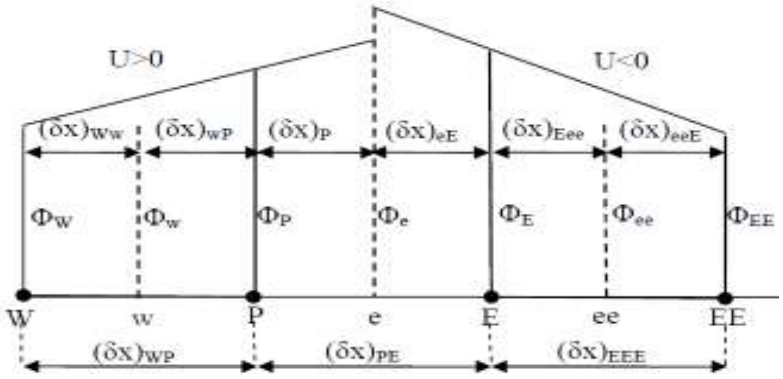

Figure 13 : Principle of second order differencing scheme

The principle of SOU scheme is illustrated in Figure 13. The cell face value of Φ is estimated from the two upstream neighboring nodes by extrapolation.

The value of Φ_e can be expressed as

$$\Phi_e = \Phi_P + (\Phi_P - \Phi_W)\frac{(\delta x)_{pe}}{(\delta x)_{WP}} \quad \text{if} > 0 \qquad (4.6)$$

$$\Phi_e = \Phi_E + (\Phi_E - \Phi_{EE})\frac{(\delta x)_{eE}}{(\delta x)_{EEE}} \quad \text{if} < 0$$

The one- dimensional discretization equation for Φ become

$$a_P \Phi_P = a_E \Phi_E + a_W \Phi_W + a_{EE} \Phi_{EE} + a_{WW} \Phi_{WW} + b \qquad (4.7)$$

4.4.4 SIMPLE algorithm (Pressure -Velocity Coupling)

The SIMPLE iterative algorithm [25] is used by Fluent to relate the velocity and pressure corrections to recast the continuity equation in terms of a pressure correction calculation.

For this method to work, a state equation that relates solids pressure to solids volume fraction is needed:

$$P_s = P_s \varepsilon_s \tag{4.8}$$

and the derivate of solids pressure with respect to solids volume fraction, K_S, is defined as:

$$K_s = \frac{\partial P_s}{\partial \varepsilon_s} \tag{4.9}$$

A small change in solids pressure, P_S', can be calculated as a function of the change in solids volume fraction, ε_s:

$$P_s' = K_s * \varepsilon_s' \tag{4.10}$$

An equation for volume fraction correction can then be written as:

$$a_p(\varepsilon_s')_p = \sum_{nb} a_{nb} (\varepsilon_s')_{ab} + b \tag{4.11}$$

where the terms on the right hand are the convective terms and the source term respectively.

The coefficient on the east neighboring point can be expressed as:

$$a_E = \max(F_{s,e}, 0) + D_E \tag{4.12}$$

$F_{s,e}, and\ D_E$ are expressed as :

$$F_{s,e} = (\rho_s)_E (U_S)_e^* A_e \qquad \text{and } D_E = (\rho_s \varepsilon_s)_e^* e_e (K_s)_E A_e \tag{4.13}$$

The velocity field $(U_S)_e^*$ is the velocity field after correcting for the fluid pressure correction.

The actual solid velocity can be represented as:

$$(U_S) = (U_S)_e^* + (U_S')_e \tag{4.14}$$

where the velocity correction, $(U_S)_e$ is related to the solids pressure field as, [34]:

$$(U_S')_e = e_e\left[(P_s')_p - (P_s')_E\right] \tag{4.15}$$

P_s' is the solid pressure correction and e_e is the coefficient linking velocity correction to the solid pressure correction. Substituting from (4.10) gives the following equation for the solid velocity correction:

$$(U_S')_e = e_e\left[(K_S)_P(\varepsilon_s')_p - (K_S)_E(\varepsilon_s')_E\right] \tag{4.16}$$

The source term, b, in eq. 4.11 can be expressed as, [34]:

$$b = -(\rho_s \varepsilon_s{}^*)_E (U_S)^*_e A_e + (\rho_s \varepsilon_s{}^*)_w (U_S)^*_w A_w - (\rho_s \varepsilon_s{}^*)_n (V_S)^*_n A_n + (\rho_s \varepsilon_s{}^*)_s (V_S)^*_s A_s - (\rho_s \varepsilon_s{}^*)_t (W_S)^*_t A_t + (\rho_s \varepsilon_s{}^*)_b (U_S)^*_b A_b - \left[(\rho_s \varepsilon_s{}^*)^*_p - (\rho_s \varepsilon_s{}^*)^*_p\right] \frac{\Delta V}{\Delta t} \quad (4.17)$$

After calculating the solids volume fraction correction, $\varepsilon_s{}'$, the solid volume fraction is updated:

$$\varepsilon_s = \varepsilon_s{}^* + \varepsilon_s{}' \quad (4.18)$$

In regions where the solid volume fraction is close to maximum packing, a small increase in the solid volume fraction will cause a large increase in the solid pressure. Such rapid changes in the solids pressure leads to numerical instability. Selective under relaxation is applied in densely packed regions to avoid these rapid changes. The equation of solid volume fraction under dense packed condition is expressed as:

$$\varepsilon_s = \varepsilon_s^* + \omega_{ps} \varepsilon_s' \quad (4.19)$$

When

$$\varepsilon_s > \varepsilon_{s,max} \; and \; \varepsilon_s' > 0$$

ω_{ps} is the relaxation factor for the solid volume fraction correction.

The velocity corrections for the solids phases are calculated and the solids velocity field is updated according to equation (4.14). The void fraction is calculated from:

$$\varepsilon_s = 1 - \sum \varepsilon_s \quad (4.20)$$

The solid phase pressure is calculated from the state equation. The procedure for the calculations is shown in Figure 14.

The time step size of 0.001s has been used. The convergence criteria for all the numerical simulations are based on monitoring the mass flow residual and the value of 1×10^{-4} is specified as converged value for the relative error between successive iterations.

The main parameters of the flow inside the system are calculated using an iteration calculation procedure performed by FLUENT. An iterative cycle starts with the introduction of initial data and/or initial guessed values, boundary conditions, physical conditions and constants. In a second step the program calculate the velocity field from the momentum equation. Then, the mass balance equations as well as the pressure equations are solved. The next step is to update the values of the parameters for both phases. The final step to check on the convergence which criterion is fixed based on the model date and property of the fluid that set. If the convergence

criterion is archived the simulation will stop and the final result of the system. If not, certain correction values are used to adjust the calculated values and the calculation will start over again, using an initial data these last corrected values of each parameters.

The following steps were followed in the simulations:

1. Initially the physical properties and exchange coefficients are calculated.
2. Velocity fields based on the current pressure field and the corresponding u_m*,v_m* (m = 0, 1 for solid and gas phases) are evaluated.
3. The fluid pressure correction P_g' is calculated.
4. The fluid pressure field is updated applying an under-relaxation, $P_g = P_g^* + w_{sg}P_g'$.
5. The fluid velocity corrections from P_g' are evaluated, and the fluid velocity fields are updated using, $U_m = U_g^* + U_m'$. (Similarly the solid phase velocities U_s as denoted in step 9 are updated).
6. The pressure gradients, $K_s = \frac{\partial P_s}{\partial \varepsilon_s}$, are evaluated for use in the solid volume fraction correction equation.
7. The solid volume fraction correction, ε_s' is evaluated.
8. The solid volume fraction is updated. That is, $\varepsilon_s = \varepsilon_s^* + \omega_{ps}\varepsilon_s'$.
9. The velocity corrections for the solid phase are estimated and the solid velocity fields are updated. That is, $U_S = U_S^* + U_S'$.
10. The solid pressure is evaluated.
11. The granular temperatures and the turbulence property are evaluated.

The normalized residuals calculated in Steps 2, 3, 5, and 9 are used to check for convergence. If the convergence criterion is not satisfied, then the iterations starting with Step 2 are repeated. The flowchart of the simulation algorithm for one time step is shown in Fig. 14.

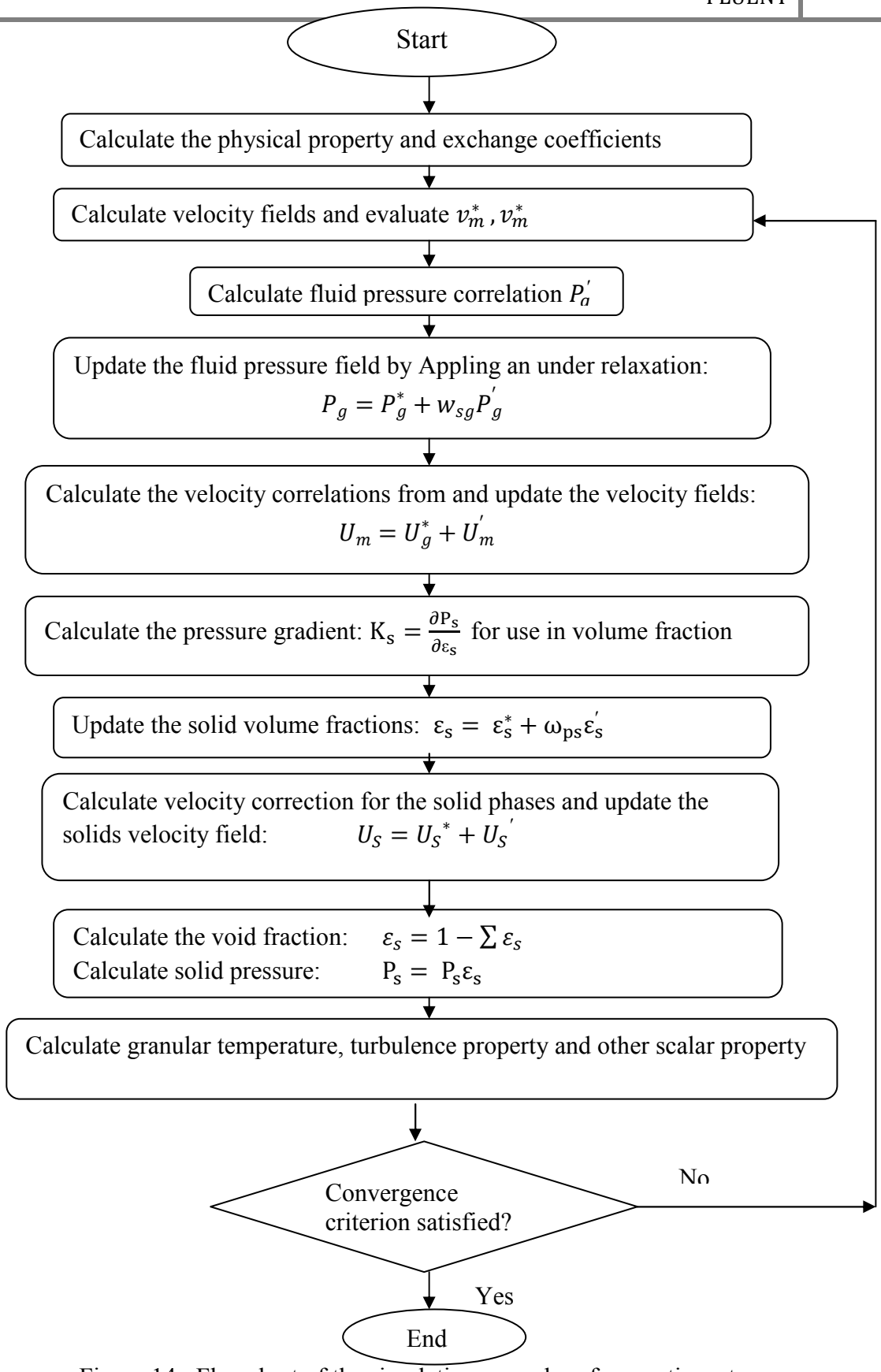

Figure 14 : Flowchart of the simulation procedure for one time step.

5. RESULTS & DISCUSSION

5.1 Model Description

In the simulation, bagasse and air was fed to the CFB, as solid particle and gas respectively. The simulations were divided in two cases. The first case, using 3-D full CFB geometry effect of superficial gas velocity and particle diameter on the solid distribution was studied. The second one, 2-D CFB riser geometry only was considered in order to observe the effect of solid circulation and effect of two symmetric solid inlets.

In each of the simulations, computations start from a situation where solids are in static condition within the riser. The simulation was conducted on laptop computer with 2GB memory for ten sec of real fluidization time corresponding to two weeks of computational time for 3-D and 1 week of computational time for 2-D. The unsteady-state flow after 10 second fluidization solid particle reaches steady-state condition throughout the CFB. That means a stable and time independent solution was reached. Averaging is then performed for another one second, to take the time averaged result. For case two, the mass flow rate of solids entering the system through the return channel is adjusted in such a way that, at any instant of time the mass in the riser remains the same at constant solid circulation rate and steady state was determine from the simulation when the total solids inventory in the riser don't show any large fluctuations over time. The results presented in this paper are all obtained in such a state (after steady-state achieved).

Several simulations have been performed in order to investigate the effect of different operating conditions and model assumptions to get an adequate description of the observed two-phase flow patterns from simulated CFB. Solid-gas phase dynamics have been represented in the form of contour plot. Figure 15 shows time-averaged contours of bagasse and air volume fraction field at the four different times of 0.03, 2.7, 5 and 10 sec from the beginning of the simulation at gas velocity of 3 m/s and particle size 337.5 μm. the last contour when the time is 10 sec indicate the flow dynamics after steady state is reached.

Once air is introduced, the bagasse begins to expand, with some particles hitting the top wall and falling down. Some particles close to the cyclone are dragged by gas into the cyclone. At the initial stage, the flow of particles into the cyclone is high, leading to particle accumulation at the apex of the cyclone. After 10 seconds, the particles flowing into the cyclone begin to decrease.

Finally, macroscopically steady state flow is established, where the input and output rates of particles for each of the flowing units involved are equal.

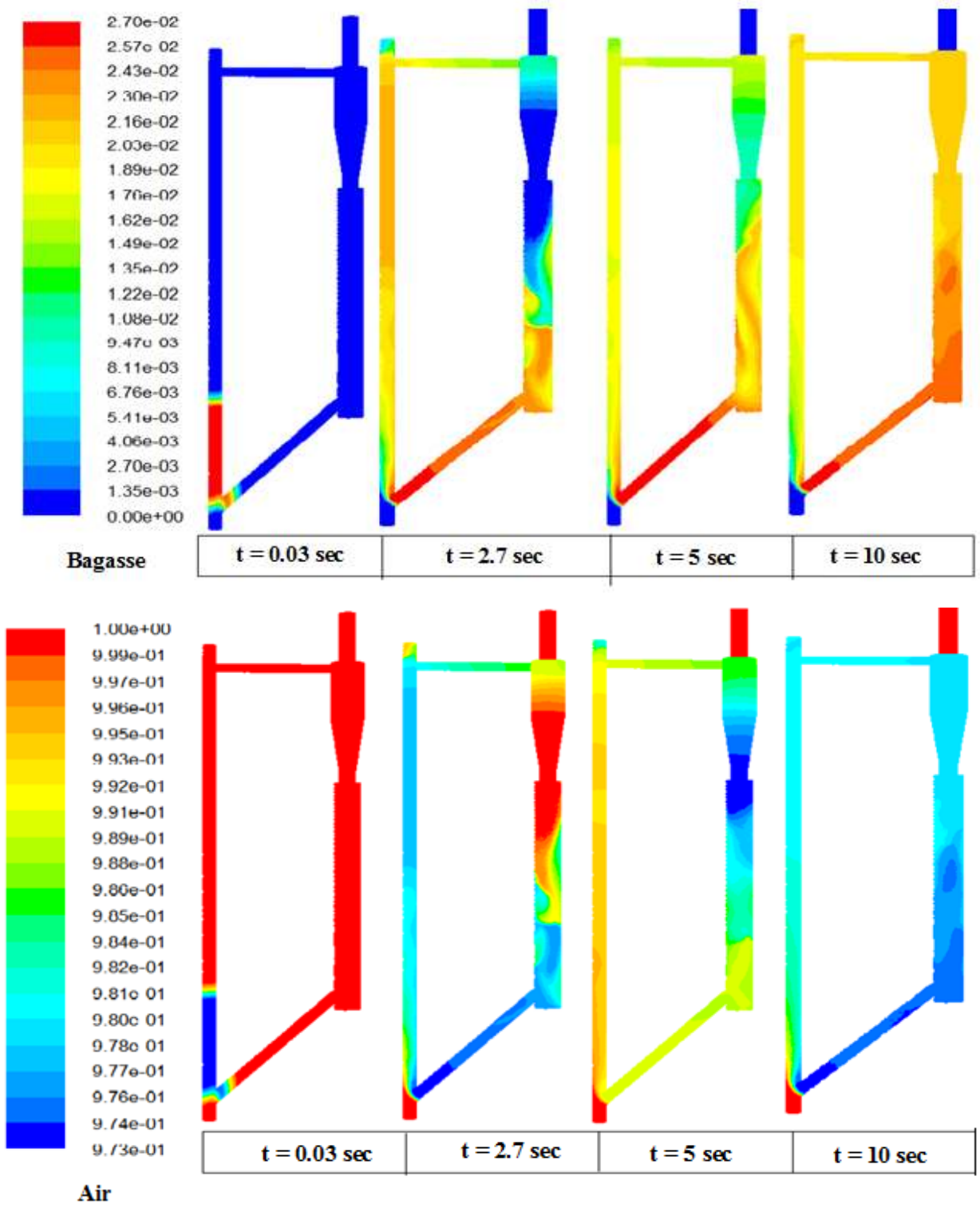

Figure 15 : Contour plot for bagasse and air

The color scale given to the left of each contours gives the value of volume fraction corresponding to the color. The contours for bagasse particle illustrates that bed is in fluidized condition. The contour for air illustrates that gas holdup is significantly more in fluidized part of the bed compared to remaining part. The bagasse particle it takes less than 2.7 sec to circulate one full circulation.

5.2 The Influence of Solid Inlet Position

5.2.1 Velocity Distribution

Fig. 16 shows the simulated distribution of solids velocities along the radial direction at six different bed height 0.3, 0.5, 0.8, 1.1, 1.5 and 1.75 m in the CFB riser at velocity 3 m/s for 3-D CFB model. All these lines represent the axial velocity magnitude at respective bed height along radial direction. The radial position (r/R) on the x-axis represents the distance from the center of the CFB riser. +0.025 and -0.025 represent the right and the left side of the riser wall and 0 represent the center of the riser. The result shows that, velocity distribution along the CFB not symmetric between two opposite side of the wall at the lower zone of the riser due to the effect of solid inlet position. The comparison among these six heights from Figure 16 confirms that vertical particle velocity profiles hardly change from a height of 1.1 m, indicating that the flow can be considered to be fully developed above this height. At a height between 0.3 m, 0.5 and 0.8 m the flow is still developing with the particles accelerating and acquiring more energy.

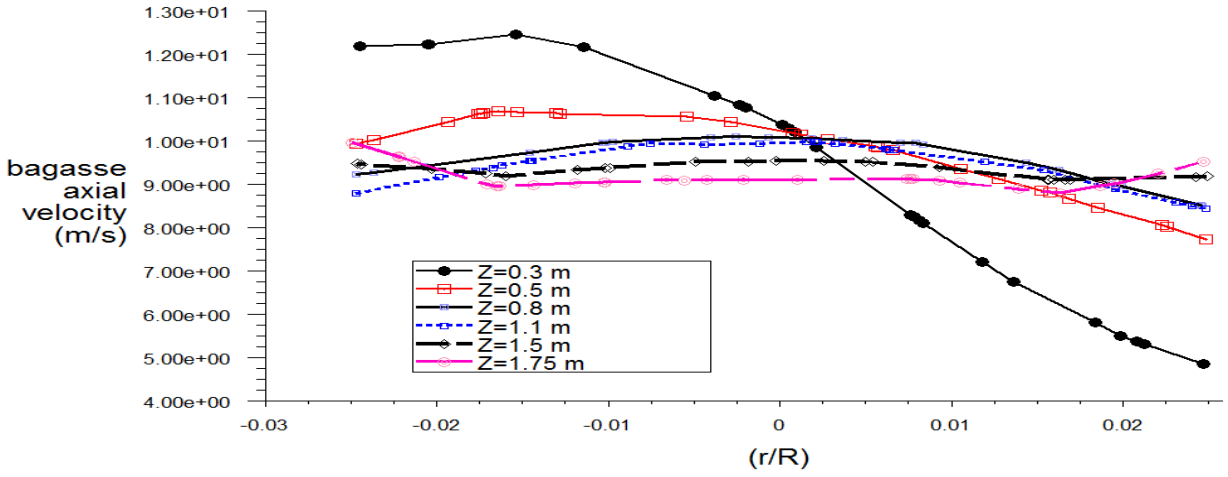

Figure 16 : Time-average axial solids velocity distribution along the radial at Ug =3 m/s for [Z =0.3 m, Z=0.5 m,Z= 0.8 m, Z =1.1 m, Z =1.5 m and Z=1.75 m]

To see the effect of solid inlet position on particle distribution and to get a symmetrical velocity distribution, that lacks case one result. Result from case two give a good agreement with the known property of CFB. Also case two simulations seems to be in many features closer to the real known CFB since the 3-D simulation consists of only one inlet and outlet. The inlet solid velocities were $U_x = V_y = 0.0146$ m/s with a feed inclination of 45^o, and a minimum fluidization solid volume fraction of 0.1158. This assured a 5.5 kg/m^{2}s solid mass flux in the riser. The bagasse particle velocity profile shows the minimum velocity at center of the radius and it increases to attain the maximum velocity away from the center. Due to the particle cluster drop formation and wall effect, the velocity decreases near the wall.

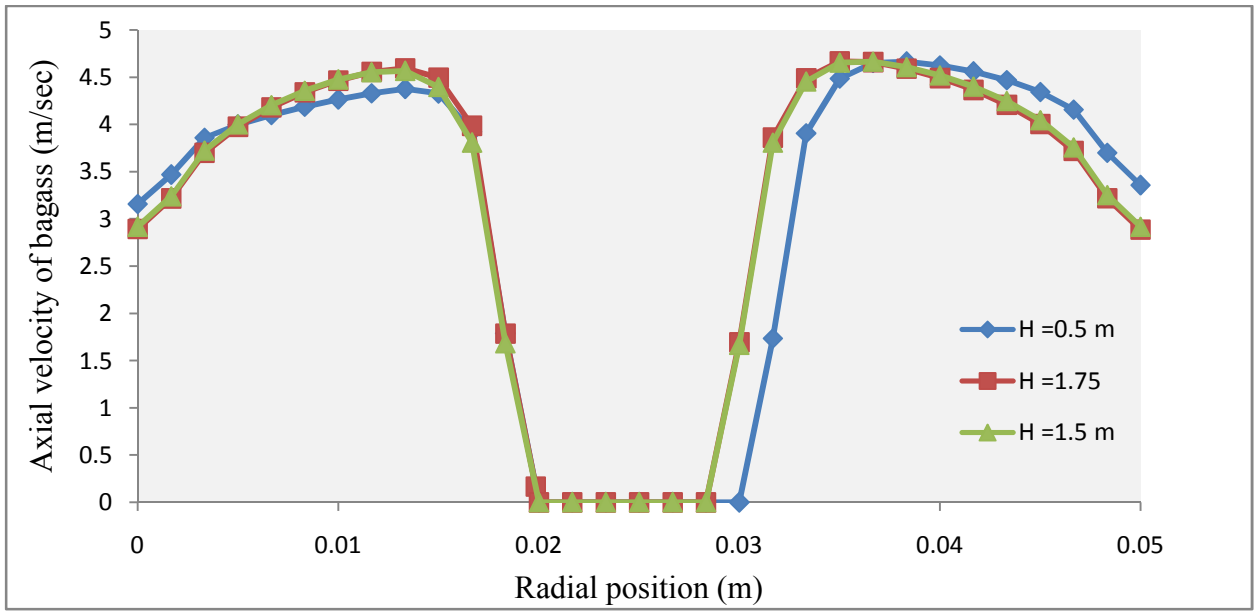

Figure 17 : Time averaged simulated particle velocities at heights [Z=0.5m, Z=1.5m and Z= 1.75m for dp =350 μm and Vg = 3m/s]

The results depicted in Fig. 17 are more complex than those in Fig. 16. The core–annulus structure can be confirmed in Figure. 17, showing falling particles near the walls while rising particles in the near center. However, the solids velocity profiles are more fluctuating along the axial direction in the sense that it fluctuates between two maximum rising velocities and solid uneven distribution of solid along the radial direction are the drawbacks of 2-D result. To sum up to the above results of Figures it is clearly show that axial flow distribution is uniform for 3-D model. 2-D model simulation cannot be viewed as a reliable simplification to the real 3-D case. But 2-D model result show easily the core-annulus structure.

5.2.2 Particle Distribution

In addition to the trend described above, Figure 18 illustrate, radial variation of solid distribution at different bed height. The result confirms that the solid volume fraction is not symmetrical and the values towards the gas and solid feeding side are higher than on the opposite side.

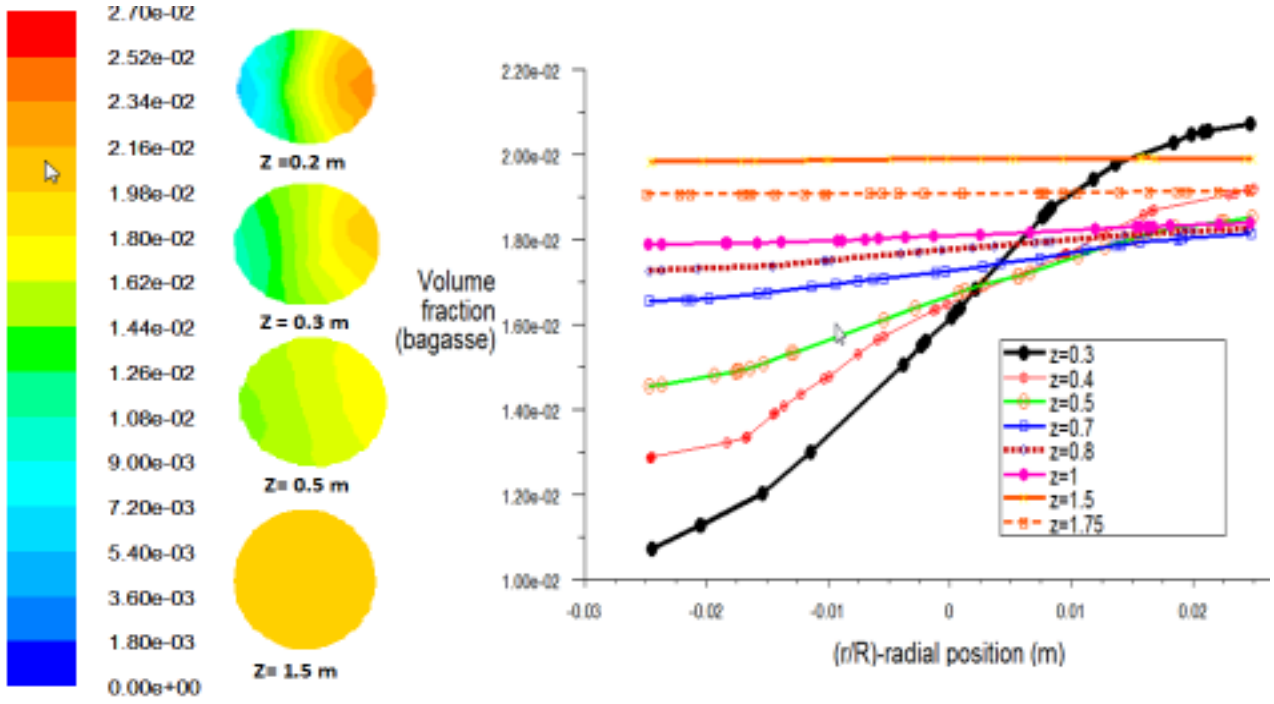

Figure 18 : Bagasse particles concentration at different radial positions with inlet velocity, V = 5.2 m/s, across different heights for 3-D model.

Contour plot from 3-D model shown in the Figure 18 illustrate that, particle concentration at height Z=0.2 m and Z=0.3 m is higher toward the positive radial direction. The variation of bagasse particle voidage at the bottom Z= 0.2 m is more apparent than near the upper bottom Z=0.3 m in dense zone of the riser, but tended to disappear along the flow direction (higher position of the column). The above phenomenon resulted from the side inlet configuration and the location of the re-circulated solid feed inlet, which significantly affect the distribution of the gas and the solid volume fraction.

According to the axial solid volume concentration profile in Figure 18 above, the riser is axially divided into the bottom zone and the upper zone. The lower region of CFB riser is denser than

the upper-dilute region even though the solids mainly accumulate in both sides the wall for 2D model and on one side only for 3-D model. From the simulation result in the figures above, the hydrodynamic model is able to describe quantitatively the accumulation of solid at the wall. Solid concentrations appear flat in the core and increase near the wall.

5.3 Core-Annulus Flow Structure

the core–annulus structure from simulation can be clearly observed by showing that the solid and gas velocities distribution along the radial position from Figure 19, for both phase the velocity in the core region are upward and much higher than that in the annulus region, while solid and gas velocities near wall are decreases, and this may lead to the back-mixing behavior or accumulation of particles. At the height of 1.75 m, the time-averaged solid and gas velocities near wall change positive, and the radial profile of gas velocity seems much flatter due to the less solid concentration in this region.

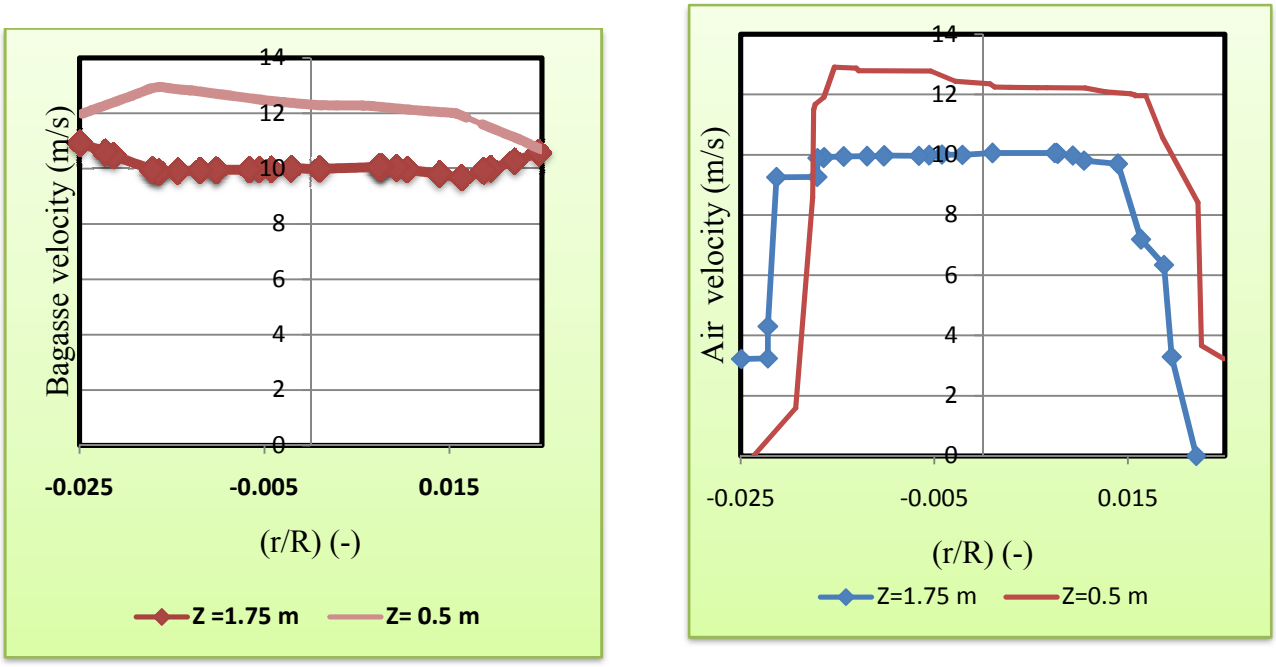

Figure 19 : Time-averaged value of simulated solid and gas axial velocities at [U_g =3 m/s and dp =350 μm]

Figure 20 shows the time-averaged distribution of axial solid velocity contour (a) in the lower dense region for 3-D CFB, and axial solid velocity (b) for 2-D CFB riser. It's clearly seen that the solids have low velocity near the wall as shown from the couture plot on the bottom of the

CFB riser side. It shows that more bagasse particles concentrate towards the re-circulated solid inlet side and form dense zone, which is a yellow color at the bottom but tended to flow up on the opposite side of this zone.

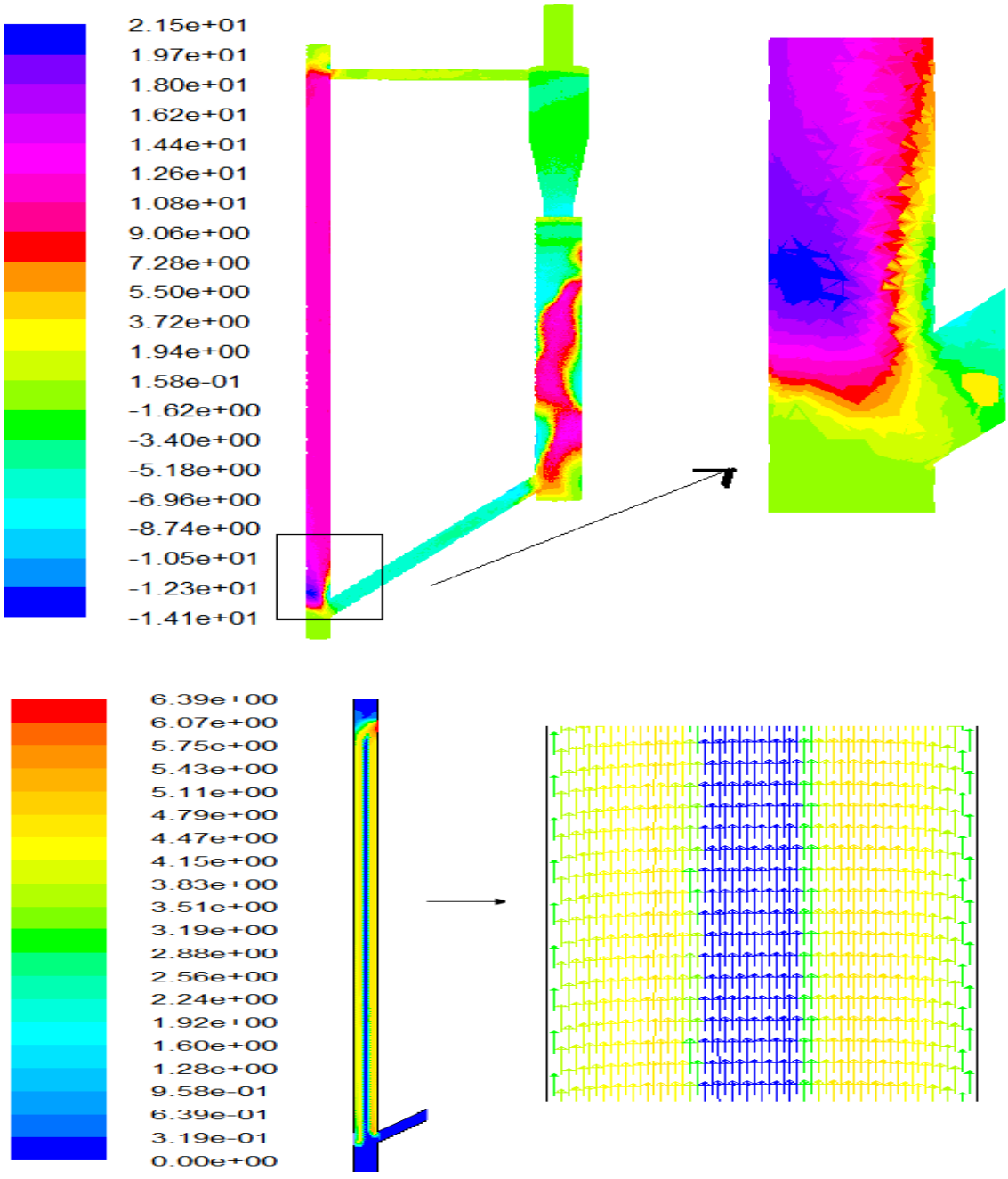

Figure 20 : Magnified solid axial velocity contour plot for for 3-D (a) and axial velocity vector for 2-D (b)

The two distributions clearly illustrate the core-annular pattern of the flow. The solid mainly accumulates and moves downward at the wall, whereas a dilute gas-solid stream flows upward in the core of the riser. The lower region of the riser is denser than the upper-dilute region even though the solid mainly accumulates at the walls in both regions. In the lower portion of the riser, only a slightly larger downflow is observed at the left hand-side wall, whereas, in the upper part, no downflow is observed.

5.4 The Influence of Solid Circulation Rate

5.4.1 Axial Distribution of Solids Holdup

Figure 21 shows the result obtained from CFD simulation of axial bagasse voidage profile for three different solid circulation rate at 5.5, 9.1 and 14.9 kg/m^{2}s for constant gas velocity of 4.2 m/s and 337.5 µm particle diameters. The voidage profile for low solid circulation of 5.5 kg/m^{2}s seems a C-shaped profile, when solid circulation increases from 5.5 kg/m^{2}s to 9.1 kg/m^{2}s and then to 14.9 kg/m^{2}s, a condition is reached at which U_g is insufficient to entrain all the solids entering into the riser without solid accumulation at the bottom of the riser so that solid particles begin to accumulate at the bottom of the CFB riser to form a dense phase and results S-shaped voidage profiles. Besides, voidage profile for 9.1 kg/m^{2}s and 14.9 kg/m^{2}s solid circulation have no big difference in their profile shape, while it seems an approximately zero increase in voidage at the dense zone. Therefore, when operating with the CFB riser in the S-shape profile the voidage in the bottom dense region of the riser does not change appreciably with changes in solids flow rate as long as the riser velocity is constant.

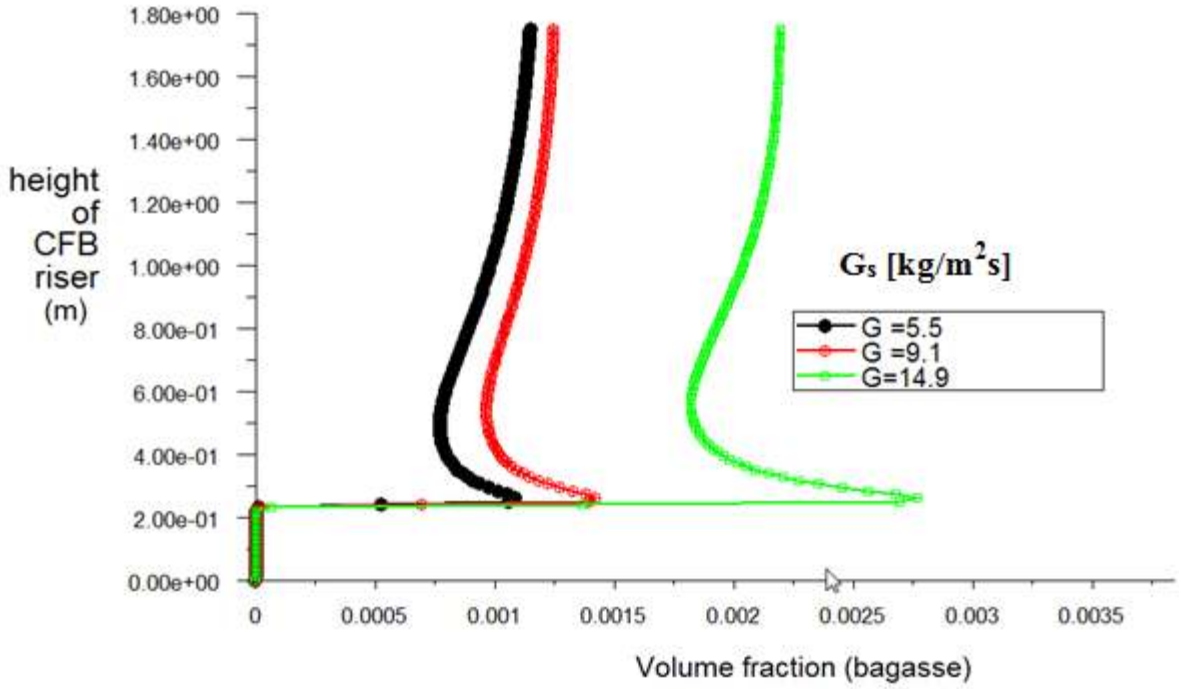

Figure 21 : Axial distribution of bagasse particle for different solid circulation of Gs =5.5 kg/m^{2}s, Gs =9.1kg/m^{2}s and Gs =14.9kg/m^{2}s

The axial solid holdup distributions of bagasse particles with variations of solid circulation rate at a given gas velocity, normally it seems, bagasse particle distribution in the CFB riser increases with increasing solid circulation in dense zone but the effect of solid circulation on bagasse particle holdup is very small. Once the S-shape profile is fully developed with a constant solids fraction at the bottom and top, gradually increasing the circulation rate resulted in an increased dense bed height.

5.4.2 Radial Distribution of Gas Holdup

In Figure 22, effect of three different solid circulation rates on averaged radial distribution of solid for a constant gas velocity Ug = 6.2 m/s is illustrated. The void fraction profile does not change significantly from height 0.5 m to 1.75 m in the core region. But close to the bottom, at height 0.5 m, the void fraction is highest in the wall as the solid circulation increases. At height 1.75 m for 5.5 kg/m^{2}s solid circulation rate the void fraction profile is rather flat as compared to14.9 kg/m^{2}s. Therefore on the rivers side for the solid holdup from the Figure 19 it can conclude that as the solid circulation increases the solid concentration distance from the wall to

the core region become increases. The solids flux has a large effect on the extent of solids down flow.

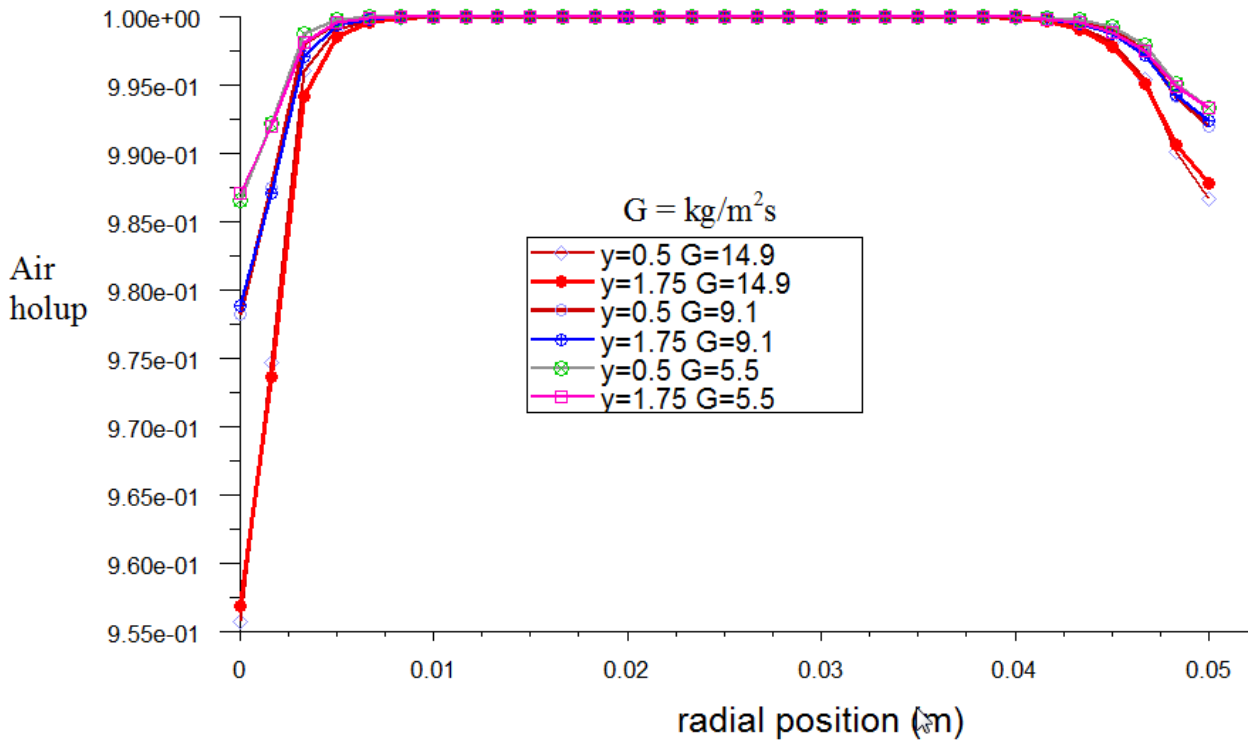

Figure 22 : Radial distribution of gas holdup at solid circulation [Gs =5.5 kg/m^{2}s, 9.1 kg/m^{2}s and 14.9 kg/m^{2}s with gas velocity of Ug =6.2 m/s]

To sum up, the simulation result of Figure 21 and 22 is that, CFB riser contains a dense phase transport region topped by a region of dilute-phase transport zone. Even though at any given solid circulation rate for a given gas velocity in a fast fluidization regime condition of the CFB riser, it is difficult to a distinct bed surface separating the dense region in the lower part of the bed and the dilute (freeboard) zone in the upper part of the bed since, at lower solid circulation rate, the axial solid holdup distribution in the whole column becomes uniform. Increasing solids fluxes increases the cross-sectional average solids holdup. The solids flux has a large effect on the extent of solids down flow, but only little influence on the lateral profile of the axial solids velocity.

5.5 The Influence of Superficial Gas Velocity

5.5.1 Axial solid velocity

The average particle velocity distribution at superficial gas velocities of 3 m/s and 5.2 m/s are shown in Figure 23 and the result shows that superficial gas velocity has an important influence on the flow in a CFB riser. The vertical velocities are high in the negative side of the radial position and decrease along the radial direction toward the positive side. As the superficial gas velocity increases from 3 m/s to 5.2 m/s the axial velocity increases. even for a fully developed height at Z =1.1 m for gas velocity of 3m/s the axial velocity increases for gas velocity of 5.2 m/s which indicates that the superficial gas velocity has a strong influence on the axial solid velocity.

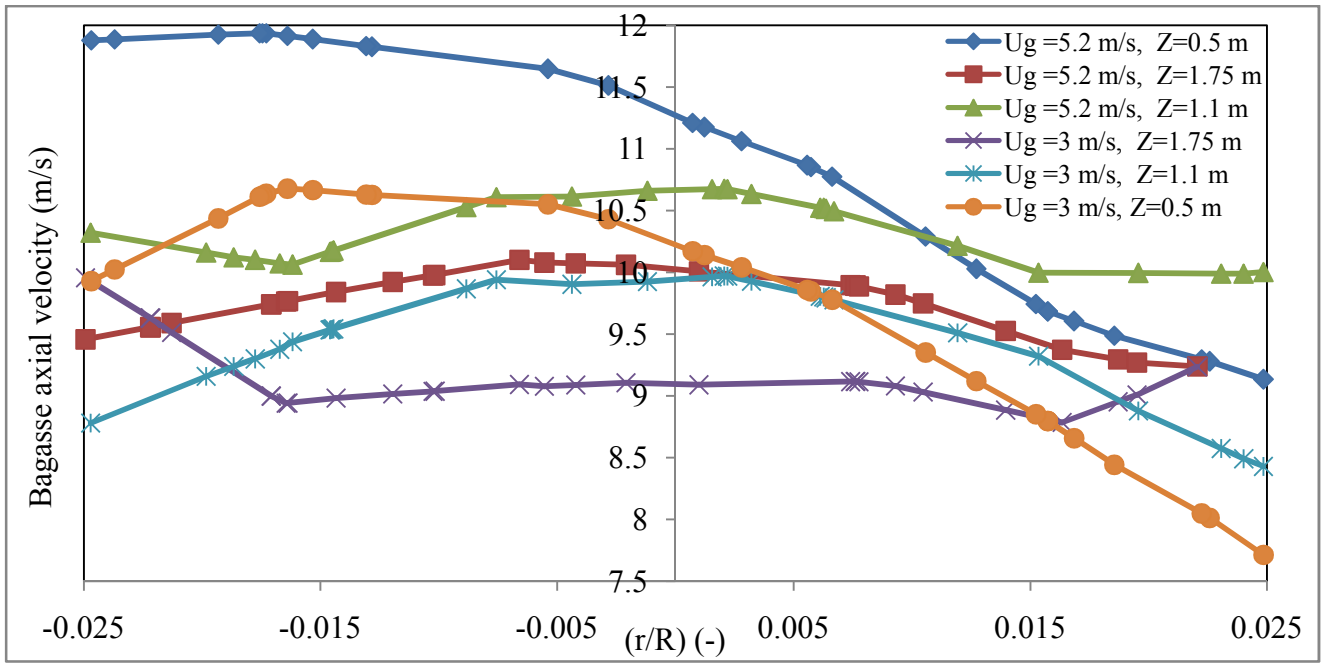

Figure 23 : Average particle velocity distributions at various superficial gas velocities [z=0.5 m, z=1.1 m and z=1.75 m]

5.6 The Influence of Particle Size

Fig. 24 shows the particle volume fraction distribution at the superficial gas velocity of 5.2 m/s. In order to investigate the effect of particle diameter on the flow behavior in the CFB riser, among the different particle diameters considered during the simulation, diameters of big particles 450 µm and small particles 350 µm, is shown on the Figure. The volume fraction of particles is lower in the center than that at the walls. The volume fraction of particles increases toward the walls. It can be seen that the volume fraction of smaller particles is higher in the upper region (z=1.75 m) than that in the lower portion (Z=0.2 m) of the riser. The volume fraction of big particles, however, is lower in the upper region than that in the lower portion of the riser. The larger particles tend to accumulate in the lower portion of the riser. This is due to the fact that the smaller particles follow the gas more effectively than larger ones. Larger particles will not follow the gas effectively and start accumulating, particularly in the wall region where the gas velocity is low.

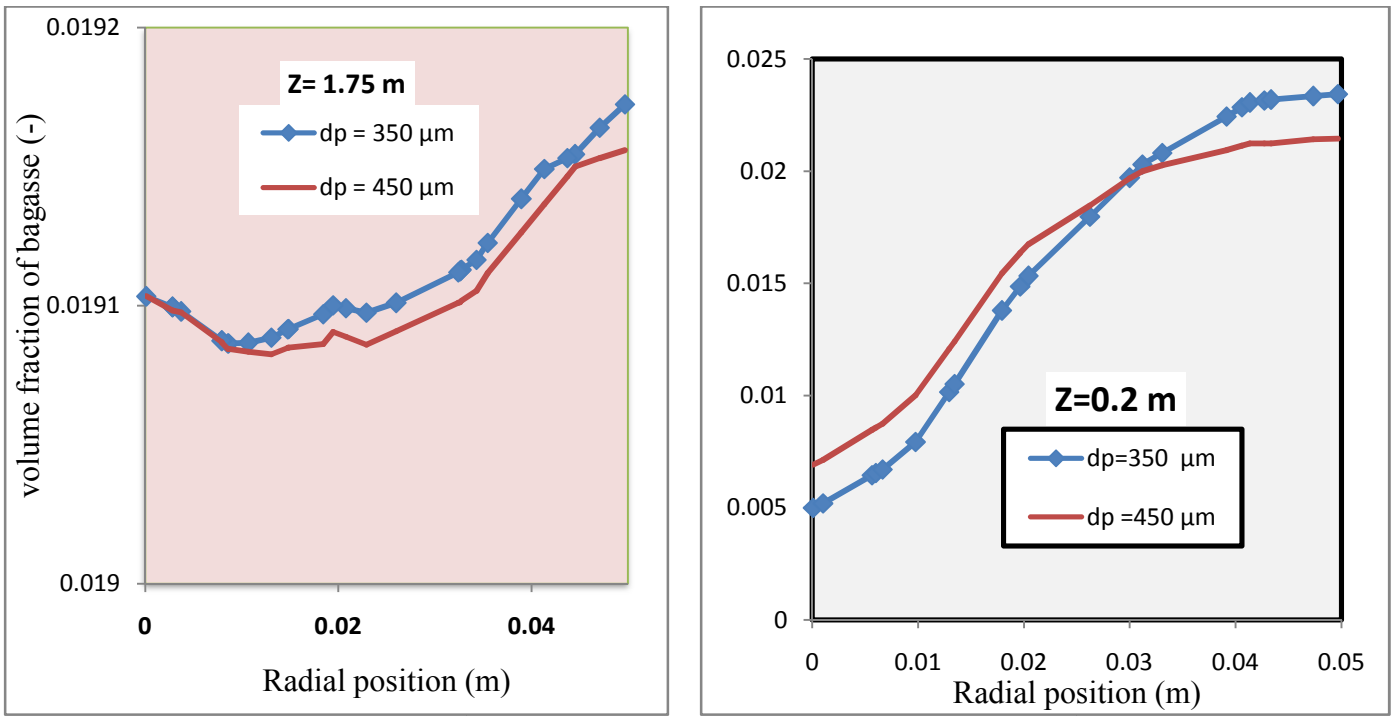

Figure 24 : Particle distribution along the radial at [Z=1.75 m and Z=0.2 m for dp =350µm and dp =450µm]

Effect of inert material (sand)

Fig. 25 shows the computed time-averaged volume fraction of particles at heights of 0.5 and 1.75 m and at a gas velocity of 5.2 m/s. On gasification of biomass using inert material like sand has also a great effect on hydrodynamics of CFB. Since the process it needs inert material with a particle size of less than that of the fuel. When sand with 60 µm particle size and having 2650 kg/m^3 is used it shows similar characteristics from what is shown in the above Figure 24 for particles of the same material with different size regardless of its high density.

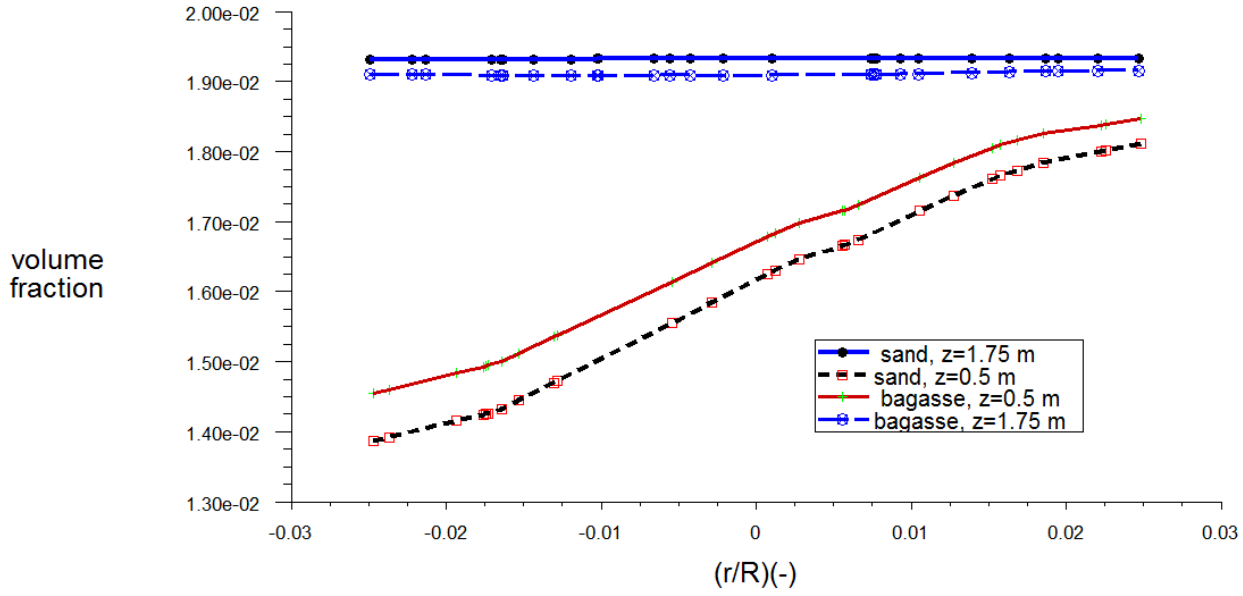

Figure 25 : Time-average distributions of solids concentration with using two different particle diameter at [Z=0.5 m, Z=1.75 m and Ug =5.2 m/s]

Particle velocity profile

The computed particle velocity distribution is shown in figure 26 and 27 at a superficial gas velocity 5.2 m/s. The simulated results showed that in the center part of the riser, the big and small particles flow upward with a high velocity of particles. In the wall region, the velocities of the big and small particles decrease from the core toward the wall. The velocities of the small particles are larger than that of the big particles in the lower zone due to high slip attain from the gas on the bottom side. The relative velocities between particles of different sizes are larger in the center than that at the wall.

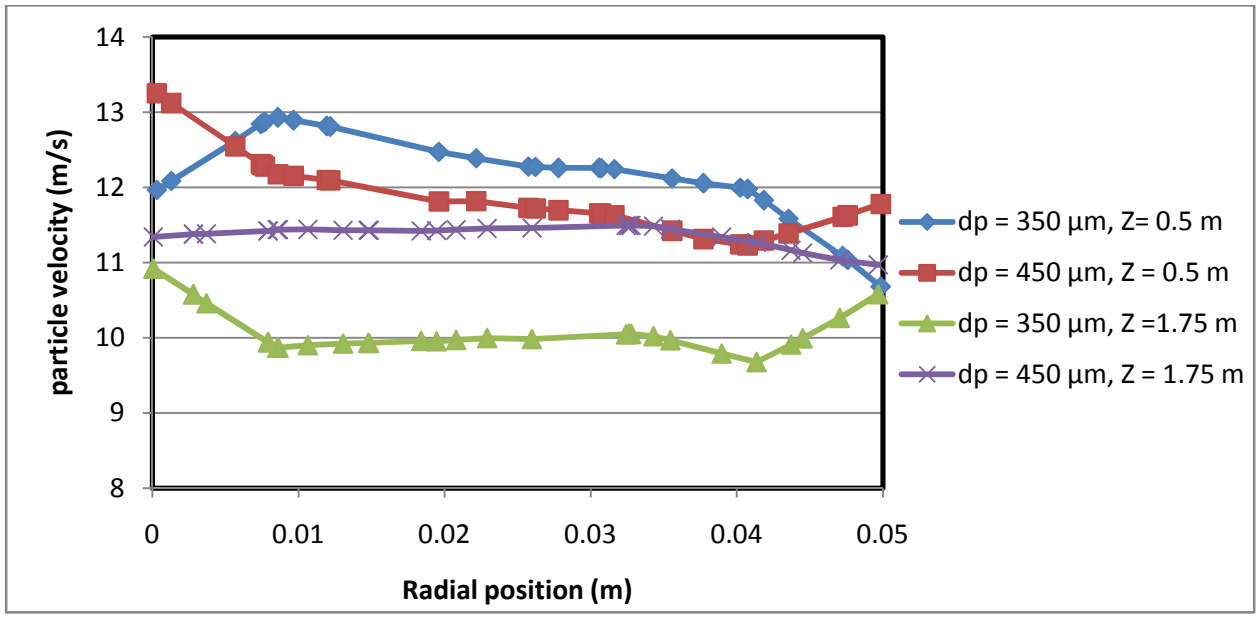

Figure 26 : Particle axial velocity distribution along the radial at Z=1.75 m for [dp =350µm and dp =450µm]

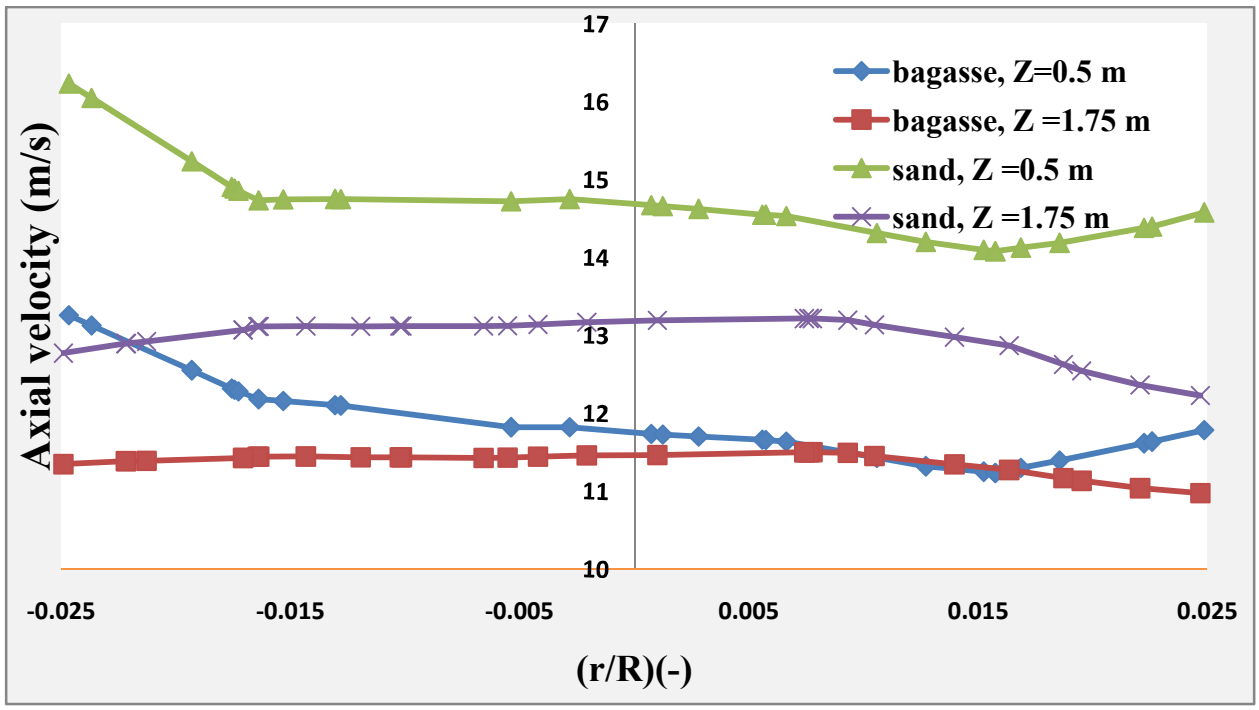

Figure 27 : Time-average averaged axial of solids velocity with using two different two different particle diameter [60 µm sand and 450 µm bagasse for Z=0.5 m, and Z=1.75 m at Ug =5.2 m/s]

5.7 Model Validation

Although, most of previous published works are focused on FCC and coal, the model and the simulation results of this thesis work is compared with some experimental published results on biomass. The simulation results show a similarity on some common behavior of CFB. For transient CFD calculations it is important to find minimum sufficient simulation times and time periods necessary for the averaging. The modeled 3-D full CFB loop in this work reaches at steady state after 10 sec flow, since it is fast fluidization the time it take to reach is small compared to bubble fluidization. A similar finding by K.W. Chu and A.B. Yu [37] perform a numerical simulation of CFB on 6 cm height riser and 1.2 cm diameter using DPM operated at superficial gas velocity of 5 m/s and steady state was reached after 0.6 sec. Zhang, M.H.at el. [38] Perform the simulation of 0.02 m width and 0.14 m height of CFB riser with inlet gas velocity of 4 m/sec and the simulation come to steady-stat after 2 sec. Hence this give the reliability of the results from this work. All the results taken from this simulation work has quite correct steady state results and all operating conditions that varies after achieving steady state was time independent results.

The simulation results of this work conclude on the flow behavior of CFB riser was that, a nonlinear, axial solid volume fraction profile, upward motion in the core of the riser and downward motion along the wall (core-annulus flow) and solid has a tendency to accumulate near the wall. Similar findings have also been reported by park, J.Y. [39] study using palm shell as fuel feed and come with similar findings. Somchai Suaysa-ard [36] using bagasse and sand mixture, the experiment was conducted on a similar geometrical dimensions used in this work and the results of her work agree with some of the results obtained in this simulation.

The basic differences observed from this simulation result and other experimental and simulation works are that a clear cluster formation was not observed in this work due to model assumptions difference on drag model. Most recent simulation works uses EMMS drag model to capture cluster formation.

6. CONCLUSION AND RECOMMENDATION

6.1 Conclusion

Modeling complex reacting flows such as combustion and gasification can be quite difficult and time taking, if the objective is to get solution as accurate as the exact values. In many cases, there are assumptions that are to be made during implementation of commercial code in CFD modeling work. The assumptions are usually aiming to achieve some simplification from many perspectives. However, these simplifications might also intern compromise the accuracy of the results from the simulations. Some of the assumptions that were made in this work are uniform particle size distribution, isothermal, non-reactive condition and modification of geometry at circulated solid inlet are among the basic one.

Based on the results obtained in the simulation from this study, the following conclusions are drawn:

- Uniform axial solid distribution clearly observed from 3-D model while the core-annulus structure was easily observed from 2-D model with less cost of time.
- Solid inlet configuration and the location of the re-circulated solid feed inlet, significantly affect the distribution of the gas and the solid volume fraction.
- The hydrodynamics model able to describe quantitatively the accumulation of solid at the wall. Solid concentrations appear flat in the core and increase near the wall.
- The lower region of the riser is denser than the upper-dilute region even though the solid mainly accumulates at the walls in both regions. In the lower portion of the riser, only a slightly larger down-flow is observed at the left hand-side wall, whereas, in the upper part, no down-flow is observed.
- Back-mixing behavior or accumulation of particles has been perfectly exist in the CFB, since the velocity in the core region are upward flow and much higher than that in the annulus region, while solid and gas velocities near wall are decreasing.
- Once fast fluidization is fully developed with a constant solid fraction at the bottom and top, gradually increasing the circulation rate resulted in an increased dense bed height only. Increasing solids fluxes increases the cross-sectional average solids holdup. The solids flux has a large effect on the extent of solids down flow.

- Increasing solids flux slows down the flow development, but increasing superficial gas velocity makes the flow development faster. Hence, superficial gas velocity has a strong influence on the axial solids velocity, and subsequently on the extent of solids down flow.
- The velocities of the small particles are larger than that of the big particles in the lower zone due to high slip attain from the gas on the bottom side.
- The volume fraction of big particles is lower in the upper region than that in the lower portion of the riser.

All the above conclusions on hydrodynamics of CFB can be used as pre-condition for CFB reactor designing part. Thus, this hydrodynamics model provides the powerful theoretical basis for next steps on CFB gasifier modeling, optimizing the operation and scale-up/down designs. The results obtained from the comprehensive simulations within this work are to be considered as reliable with respect to how the model was formulated, implemented and finally used. However, the simulation results should be compared with experimentally obtained data from CFB pilot plant (when available) before any final conclusions about the validity of results can be made and for any further predictions of the performance of CFB gasifier.

6.2 Recommendation

The simulation results agree with the known hydrodynamic property of CFB and conclude the non-uniformity in radial and axial solids hold-up is with a high concentration of solids flowing mainly downwards near the wall region and most of the gas passing through the central core region. As a result, gas-solids contact is poor in CFB riser. Hence, to reducing the non-uniformity distribution it is better to fix the baffle on the inside wall of CFB to reduce the non-uniform particle distribution in the Core–annulus region. The other option to alleviate the non-uniformity is using a symmetric small secondary air inlets hole along the whole column. Therefore the next step on designing CFB based on the results of the hydrodynamics model, it's better to focus on other options to reduce the non-uniformity of the axial and radial solid holdup, effect of using baffle on hydrodynamics, types of different kind of baffles, cost of power to supply secondary air as compared with installing baffle, and studying on the two next steps thermodynamic equilibrium modeling and reaction kinetics modeling to complete the full design.

Considering the real operation of CFB gasifier, operate at a very high temperature, solid fuel does not have uniform size and solid particle size change and finally converted to gas, char and ash and other very important property of the actual operation of the gasifier was not considered in this work. These are some of the limitation of this work to apply directly to the industrial scale gasifier. To consider the reaction part of the CFB, I recommend the next study to use the new version of the FLUENT 12 since it has some new future like modeling gasification with reaction rather than using FLUENT 6.3 with User Define Function (UDF) for shrinking core model to consider particle size change with reaction.

List of References

[1] Anshul Y. Energy saving opportunities in Sugar industry, ANSH Energy Solutions Pvt. Ltd, 2009.

[2] http://liveenergyng.com/about.html

[3] http://www.seminarprojects.com/Thread-biomass-gasification-for-production-of-producer-gas-using-wood-chip-saw-dust-trash

[4] Zhang, N., Lu, B., Wang, W., Li, J., 3D CFD simulation of hydrodynamics of a 150MWe circulating fluidized bed boiler, Chemical Engineering Journal, 162 (2010) 821–828

[6] Wang, Y. and Yan, L.(2008) CFD Studies on Biomass Thermo-chemical conversion, International Journal of Molecular Science 9: 1108-1130.

[7] Heshmat Massah, Lanre Oshinowo. Advanced Gas-Solid Multiphase Flow Models Offer Significant Process Improvements,journal article by FLUENT software users, Lebanon, New Hampshire, 2000.

[8] Ethio Resource Group (ERG), Diversity and security for the Ethiopian Power System, August 2009.

[9] Hiber Sugar Share Company, prospectus, No. 01/01July 2009

[10] Sintayehu Mekuria, Nurelegne Tefera, A.Venkata Ramayya. Energy System Analysis of Wonji/ Shoa Sugar Factory, Journal of Ethiopian Society of Chemical Engineers, Vol. 10, No.1, May 2007

[11] Yohannes Berhane, Energy assessment, generation and utilization efficiency in Ethiopian sugar factories Case study: Metehara Sugar Factory, M.Sc Thesis, Addis Ababa University, Faculty of Technology Department of Mechanical Engineering, June 2007.

[12] R. Deshmukh, “Thermal gasification or direct combustion a technical assessment of energy generation in Indonesian sugar factories.”M.Sc Thesis, Faculty of Humboldt State

University, Dec, 2008.

[13] Cogeneration Opportunities in the World Sugar Industries, International Sugar Organization, MECAS (09)05, April 2009.

[14] Kunii, D. and Levenspiel, O' Fluidization Engineering', 2nd Edition, ButterWorth-Heinemann, London. . (1997)

[15] Waqar Ali Khan, Khurram Shahzad, and Niaz Ahmad Akhtar, Hydrodynamics of Circulating Fluidized Bed Combustor: A Review, Journal of Pakistan Institute

[16] Hugo A. Jakobsen, Chemical Reactor Modeling, Multiphase Reactive Flows, 2008 Springer-Verlag Berlin Heidelberg

[17] Basu P., "Combustion and Gasification in Fluidized Beds", Taylor and Francis Group LLC, Boca Raton, FL, 2006.

[18] Go´ mez-Bare. A., Leckner B., Modeling of biomass gasification in fluidized bed, Progress in Energy and Combustion Science 36 (2010) 444–509

[19] Desta Lemma Gebrewold, CFD Modeling of Pressurized Entrained Flow Biomass Gasification (PEBG)-Design Simulation of the Oxygen Register in a Pilot Reactor, Luleå University of Technology, Applied Physics and Mechanical Engineering

[20] Gayan, P., J. Adanez, L. F. de Diego, F. Garca-Labiano, A. Cabanillas, A. Bahillo, M. Aho and K. Veijonen, "Circulating Fluidized Bed Co-Combustion of Coal and Biomass," Fuel 83, 277–286 (2004).

[21] Jose Corella, Alvaro Sanz, Modeling circulating fluidized bed biomass gasifiers, A pseudo-rigorous model for stationary state, Fuel Processing Technology 86 (2005) 1021–1053

[22] Yerushalmi, J. "High Velocity Fluidized Bed" Fluidization Technology, John Wiley and Sons Ltd; 155. (1986)

[23] Gasdos, L. J., and Bierl, T. W., 'Studies in Support of Re-circulating Bed Reactors for Processing of Coal', Report by Carnegie Mellon, University, Pittersberg. (1978)

[24] Brereton, C. M.H. and Grace, J.R. Microstructure aspects of the behavior of Circulating Fluidized Beds, Chemical Engineering Science 48:2565-2572, (1993)

[25] Shuyan, W, Huilin L,Wentie L and Wei. L, Flow behavior of clusters in a riser simulated by direct simulation Monte Carlo method. Chemical Engineering journal 106: 197-211, (2005)

[26] K Kato, H Shibasaki, K Tanura, S Arita, C Wang and T Takarada, 'Particle Hold up in Fast Fluidized Bed.' Journal of Chemical Engineering. Japan, vol 22, 1989, no 2, p 130.

[27] Gungor Afsin, Predicting axial profile of a CFB, Chem. Eng. J, 140 (2008) 445-446

[28] Idris M.N, and Burn. A, CFD Modeling Gas-solid flow in CFB/FCCriser reactors: simulation using KTGF in a fully developed flow situation, AIChE 2008, November 16-21, 2008.

[29] Adman Almuttahar, Farborz Taghipour. Computationam fluid dynamics of a circulating fluidized bed under various fluidization conditions, Chemical Engineering Scincies 63 (2008) 1696-1709

[30] Yanping Li Bingjie Ma Jinbang Hu Kai Zhao, Numerical Simulation of the Hydrodynamics of Gas/Solid Two-Phase Flow in a Circulating Fluidized Bed with Different Inlet Configurations, Research Article, Chem. Eng. Technol. 2009, 32, No. 6, 964–970

[31] Zhou. W , Zhao C.S, Duan L.B, Qu. Cr, Chen X.P, Two –dimensional computational fluid dynamics simulation of cola in circulating fluidized bed combustor, Chem. Eng. J (2010)

[32] Cabezas-Gómez. L, Silva. R. C, and Milioli. F. E, SOME modeling and numerical Aspects of the two-fluid Simulation of the Gas-solids flow in a CFB riser, Brazilian Journal of Chemical Engineering , Vol. 23, No. 04, pp. 487 - 496, October - December, 2006

[33] Huilin, L., Gidaspow, D. (2003b), Hydrodynamics of binary fluidization in a riser: CFD simulation using two granular temperatures, Chemical Engineering Science 58, pp. 3777-3792.

[34] FLUENT 6.3 User's Guide, 20.4, Modeling Basic Fluid Flow, Chapter 9 Fluent Inc. (2001)

[35] Schaeffer, D.G. (1987) Instability of Evolution Equations Describing Incompressible Granular Flow, J.Differ. Eqs., 66, pp. 19.

[36] Somchai Suaysa-ard, Hydrodynamics of mixed feed in circulating fluidized bed**,** thesis, Chulalongkorn University, 2004, ISBN 974-17-6038-8.

[37] K.W. Chu, A.B. Yu., Numerical simulation of complex particle–fluid flows, Powder Technology 179 (2008) 104–114

[38] Zhang, M.H., Chu, K.W., Wei,F., Yu A.B., A CFD–DEM study of the cluster behavior in riser and downer reactors, Elsevier, Powder Technology 184 (2008) 151–165

[39] Park, J.Y. The cluster dense phase models for group A fluidization: Dense phase hydrodynamics, Chemical Engineering Sinence, Vol.58: 193-202, 2003

APPENDICES

Appendix 1 : procedure

General Operation Sequence of GAMBIT

- **Initial setup**
  - Solver selection, select solver 5/6.
- **Geometry Creation**
  - Create full geometry
  - Decompose into mesh-able sections
- **Meshing**
  - Local meshing: Edge and Boundary layers
  - Global meshing: Face and/or Volume
- **Mesh examination**
- **Boundary assignment**
  - Continuum and Boundary assign for inlet and outlet
- **Mesh export to be used in FLUENT**

General Steps for working multi-phase model on FLUENT

Grid

1. Reading and Importing GAMBIT Mash File: **File → Read → Case**
2. Check the Grid: **Grid → Check**
3. Smooth (And Swap) the Grid: **Grid → Smooth / Swap ...**
4. Scale the Grid: **Grid → Scale**
5. Display the Grid: **Display → Grid**

Models

1. Define the Model: **Define → Models → Solver**
2. Select multiphase model: **Define → Model→ Multiphase → Eulerian and select phase number.**
3. Select the Standard $k-\varepsilon$ Turbulence Model: **Define → Models → Viscous** and select dispersed multiphase model.

Material

1. Define the Material : **Define → Material**

   Specify primary phase: Air→ specify the property

   Specify Secondary phase: Biomass/Bagasse → specify the property

Phase type

1. Enable the phase to the continuous phase flow prediction:

   Define→ phase →primary phase→ Air→ Set

   Secondary phase→ Bagasse→ Granular→ set based on the model

Operating Condition

- Keep the default operating conditions **Define → Oprating Conditions ...**
- add effect of gravitational effect g = 9.81m/s^2 , direction based on geometry axis.
- keep the operating pressure at atmospheric pressure.

Boundary Condition

2. Define the Boundary Condition: **Define → Boundary Conditions ...**
3. Select the following condition for the **Gas velocity-inlet** zone
4. Select the following condition for the **Solid velocity-inlet** zone
5. Select the following condition for the **pressure-outlet** zone
6. Set condition for the wall zone

Solution

1. Set the under relaxation factor, Discretization and pressure-velocity couple SIMPE type.
   Solve → Controls → Solution
2. Initialize the flow field using condition at minimum fluidization condition or at stationary condition.

   Solve→ initialize→ select all zone to compute→ initialize

A. Enable the display of residual during the solution process:
   Solve → Monitors → Residual...

Packing the CFB gasifier (Adapting)

- Initially to start CFB gasifier may need to pack a certain amount of biomass, to set this initial static height.
  Adapt→ Region→ Mark

- To consider the solid packed region in the simulation need to specify volume fraction at that condition.
  Solve→ initialize → patch

  Save the case file: **File → Write → Case**

Save each time flow condition and data for a certain time gap and any animation picture or data is saved.

File→ Write →Autosave

Began the calculation by requesting 500,000 iteration: **Solve → Iterate…**

Save the Converged flow data: **File → Write → Data…**

Post processing: **Display → Contours**

1. Display the volume fraction distribution for each phases
2. Display velocity profile for each phase along different direction

Display → pathlines

To see the flow direction for both phases need to see path of the flow: Display the pathlines of both phases

Appendix 2 : FLUENT report for 3-D CFB gasifier

```
FLUENT
Version: 3d, dp, pbns, eulerian, ske, unsteady (3d, double precision,
pressure-based, Eulerian, standard k-epsilon, unsteady)
Release: 6.3.26
Title:

Models
------

   Model                         Settings
   ------------------------------------------------------------------
   Space                         3D
   Time                          Unsteady, 1st-Order Implicit
   Viscous                       Standard k-epsilon turbulence model
   Wall Treatment                Standard Wall Functions
   Multiphase k-epsilon Models   Dispersed Approach
   Heat Transfer                 Disabled
   Solidification and Melting    Disabled
   Species Transport             Disabled
   Coupled Dispersed Phase       Disabled
   Pollutants                    Disabled
   Pollutants                    Disabled
   Soot                          Disabled

Material Properties
-------------------

   Material: air (fluid)

      Property                         Units      Method     Value(s)
      ------------------------------------------------------------------
---
      Density                          kg/m3      constant   1.225
      Cp (Specific Heat)               j/kg-k     constant   1006.43
      Thermal Conductivity             w/m-k      constant   0.0242
      Viscosity                        kg/m-s     constant
1.7894001e-05
      Molecular Weight                 kg/kgmol   constant   28.966
      L-J Characteristic Length        angstrom   constant   3.711
      L-J Energy Parameter             k          constant   78.6
      Thermal Expansion Coefficient    1/k        constant   0
      Degrees of Freedom                          constant   0
      Speed of Sound                   m/s        none       #f

   Material: biomass (solid)

      Property               Units    Method     Value(s)
      ------------------------------------------------------
      Density                kg/m3    constant   630
```

```
   Cp (Specific Heat)     j/kg-k   constant   871

   Thermal Conductivity   w/m-k    constant   202.4
```

Boundary Conditions

```
   Zones

      name               id   type
      ---------------------------------------
      fluid              2    fluid
      wall               3    wall
      out_let            4    pressure-outlet
      gas_inlet          5    velocity-inlet
      default-interior   7    interior

   Boundary Conditions

      fluid

         Condition                                                  Value
         ------------------------------------------------------------------
         Material Name                                              air
         Specify source terms?                                      no
         Source Terms                                               ()
         Specify fixed values?                                      no
         Local Coordinate System for Fixed Velocities               no
         Fixed Values                                               ()
         Motion Type                                                0
         X-Velocity Of Zone (m/s)                                   0
         Y-Velocity Of Zone (m/s)                                   0
         Z-Velocity Of Zone (m/s)                                   0
         Rotation speed (rad/s)                                     0
         X-Origin of Rotation-Axis (m)                              0
         Y-Origin of Rotation-Axis (m)                              0
         Z-Origin of Rotation-Axis (m)                              0
         X-Component of Rotation-Axis                               0
         Y-Component of Rotation-Axis                               0
         Z-Component of Rotation-Axis                               1
         Deactivated Thread                                         no
         Laminar zone?                                              no
         Set Turbulent Viscosity to zero within laminar zone?       yes
         Porous zone?                                               no
         Porosity                                                   1

      wall

         Condition                                                Value
         ----------------------------------------------------------------
```

```
   Enable shell conduction?                                no
   Wall Motion                                             0
   Shear Boundary Condition                                0
   Define wall motion relative to adjacent cell zone?      yes
   Apply a rotational velocity to this wall?               no
   Velocity Magnitude (m/s)                                0
   X-Component of Wall Translation                         1
   Y-Component of Wall Translation                         0
   Z-Component of Wall Translation                         0
   Define wall velocity components?                        no
   X-Component of Wall Translation (m/s)                   0
   Y-Component of Wall Translation (m/s)                   0
   Z-Component of Wall Translation (m/s)                   0
   Wall Roughness Height (m)                               0
   Wall Roughness Constant                                 0.5
   Rotation Speed (rad/s)                                  0
   X-Position of Rotation-Axis Origin (m)                  0
   Y-Position of Rotation-Axis Origin (m)                  0
   Z-Position of Rotation-Axis Origin (m)                  0
   X-Component of Rotation-Axis Direction                  0
   Y-Component of Rotation-Axis Direction                  0
   Z-Component of Rotation-Axis Direction                  1
   X-component of shear stress (pascal)                    0
   Y-component of shear stress (pascal)                    0
   Z-component of shear stress (pascal)                    0
   Specularity Coefficient                                 0

out_let

   Condition                                        Value
   -------------------------------------------------------
   Gauge Pressure (pascal)                          0
   Backflow Direction Specification Method          1
   is zone used in mixing-plane model?              no
   Radial Equilibrium Pressure Distribution         no

gas_inlet

   Condition                                  Value
   -----------------------------------------------
   is zone used in mixing-plane model?        no

default-interior

   Condition   Value
   -----------------
```

Solver Controls

```
--------------

   Equations
```

Equation	Solved
Flow	yes
Volume Fraction	yes
Turbulence	yes

Numerics

Numeric	Enabled
Absolute Velocity Formulation	yes

Unsteady Calculation Parameters

Time Step (s)	0.001
Max. Iterations Per Time Step	100

Relaxation

Variable	Relaxation Factor
Pressure	0.30000001
Density	1
Body Forces	1
Momentum	0.69999999
Volume Fraction	0.2
Granular Temperature	0.2
Turbulent Kinetic Energy	0.80000001
Turbulent Dissipation Rate	0.80000001
Turbulent Viscosity	1

Linear Solver

Variable	Solver Type	Termination Criterion	Residual Reduction Tolerance
Pressure	V-Cycle	0.1	
X-Momentum	Flexible	0.1	0.7
Y-Momentum	Flexible	0.1	0.7
Z-Momentum	Flexible	0.1	0.7
Volume Fraction	Flexible	0.1	0.7
Turbulent Kinetic Energy	Flexible	0.1	0.7
Turbulent Dissipation Rate	Flexible	0.1	0.7

Pressure-Velocity Coupling

Parameter	Value
Type	Phase Coupled SIMPLE

Discretization Scheme

Variable	Scheme
Momentum	Second Order Upwind
Volume Fraction	First Order Upwind
Turbulent Kinetic Energy	Second Order Upwind
Turbulent Dissipation Rate	Second Order Upwind

Solution Limits

Quantity	Limit
Minimum Absolute Pressure	1
Maximum Absolute Pressure	5e+10
Minimum Temperature	1
Maximum Temperature	5000
Minimum Turb. Kinetic Energy	1e-14
Minimum Turb. Dissipation Rate	1e-20
Maximum Turb. Viscosity Ratio	100000

BIOGRAPECAL SKETCH

- Author: Beniyam Kebede W/kidane
- City: Addis Ababa
- Phone: +251-911-11-69-80
- E-mail : kebedebeniyam@gmail.com

- Date: July,2011
- Degree: Master of Science in Chemical Engineering under Process Engineering

Undergraduate and Graduate Education

❖ Master of Science in Chemical Engineering under Process Engineering

- ✓ Addis Ababa Institute of Technology (AAiT), Addis Ababa University, Addis Ababa, Ethiopia, 2011
- ✓ Thesis Title: CFD Modeling & Simulation on Hydrodynamics of CFB Biomass Gasifier using FLUENT
- ✓ Advisor: Dr.-Ing. Zebene Kiflie

❖ Bachelor of Science in Chemical Engineering

- ✓ Bahir Dar University Engineering Faculty, Bahir Dar University, Bahir Dar, Ethiopia, 2009
- ✓ Project Title: BIO-OIL Plant Design
- ✓ Advisor: Mr. Moges Ashagrie